Contents

1	Inti	roduction	3			
2	Tec	hnical aspects of high pressure experiments	8			
	2.1	Generation of high pressure	8			
	2.2	Pressure measurement	12			
	2.3	Pressure transmitting media	14			
3	The	eoretical aspects	16			
	3.1	Thermodynamical relations	16			
	3.2	Equations of state	18			
	3.3	Transport properties	18			
4	Structural phase transitions in Ln_2CuO_4 ($Ln = La, Pr, and Nd$)					
	4.1	Structural distortion, magnetism and superconductivity	21			
	4.2	Structural phase transitions in $\rm La_{2-x}Nd_xCuO_4$ (0.6 $\leq x \leq$ 2) and $\rm Pr_2CuO_4$	24			
	4.3	Compressibility of $\rm Ln_2CuO_4$ compounds (Ln = La, Pr and Nd) $\ \ldots \ \ldots \ \ldots$	28			
5	Hig	\mathbf{h} – T_{c} superconductors under high pressure	32			
	5.1	Role of pressure in the discovery of high– $T_{\rm c}$ compounds	33			
	5.2	Pressure–induced charge transfer	34			
	5.3	Intrinsic pressure effects on $T_{\rm c}$	37			
	5.4	Uniaxial pressure dependence of $T_{\rm c}$	40			
	5.5	Inequivalent CuO2–layers in Tl– and Hg–based compounds $\ \ldots \ \ldots \ \ldots$	42			
	5.6	Other models to explain pressure–induced changes in $T_{\rm c}$	45			
6	Str	ongly correlated f–electron systems	47			
	6.1	Some characteristics of heavy–fermion compounds	48			
	6.2	Exchange interaction and Doniach phase diagram	50			

7	Cor	clusio	n	76				
	6.6	Super	conductivity on the verge of magnetic order	72				
	6.5	Anom	alies in the residual resistivity	68				
		6.4.2	Temperature dependence of the electrical resistivity	64				
		6.4.1	Different models to account for unusual low temperature properties	62				
	6.4	Non–Fermi–liquid behaviour						
	6.3	From magnetism to heavy–fermion behaviour and vice versa						

Chapter 1

Introduction

The discovery of the cuprate superconductors in 1986 [1] triggered a tremendous effort to synthesize new materials with higher transition temperatures and has led to $T_c = 133$ K in a Hg-based compound [2]. The unusual normal and superconducting state properties of these materials renewed the interest of physicists in strongly correlated electron systems. In this field an intensive research had already begun after superconductivity in the ternary intermetallic compound CeCu_2Si_2 ($T_c = 650$ mK) was discovered in 1979 [3]. Later on, it was found that also U-based intermetallics superconduct. The low temperature properties of these systems are dominated by the strong correlation of electrons which can be accounted for in Fermi-liquid (FL) theory. Despite the large difference in T_c of more than two orders of magnitude, superconductivity in cuprates and in compounds with 4f- or 5f-elements has one crucial feature in common: it emerges on the brink of magnetic order.

Both systems show a remarkable resemblance in their phase diagram (Fig. 1.1) although they belong to different chemical substance classes. The phase diagram of $La_{2-x}M_xCuO_4$ (M = Sr or Ba) in Fig. 1.1(a) stands in place for the hole–doped cuprates. It is quite similar to that of the electron–doped compounds like $Nd_{2-y}Ce_yCuO_4$. In the slightly doped region (small x values) the cuprate materials exhibit a long–range antiferromagnetic (AFM) order. It is manifest in the ordering of the magnetic moments of the copper ions in the CuO_2 –layers, that are a common structural element of the cuprate superconductors. The doping can be achieved either by substituting the trivalent by a divalent ion or varying the oxygen content. It should be noticed that in this region of the phase diagram non–metallic behaviour is found. Thus, close to the paramagnetic–AFM transition a metal–insulator transition occurs (shaded region in Fig. 1.1(a)). If the doping reaches a certain value, i. e. a critical number of free carriers in the CuO_2 –layers, the long–range magnetic order is destroyed and superconductivity appears. This

4 1 Introduction

does not mean however, that spin correlations are not important for superconductivity. Several models have been discussed in literature relating AFM order and superconductivity, for example a pairing mechanism mediated by magnons instead of phonons [4].

The unconventional nature of the cuprate systems in the superconducting as well as in the normal state, is manifested for example by the symmetry of the superconducting phase (not s- but $d_{x^2-y^2}$ -like [5]) and by the unusual temperature dependence of several physical properties above T_c , respectively. An example for the latter is the temperature dependent rate of nuclear magnetic resonances $1/T_1$. This quantity probes the low-lying spin excitations and has a maximum at T_{SG} , the spin-gap temperature [6]. Inelastic neutron scattering experiments confirmed the existence of such a gap above T_c in underdoped YBa₂Cu₃O_{6.69} ($T_c = 59$ K) [7] (see Fig. 1.1(a)). Furthermore, also the charge excitations seem to have anomalies, revealed for example by electrical resistivity $\rho(T)$. The in-plane resistivity $\rho_{ab}(T)$ starts to deviate from the linear temperature dependence at T^* , while the c-axis resistivity shows a minimum at T^* , well above T_c [8]. Although $T^* > T_{SG}$, the anomalies in the spin and charge excitation spectrum seem to be related [9]. These unusual properties suggest that the normal state cannot be describe within FL theory as the Bardeen-Cooper-Schrieffer (BCS) theory for conventional superconductors is not an appropriate framework to account for the superconducting properties.

The cuprates, in particular the $\rm La_{2-x}M_xCuO_4$ compounds, are interesting materials also from the structural point of view. A structural phase transition from the orthorhombic (O) into the tetragonal T-phase can be achieved by temperature, doping or pressure. In this transition a cooperative tilt of the $\rm CuO_6$ octahedra is involved. They are part of the $\rm CuO_2$ -layers where the superconductivity takes place. The connection of this lattice instability with superconductivity is subject of intensive research.

Pressure is a suitable and a clean mean to study the evolution of structural parameters and of $T_{\rm c}$. In the schematic phase diagram shown in Fig. 1.1(a) the doping concentration x has then just to be replaced by pressure. As examples, we will present detailed studies of the structural phase transitions in non-superconducting La_{2-x}Nd_xCuO₄ (0.6 $\leq x \leq$ 2.0) and Pr₂CuO₄ and pressure–induced changes of $T_{\rm c}$ in Hg– and Tl–based high– $T_{\rm c}$ cuprates.

The phase diagram of the intermetallics with 4f- or 5f-elements exhibits some features quite similar to those discussed above. In $CeCu_2Si_2$ no long-range magnetic order is observed at high temperature and it can therefore be placed in the non-magnetic region, i. e. just above a critical parameter g_c , in the phase diagram of Fig. 1.1(b). The control parameter g can either be the content of a substitute or pressure. Substitution of Si by Ge yields the antiferromagnetically

1 Introduction 5

ordered $CeCu_2Ge_2$. Hence, it is placed at the left of g_c in Fig. 1.1(b). The Néel temperature $(T_N = 4.1 \text{ K})$ decreases as pressure is applied and a superconducting phase $(T_c = 700 \text{ mK})$ is induced at P = 9.4 GPa which disappears close to 20 GPa [10]. Consequently, superconductivity emerges close to the magnetic instability as in the cuprates.

The discovery of superconductivity in CeCu_2Si_2 and CeCu_2Ge_2 was rather surprising since their La counterparts are normal metals down to a few millikelvin. Thus, the 4f-electrons are responsible for superconductivity and for the local magnetic moments. In CeCu_2Si_2 these moments are screened by the conduction electrons below the Kondo-temperature $T_K \approx 15 \text{ K}$ where a magnetic singlet state is formed. In such a "Kondo-lattice" the mass of the f-electrons increases enormously, up to several hundreds of the bare electron mass, as temperature approaches zero. The physical properties can be well described if the picture of quasi-particles is used (FL theory). It is believed that the large jump in the specific heat of CeCu_2Si_2 at T_c is caused by these heavy-fermions (HF), forming the Cooper-pairs. The nature of the attractive interaction responsible in this pairing mechanism is still a matter of discussion.

So far, thirteen HF systems are known to become superconducting or exhibit traces of superconductivity below ≈ 2 K at ambient or high pressure. The majority of HF compounds are either magnetic and can be tuned by alloying or pressure to the paramagnetic side or they are non-magnetic and exhibit FL behaviour below a temperature $T_{\rm FL}$. In the past years detailed measurements close to the magnetic instability, i. e. around $g_{\rm c}$, have revealed very unusual low temperature properties in some HF systems. They are manifested in a deviation from the FL (quadratic) temperature dependence in $\rho(T)$ or in a logarithmic divergence of the specific heat and the magnetic susceptibility. Apparently, this non-Fermi-liquid (NFL) behaviour (dashed region in Fig. 1.1(b)) is somehow related to superconductivity as was recently reported for CePd₂Si₂ [11] and could be a generic feature of a quantum critical point (QCP) [12]. But other concepts are developed and recently a model was proposed, taking into account the competition between magnetic order and the Kondo effect and the disorder of the system [13].

The importance of pressure as external parameter for these systems was clearly demonstrated by the pressure–induced superconductivity in CeCu₂Ge₂. Very often experiments on solid–solutions, i. e. nonstoichiometric compounds are done to simulate external by chemical pressure. This provides an understanding of the physical properties, but the interpretation has always to consider the inhomogeneity of the system. The investigation of the unusual low temperature properties in the vicinity of the magnetic instability however, needs a clean tool to be applied on (stoichiometric) compounds, where inhomogeneity and disorder effects have been re-

6 1 Introduction

duced as much as possible. The high pressure experiments we have performed on stoichiometric (single crystalline) Ce—based intermetallics have revealed NFL behaviour close to the magnetic instability and will be presented in this work.

In the field of strongly correlated electron systems several ten thousand publications appeared so far. Among these are more than thousand articles dealing with the influence of high pressure on structural, phononic, and electronic properties. It would be quite difficult and beyond the scope of the present work, to cover thoroughly these high pressure results. Therefore, after a brief presentation of the high pressure techniques in chapter 2 and some theoretical aspects (chapter 3), we shall concentrate on the more modest goal of describing the progress achieved (i) in the understanding of the structural evolution of the undoped rare–earth based cuprates (chapter 4), (ii) in the picture of a pressure–induced charge transfer in high– T_c cuprates (chapter 5), and (iii) in collecting more experimental evidence of the unusual low temperature properties in heavy–fermion compounds that are driven by pressure towards the magnetic instability (chapter 6). A conclusion will be given in chapter 7.

1 Introduction 7

Figure 1.1: a.) Schematic doping (x)—temperature (T) phase diagram of $\text{La}_{2-x}\text{M}_x\text{CuO}_4$ (M = Sr, Ba). At low x an insulating (INS) and an antiferromagnetically ordered phase (AFM) exists. The superconducting phase (SC) sets in as the AFM order is destroyed. In the metallic phase (M), anomalies in the charge and spin excitations are visible below characteristic temperatures T^* and T_{SG} , respectively. A metal—insulator transition occurs in the shaded region. Furthermore, a transition between an orthorhombic (O) and a tetragonal (T) structure can be induced either by changing T or x. b.) Schematic phase diagram of heavy–fermion systems. The AFM order scales to zero at a critical value g_c of a control parameter g which can be either the content of a substitute or pressure. Superconductivity seems to occur also in the AFM region in some systems. In non–superconducting compounds the Fermi–liquid (FL) behaviour is manifest in several physical properties below a temperature T_{FL} . Some systems show non–Fermi–liquid (NFL) behaviour close to g_c . The question arises whether this behaviour is determined by a quantum critical point (QCP) or other mechanisms.

Chapter 2

Technical aspects of high pressure experiments

The indispensable tool for all the discussed experiments in this work is an appropriate high pressure device. By the expression "high pressure" we mean pressures of several gigapascals $(1 \text{ GPa} = 10^9 \text{ N/m}^2 = 10 \text{ kbar})$ up to 40 GPa. The basic principle of such high pressure devices, which are not larger than a fist, are explained at the beginning of this chapter. In this pressure range, conventional pressure gauges do not work anymore. The high pressure manometers utilized in this work are described in section 2.2. The results presented here were obtained in (quasi)hydrostatic pressure conditions achieved with different kind of pressure transmitting media. Some aspects of them, like pressure gradients developing at high pressure, are discussed briefly in section 2.3.

2.1 Generation of high pressure

An overview of different high pressure techniques was given recently by Eremets [14] but still the early review articles by Jayaraman are very instructive [15, 16]. The highest pressures can be achieved with a diamond anvil cell (DAC). Other anvils like sapphire, tungsten—carbide or sintered diamond are also used, if a pressure range up to 30 GPa is sufficient. In this work we consider only static pressures, which can be maintained for as long a period of time as desired. Static pressures are limited by the available strengths of materials used in the DAC technique. It is possible to extent the pressure range considerably through the use of so called dynamic techniques by means of shock waves. Pressure of several hundred gigapascals can be attained in this way, but it lasts for only a few microseconds. For further details the reader is referred to

Figure 2.1: An accurate scale view of the inner part of a DAC. In between the two diamond anvils a preintended (metallic) gasket is placed. In its center a hole is drilled which serves as sample chamber. It contains also the pressure gauge, for example a small ruby chip (not drawn), and a suitable pressure transmitting medium.

Ref. [14] and references therein.

The principle of the generation of high pressure will be described with the DAC as an example (Fig. 2.1). On the tip of a diamond anvil a preintended metallic gasket is placed. A hole centered in the middle of the gasket contains the sample and a pressure gauge. The sample chamber is completely filled with a suitable (hydrostatic) pressure transmitting medium. For experiments up to 20 GPa the typical dimensions are 500–900 μ m diameter for the diamond tip face, a hole diameter of 200–300 μ m, and a starting gasket thickness of around 100 μ m. The gasket thickness becomes reduced to $\approx 50~\mu$ m at the highest pressure. The pressure is achieved by a force applied to the diamonds, reducing the volume of the pressure chamber. As a consequence the sample is uniformly compressed. The big advantage of a DAC is the optical access to the sample. This allows in principle the pressure determination at any temperature. Such cells are mainly used for optical and x-ray studies.

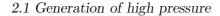
Several difficulties arise if a DAC is used for electrical transport measurements, such as electrical resistance [17]. In this case, at least four electrical leads have to withstand the plastic deformations during pressurization and the probing leads have to be insulated against the metallic gasket. To circumvent these problems a composite gasket is often used (as in the experiments discussed in chapter 5). It is made out of a stainless steel foil and a polyamid film (KaptonTM),

glued to the gasket with a mixture of a two component epoxy adhesive and fine Al₂O₃ powder.

Using a clamp device, derived from the Bridgman type cell with tungsten–carbide or sintered diamond anvils, a non–metallic gasket avoids the fabrication of a composite gasket [18]. An often used material is pyrophyllite (a sheet silicate, $Al_2(Si_4O_{10})(OH)_2$). The soft mineral steatite $(3MgO\cdot4SiO_2\cdot H_2O)$ serves as pressure transmitting medium. The initial internal diameter ϕ and thickness h of the gasket are $\phi = 0.6 - 2$ mm and $h = 0.125\phi$, respectively. The anvil flat diameter is about 2ϕ . At the highest pressure (≈ 30 GPa) the thickness of the pyrophyllite ring becomes reduced to $h \approx 0.1\phi$. Such a high pressure cell was used in the experiments discussed in chapter 6 and further technical details are described elsewhere [18].

The electrical contact between the sample and the measuring equipment is provided by Au or Pt wires ($\phi = 50 \ \mu m$), wedged into small gorges in the pyrophyllite ring (Fig. 2.2). Eight leads allow different possibilities for transport measurements. For instance, the four–point resistance of two samples in series with a pressure manometer can be determined. In another configuration, two different parts of the manometer (here a thin Pb foil) and of the sample can be studied (see Fig. 2.2(a)). The former set–up allows, for example, to compare the behaviour of two samples in almost identical experimental conditions. The latter provides hints on a pressure gradient or a possible discrepancy in the pressure response across the sample on a length scale down to $100 \ \mu m$, which is the minimum distance between two voltage leads. This technique has been developed further to measure four samples at once. Then twelve wires have to be put across the pyrophyllite ring. The electrical resistivity of CeCu₅Au, presented in chapter 6, was measured in such a high pressure cell.

This kind of pressure cell also allows to measure the absolute thermopower of a sample under high pressure. The sample is placed in the middle of the cell and a local heater (Chromel strip) is carefully aligned at the short edge of the sample (Fig. 2.2(b)). On this end of the sample two 12 μ m thermocouple wires (AuFe and Chromel) are placed, ideally at exactly the same distance from the heater. With a current up to 70 mA through the heater a temperature gradient $\Delta T \approx 50$ mK is achieved. It decreases roughly as $\exp(-L/h)$, where L is the distance from the heater. Tests showed that the other end of the sample can be considered to be sufficiently far away from the heater to remain at T_0 . Therefore, a Au wire ($\phi = 10 \ \mu$ m) is chosen as additional lead to connect this reference point for the thermopower measurement. The electrical contact through the gasket is maintained by 25 μ m Au leads. The two voltages measured in the experiment are V_{AuFe} , between the AuFe thermocouple and the common Au wire and $V_{Chromel}$ between the Chromel wire and the Au wire. The absolute thermopower S_x of the sample at



11

Figure 2.2: (a) Top view of a pyrophyllite gasket with a sample (CeRu₂Ge₂) and the pressure gauge (Pb) placed on a disk of steatite, i. e. the pressure transmitting medium. Thin ($\phi = 10~\mu m$) Au wires are attached on the sample and the Pb foil. Pt wires ($\phi = 50~\mu m$) are led through the gasket and establish the electrical contact outside the pressure cell. The sample chamber will be closed with a second disk of steatite. (b) Same principle as before but now the absolute thermoelectric power of the sample can be measured. A heating current I_{heating} produces a temperature gradient that leads to two thermovoltages V_{Chromel} and V_{AuFe} . They are used to determine the absolute thermopower of the sample (see text). The thin Pb foil serves as pressure gauge.

 $T_0 + \Delta T/2$ is then determined by

$$S_{\rm x} = S_{\underline{\rm Au}} F_{\rm e} + \frac{S_{\rm Chromel} - S_{\underline{\rm Au}} F_{\rm e}}{1 - V_{\rm Chromel} / V_{\rm Au} F_{\rm e}}$$
(2.1)

with $S_{\underline{Au}Fe}$ and $S_{\underline{Chromel}}$ the absolute thermopower of the $\underline{Au}Fe$ and $\underline{Chromel}$ wires, respectively.

The total uncertainty in the absolute thermopower (about 15% at 10 GPa) has several origins. A systematic error occurs, whose magnitude depends strongly on the accuracy of the positioning of the thermocouple wires, which should be considered to be of the order of the wires diameter (12 μ m). Thus, if $\Delta T \propto \exp(-L/h)$, ΔT decreases by 13% on a distance $L=12~\mu$ m with $h = 90 \ \mu \text{m}$ for a pressure cell of internal diameter $\phi = 1 \ \text{mm}$. Therefore, a small difference in the distances of the two thermocouples from the heater may lead to a considerable temperature difference. On the other hand, the absolute thermopower of the <u>Au</u>Fe and Chromel wires are taken to be pressure independent. This is of course, a crude approximation. In the case of <u>Au</u>Fe, measurements in the temperature range 1.2 < T < 4.2 K and up to 1 GPa showed that pressure has almost no influence on the thermovoltage measured [19]. Diatschenko and Chu [20] found that the thermal voltage of a Chromel/Alumel thermocouple does not shift more than 1 μ V from its atmospheric pressure value up to 2.2 GPa between 4.2 and 300 K. This, however, does not necessarily imply a small pressure effect on the Seebeck coefficient of Chromel/Alumel thermocouples. Taking into account these uncertainties one has to be careful in the interpretation of small pressure-induced variations in the absolute thermopower. Nevertheless, the large thermopower observed in HF systems makes it possible to obtain substantial information about these compounds, even at very high pressure.

2.2 Pressure measurement

Any physical quantity can be measured either in a direct way using the definition of the quantity or indirect methods. The former measurements are called primary and the latter secondary. Pressure is defined as force per unit area and then a primary pressure gauge must separately and explicitly measure an appropriate force and an appropriate area (the "force–piston gauge"). All other devices used for pressure measurements are secondary gauges and need calibration against the primary gauge. Many physical properties show a sufficiently large pressure dependence and are used as secondary gauges. Here only the ruby fluorescence and the pressure–induced shift of the critical temperature T_c of some elements will be discussed.

The pressure dependence of the ruby fluorescence is an easy way and now a commonly used method for pressure determination in the DAC at any temperature. Ruby (α -Al₂O₃ with 0.05-

2.2 Pressure measurement 13

0.5wt% Cr^{3+}) has a strong fluorescence doublet at $\lambda_0 = 694.33$ nm (R_1 -line) and $\lambda = 692.8$ nm (R_2 -line) which can be excited by laser-light. The ruby scale was calibrated against the Decker equation of state (EOS) for NaCl [21] up to 19.5 GPa [22, 23]. In this pressure range the R_1 -line shifts approximately linearly with pressure ($d\lambda/dP = 0.364$ nm/GPa). Further, Mao and coworkers [24] calibrated ruby up to 110 GPa against the EOS of some metals (Cu, Mo, Pd, and Ag) known from shock—wave data. They described the pressure induced R_1 -shift with

$$P = \frac{1904}{B} \left[\left(\frac{\lambda(P)}{\lambda_0} \right)^B - 1 \right] \quad , \tag{2.2}$$

where $\lambda(P)$ is the wavelength of the R₁-line in nanometer and P is the pressure in gigapascal. In hydrostatic (nonhydrostatic) conditions the parameter B is equal to 7.665 (5.0). Thus, the same shift leads to higher pressures in hydrostatic conditions.

The ruby fluorescence method provides a tool to measure pressure in situ at low temperature. The pressure—and temperature—induced R—line shifts are independent of each other [25, 26]. The temperature induced shift has been attributed to a coupling of the Cr^{3+} crystal field levels to acoustic phonons [27]. It can be well represented by the semi–empirical relation

$$\nu(T) = \nu_0 - \frac{\alpha}{\exp(\Theta/T) - 1} \tag{2.3}$$

with $\nu_0 = 14421.8 \text{ cm}^{-1}$ the frequency of the R₁-line at T = 0 K, $\Theta = 482 \text{ K}$, and $\alpha = 76.6 \text{ cm}^{-1}$, characterizing the phonon dispersion and the electron-phonon coupling, respectively [28]. This equation yields a temperature-induced shift in λ_1 which is in very good agreement with that calculated with the equation proposed by McCumber and Sturge [27]. Thus, with this temperature dependence of the R₁-line, the preceding pressure calibration (eq. (2.2)) can be used for pressure measurements at low temperature.

The position of the R_1 -line shifts with a rate of 6.8×10^{-3} nm/K close to room temperature. A temperature increase of 5 K has the same effect as an increase in pressure by 0.1 GPa. The accuracy of pressure determination is about 0.03 GPa if the doublet is well resolved. Even an accuracy of 0.01 GPa can be achieved if the lines are fitted. At low temperature the width of the R_1 -line is very small and pressure determination can be made within 0.005 GPa. It is clear that for such precise pressure determination the ruby fluorescence should be excited with as less as possible laser power to avoid heating. However, these lower limits refer more to the sensitivity of pressure changes than to the absolute pressure value. In the latter case, the hydrostaticity and the quality of ruby (Cr-concentration, internal stress introduced during grinding) are the key points and should be taken into account if an absolute pressure determination is desired.

High pressure cells with opaque anvils need other means for pressure determination. Many groups use the pressure shift of the superconducting transition of Sn, In or Pb. With the In manometer ($T_c = 3.407 - 0.43P + 5.0 \times 10^{-2}P^2$ [29], P in gigapascal) an accuracy of 0.02 GPa can be achieved for pressures below 1.2 GPa [14]. Similar accuracy can be achieved with the tin gauge $(T_c = 3.732 - 0.49P + 3.9 \times 10^{-2}P^2$ [29], P in gigapascals). The Pb gauge however, is preferred because it can be used up to 30 GPa. In our measurements, presented in chapter 6, we used a quadratic expression obtained by a least squares fit to the $T_c(P)$ data for a low and a high pressure region: $T_{\rm c}=7.199-0.366P+0.12\times10^{-2}P^2$ for P<2 GPa and $T_{\rm c}=$ $7.13-0.37P+7.2\times10^{-3}P^2$ for P>2 GPa. The pressure induced $T_{\rm c}$ -shift was calibrated by Bireckhoven and Wittig [30] using the Pb and GaP phase transitions at 14 and 22 GPa, respectively, as fixed points at room temperature. They assumed that pressure did not change upon cooling. This Pb-scale differs by about 8% (above 20 GPa) to that given by Erskine and Yu [31] who measured pressure at low temperature with the ruby fluorescence and Pb. Below 10 GPa both calibrations agree. Thomasson et al. [32] studied the influence of the pressure conditions on $T_c(P)$ of lead up to 17 GPa. They ascribed the different pressure coefficient of $T_{\rm c}(P)$ in different media to the sensitivity of $T_{\rm c}$ to shear stress. In an alcohol medium — which might be compared to steatite — the precision is about 0.5 GPa up to 14 GPa and 1 GPa at higher pressure.

2.3 Pressure transmitting media

The ideal pressure transmitting medium is He. Compared to Ar, Xe, and the 4:1 methanolethanol mixture, He gives the smallest broadening of the R_1 -ruby fluorescence line. Even if
pressure is changed at low temperature no broadening was observed [33]. Loading a DAC
with He is a simple and reliable method. The almost closed DAC is placed in a cryostat and
completely covered with liquid He. As the He is superfluid it enters the sample chamber and the
cell can be closed to seal the gasket [34]. We used a quite similar technique for loading liquid N_2 as pressure transmitting medium in the experiments presented in chapter 4. The DAC was
placed in a suitable container that can be pressurized with N_2 . Then this assembly is cooled
down to 77 K. After the pressurized N_2 has become liquid the DAC can be closed. The main
advantage of this method is that the loading procedure is quick (≈ 1 h) whereas He-loading
takes several hours.

Soft and solid pressure transmitting media are the easiest to use. The sample chamber is filled with the medium and slightly pre-pressed. The excess material is removed and the sample

and pressure gauge are added and pushed into the medium as the cell is closed. The crucial question is the choice of the medium. Salts, such as KCl, CsCl, AgCl or NaCl give rather good pressure conditions up to 5 GPa but the latter yields a larger pressure gradient. The medium chosen depends on the nature of the experiment. If ruby fluorescence is measured then the pressure transmitting medium should become transparent when pressurized. In the case of a superconducting pressure gauge an opaque medium such as steatite can be used. It might be convenient to use the sample itself as pressure medium. This is often done in the case of powered samples as we did in the $T_c(P)$ measurements of the high- T_c compounds (chapter 5). In such experiments non-hydrostaticity is not negligible, especially if the sample can not be considered as compressible in comparison with e. g. KCl or NaCl.

Pressure gradients depend on the pressure transmitting medium used. In the clamped cell used for electrical transport measurements (chapter 6) the pressure gradient was estimated. Two voltages on the Pb foil were measured (see Fig. 2.2(a)) resulting in two pressures, measured along a length of $\approx 500~\mu\text{m}$. Below 5 GPa no pressure gradient was detected and the accuracy of the pressure determination was limited by the width of the superconducting transition. We estimated a pressure gradient of 0.7 GPa at 10.8 GPa [35]. At much higher pressure ($P \approx 30~\text{GPa}$) the pressure gradient can increase up to 2 GPa [18].

Chapter 3

Theoretical aspects

At the beginning of this chapter some thermodynamic relationships, used in following chapters, are given. This part contains no references since the equations can be found in any text-book dealing with thermodynamics. Section 3.2 is devoted to equations of state that describe the volume–pressure dependence. Some theoretical considerations about transport properties, i. e. electrical resistivity and thermoelectric power, are presented in section 3.3.

3.1 Thermodynamical relations

In a homogeneous system with its volume (V) and the temperature (T) as the only external parameters, the pressure (P) can be evaluated using the free energy F(V,T) = U - TS, where U and S are the internal energy and the entropy, respectively. In the isothermal case, the total derivative dF = -SdT - PdV leads to the pressure

$$P = -\left(\frac{dF}{dV}\right)_T \qquad . \tag{3.1}$$

The variables V, T, and P are examples of thermodynamic coordinates that can be used for describing the state of a system. For all known substances at most two of these three variables are independent and can be chosen arbitrarily. The other is then fixed. This means that a relation f(V,T,P)=0— the equation of state (EOS)— exists for any substance. Possible representations of the EOS are V=V(P,T), P=P(V,T), and T=T(P,V). From these functions six partial derivatives can be obtained, and three of them define macroscopic material constants such as

$$\alpha = \frac{1}{V} \left(\frac{\partial V}{\partial T} \right)_P \tag{3.2}$$

$$\kappa_T = -\frac{1}{V} \left(\frac{\partial V}{\partial P} \right)_T \tag{3.3}$$

$$\zeta = \frac{\alpha}{\kappa_T} = \left(\frac{\partial P}{\partial T}\right)_V \tag{3.4}$$

with α , κ_T , and ζ the coefficient of volume thermal expansion, the isothermal compressibility coefficient and the pressure coefficient, respectively. The reciprocal of these quantities gives the remaining three first derivatives. Only the isothermal bulk modulus

$$B_T = -V \left(\frac{\partial P}{\partial V}\right)_T \tag{3.5}$$

is frequently used. Other derivatives may be defined, e. g. the adiabatic compressibility coefficient

$$\kappa_S = -\frac{1}{V} \left(\frac{\partial V}{\partial P} \right)_S = B_S^{-1} \quad , \tag{3.6}$$

with B_S^{-1} the adiabatic bulk modulus. In this case no heat flows into or out of the sample and thus temperature is not constant. It is related to κ_T via

$$\kappa_T = \kappa_S + \frac{\alpha^2 TV}{C_P} \quad . \tag{3.7}$$

Here C_P is the specific heat measured at constant pressure. Using the thermodynamic Grüneisen parameter

$$\gamma = \frac{\alpha V}{\kappa_T C_V} = \frac{\alpha V}{\kappa_S C_P} \quad , \tag{3.8}$$

eq. (3.7) can be rewritten in the form

$$B_S = B_T (1 + \alpha \gamma T) \qquad . \tag{3.9}$$

 γ describes the change of pressure if the internal energy is changed at constant volume:

$$\gamma = \frac{1}{V} \left(\frac{\partial U}{\partial P} \right)_V \tag{3.10}$$

Second-order phase transitions exhibit no sudden volume change or latent heat. They are characterized by discontinuous changes in α , κ_T , and specific heat $(C_P \text{ and } C_V)$ at the transition temperature T_0 . The slope of a second-order transition curve in the (P,T) diagram can be related to these discontinuities by means of the two Ehrenfest relations

$$\left. \frac{\partial P}{\partial T} \right|_{T=T_0} = \frac{\Delta \alpha}{\Delta \kappa_T} \quad , \tag{3.11}$$

$$\left. \frac{\partial P}{\partial T} \right|_{T=T_0} = \frac{\Delta C_P/T}{V\Delta \alpha} \quad . \tag{3.12}$$

The second equation is useful to calculate the pressure dependence of a phase transition temperature, e. g. the superconducting transition temperature $T_{\rm c}$ or the AFM ordering temperature $T_{\rm N}$ (see section 5.4).

3.2 Equations of state

In practice, the form of the EOS most frequently measured is V = V(P) at constant temperature. Many different (semi-empirical) EOS have been proposed to describe condensed matter under compression (see e. g. the overviews by Bolsaitis and Spain [36] and Holzapfel [37]). An often used EOS was derived by Murnaghan [38] from the expansion of the isothermal bulk modulus (eq. (3.5)) in terms of P:

$$B_T = -V \frac{\partial P}{\partial V} = B_0 + B_0' P + \dots , \qquad (3.13)$$

where B'_0 represents the pressure dependence of B_0 . Truncating this expansion at the first order leads to the Murnaghan EOS

$$P(V) = \frac{B_0}{B_0'} \left[\left(\frac{V_0}{V} \right)^{B_0'} - 1 \right] \tag{3.14}$$

which works well up to a compression of about 15%.

Based on finite-strain theory other relations can be derived. Defining the strain by $\epsilon = [(V_0/V)^{2/3} - 1]/2$ and developing the strain energy in terms of ϵ up to third order yields [39]

$$P(\epsilon) = 3B_0 \epsilon (1 + 2\epsilon)^{5/2} \left[1 + 3/2(B_0' - 4)\epsilon + \dots \right]$$
 (3.15)

From this the Birch EOS [40] is obtained if the expansion is truncated at the second order term

$$P(x) = \frac{3}{2}B_0\left\{x^{7/3} - x^{5/3}\right\}\left\{1 + \frac{3}{4}\left(B_0' - 4\right)\left(x^{2/3} - 1\right)\right\} , \qquad (3.16)$$

with $x = V_0/V$. This widely used relation works rather well up to compression of 20%. An "universal" EOS was proposed by Vinet *et al.* [41]:

$$P(x) = 3B_0(1 - x^{-1/3})x^{2/3} \exp\left\{\frac{3}{2} \left(B_0' - 1\right) \left(1 - x^{-1/3}\right)\right\} , \qquad (3.17)$$

with x as defined above. The exponential term reflects the typical form of interatomic repulsion. The success of this EOS has been demonstrated by comparing the P(x) relation derived from ultrasonic measurements of B_0 and B'_0 with (P, V) relations obtained by static compression or shock—wave data. It works for many classes of solids such as metallic, covalent, ionic, or van der Waals crystals. All three EOS agree with 2.5% at a compression of 15%.

3.3 Transport properties

The electrical resistivity $\rho(T)$ of metals at low temperature contains several basic parts:

$$\rho(T) = \rho_0 + AT^2 + BT^5 + CT^i \exp(-\hbar\omega_0/k_B T) \quad . \tag{3.18}$$

The residual resistivity ρ_0 results from electron scattering of impurities and lattice imperfections and is considered to be temperature independent. The electron–electron scattering leads to the quadratic term, whereas the electron–phonon scattering gives in the Bloch–Grüneisen approximation the T^5 contribution. It is mentioned that this approximation yields also the $\rho(T) \propto T$ dependence at temperatures well above the Debye temperature Θ_D . Electron–phonon umklapp processes give rise to the exponential part in eq. (3.18), where ω_0 is a phonon frequency and i an empirical parameter. Depending on the system under investigation the phonon energy $\hbar\omega_0$ can be replaced by a magnetic gap energy Δ , if for example an anisotropic ferromagnet (FM) is considered [42].

The transport properties, such as electrical conductivity $\sigma = 1/\rho$ and the thermopower S, are derived using the linearized Boltzmann equation [43, 44]:

$$\sigma = \frac{1}{\rho} = e^2 K_0 \tag{3.19}$$

$$S = -\frac{1}{|e|T} \frac{K_1}{K_0} . (3.20)$$

The integrals K_n are defined as [45]

$$K_n = \frac{1}{8\pi^3} \int \left[\frac{\partial E_k}{\hbar \partial k} \right]^2 \left[-\frac{\partial f_k}{\partial E_k} \right] E_k^n \tau_k dk \quad , \tag{3.21}$$

with E_k the conduction–electron energy, f_k the Fermi–Dirac distribution, and τ_k the relaxation time. The latter has to be calculated for wave vector \vec{k} and spin σ . In the most general case this has to be done along the principal axes of the lattice [45]. The challenge is to compute the integrals K_n , which account explicitly for the shape of the Fermi surface and the energy and/or spin dependence of the relaxation time. For isotropic metals and alloys this can be found e. g. in the book by Ziman [46]. The anisotropy of the transport properties of Ce–based Kondo compounds is intensively treated in Ref. [45]. It is worth noting that the third transport property, the thermal conductivity, can also be expressed as a function of the integrals K_n (see e. g. Ref. [43]).

With the assumption, that the physical properties responsible for the electron transport are analytic functions close to and at the Fermi surface (Sommerfeld expansion), $\rho(T)$ and S(T) can be obtained. This was done for Fermi-liquids and for HF systems at low temperature. In the Sommerfeld expansion it was shown [47, 48] that $\rho(T)$ obeys a quadratic temperature dependence at very low temperature, according to eq. (3.18) if phononic and other processes are negligible:

$$\rho(T) = \rho_0 + AT^2 \qquad . \tag{3.22}$$

For the thermopower the Sommerfeld expansion leads to [44, 48, 49]

$$S(T) = \frac{\pi^2 k_{\rm B}^2 T}{3 e} \left(\frac{\partial \ln \tau(E)}{\partial E} \right)_{E=E_{\rm E}} , \qquad (3.23)$$

with $k_{\rm B}$, e, and $E_{\rm F}$ the Boltzmann constant, the electron charge, and the Fermi–energy, respectively. If the electrons are considered to be free, the Fermi surface to be spherical, and the relaxation time to be energy independent, eq. (3.23) gives [43]

$$S(T) = -\frac{\pi^2 k_{\rm B}^2}{2|e|E_{\rm F}}T \qquad . \tag{3.24}$$

Thus, in a simple metal ($E_{\rm F} \approx 5$ eV) S(T) is of the order of $-2~\mu{\rm V/K}$ at 300 K. This value is certainly of the right order of magnitude but a negative sign is not always found experimentally [43]. Under the assumption that the conduction electrons belonging to two bands (in transition metals s- and d-bands) the thermopower can be written as [43, 44]

$$S(T) = -\frac{\pi^2 k_{\rm B}^2 T}{3|e|} \left[\frac{3}{2E_{\rm F}} - \frac{1}{N(E)} \frac{\partial N(E)}{\partial E} \right]_{E=E_{\rm F}} , \qquad (3.25)$$

where N(E) is the electron density of state at energy E. The first term in this equation is identical to eq. (3.24). It can be dominated by the logarithmic derivative of N(E) at $E_{\rm F}$. As was shown by Mott [50], eq. (3.25) can be used for rare—earth based intermediate valence compounds. Then N(E) has to be replaced by the density of state of f—electrons, $N_f(E)$. The sign of S(T) depends on the slope of N(E) at $E_{\rm F}$ and can either be positive or negative. These considerations show, that thermopower experiments probe the energy derivative of N(E) at the Fermi energy and is thus a very sensitive tool. For more details the reader is referred to the review article by Huebner [49] and the books by Blatt and coauthors [43] and Barnard [44].

Chapter 4

Structural phase transitions in Ln_2CuO_4 (Ln = La, Pr, and Nd)

The La– and Nd–based cuprates show only in a small doping range superconductivity. Close to the upper limit of the doping interval a structural transition from an orthorhombic (O–phase) into a tetragonal (T–phase) structure occurs (section 4.1). This transition can also be induced by pressure. As soon as the tetragonal structure is attained, T_c does not increase further. Thus a maximum in T_c seems to be correlated with flat or almost flat CuO_2 –layers. This immediately leads to the more general question about the structural stability of the undoped, i. e. the parent compounds of the high– T_c cuprates. Based on our results with conventional x–ray diffraction and the recently obtained data using synchrotron radiation, a detailed picture of the structural evolution of the $La_{2-x}Nd_xCuO_4$ solid–solution can be drawn (section 4.2). Furthermore, the synchrotron radiation data allowed the analysis of the axis– and volume compressibilities which will be compared to calculated values in section 4.3.

4.1 Structural distortion, magnetism and superconductivity

The electron–doped lanthanide–based cuprates, like $Nd_{2-y}Ce_yCuO_4$ [51] crystallize in the T'–phase (I4/mmm, Nd_2CuO_4 –type) shown in Fig. 4.1(a). In the crystal structure of the hole–doped, La–based compounds, a cooperative tilt of [CuO₆] octahedra leads to an orthorhombic (Cmca) structure (Fig. 4.1(b)) which is a distorted K_2NiF_4 –type. The latter belongs to the tetragonal crystal system (I4/mmm, Fig. 4.1(c)). Sr_2RuO_4 crystallizes in this structure and the appearance of superconductivity in this material ($T_c \approx 1 \text{ K}$) [52] reinforced the interest in compounds crystallizing in the structures shown in Fig. 4.1. Sr_2RuO_4 is the only known su-

Figure 4.1: Schematic view of the different crystal structures attained by the various $La_{2-x}Nd_xCuO_4$ solid-solution (0.6 $\leq x \leq$ 2.0) at different pressure. (a) The low pressure T'-phase (I4/mmm, Nd_2CuO_4 -type), (b) the intermediate orthorhombic O-phase (Cmca, distorted K_2NiF_4 -type), and (c) the high-pressure T-phase (I4/mmm, K_2NiF_4 -type).

perconductor with the same layered crystal structure as the La– and Nd–based cuprates that includes no copper. Apparently the main difference is that the Ba–substituted La₂CuO₄ superconducts at temperatures as high as 40 K (at P=1.3 GPa) [53] whereas in Sr₂RuO₄ the transition temperature is about 1 K. Furthermore, T_c decreases to ≈ 700 mK as a pressure of 1.2 GPa is applied on Sr₂CuO₄ [54]. This raises the question whether in both systems the same mechanism is responsible for superconductivity.

 $\text{La}_{2-x}\text{Sr}_x\text{CuO}_4$ is the simplest hole–doped copper–oxide superconductor and its systematic study has revealed an evolution from an AFM insulator to a normal metal via a superconducting state (0.07 $\leq x \leq$ 0.24; $T_c = 24$ K for x = 0.15). The AFM order is caused by the Cu–moments which are ordered below $T_N = 320$ K (La^{3+} has no magnetic moment) and the ordering temperature is largely enhanced by pressure [55]. The crystal structure contains [CuO₆] octahedra (Fig. 4.1(b)) which are distorted to relieve compressive stress on them caused by the mismatch of (La, Sr)–O and Cu–O bonds. Hence, the CuO₂ planes are buckled. As x exceeds 0.21, a structural transition into the tetragonal K_2NiF_4 structure (Fig. 4.1(c)) occurs and simultaneously the

superconducting transition temperature T_c decreases sharply as already mentioned in the introduction (see Fig. 1.1). Hydrostatic pressure experiments on samples with $x \leq 0.18$ showed that T_c increases linearly with pressure but as soon as the tetragonal phase is induced, T_c remains constant [56, 57]. This change in $\partial T_c/\partial P$ is believed to be related with the orthorhombic-tetragonal transition [58] and thus the maximum in T_c occurs when the CuO₂ planes are flat or almost flat. Pressure experiments on superconducting La_{2-x}Sr_xCuO₄ with x = 0.10 and 0.15 have shown that T_c varies inversely with the tilt angle and that T_c is maximum in the tetragonal structure, i. e. with flat and square CuO₂ planes [59].

Soon after the discovery of the hole–doped superconductors, the electron–doped materials $\text{Ln}_{2-x}\text{Ce}_{x}\text{CuO}_{4}$ (Ln = Pr, Nd, Sm, and Eu) were synthesized [51]. Murayama *et al.* [60] investigated the pressure dependence of T_{c} in Nd_{1.85}Ce_{0.15}CuO₄ ($T_{c} \approx 20$ K) and found almost no pressure effect on T_{c} ($P_{\text{max}} = 2.5$ GPa). Comparing the difference in the Cu coordination with respect to the hole–doped superconductors with T– or O–structure these authors point out the important role of the bond between copper and apical oxygen.

The parent compounds of these superconductors show a complex magnetic ordering. In Nd₂CuO₄ several magnetic phases occur as the temperature is lowered or a magnetic field is applied. At low temperature the magnetic moment of the Nd³⁺ is able to interact with (next nearest) Cu-spins and to order spontaneously [61]. Below 30 K the Cu-moments are oriented antiferromagnetically along the a-axis as well as in the basal plane of the tetragonal structure. Along the c-axis adjacent Cu-spins are coupled ferromagnetically. The same order occurs for the Nd-sublattice below 5 K. Neighboring Nd- and Cu-spins are coupled ferromagnetically. In the Nd_{1.85}Ce_{0.15}CuO₄ superconductor the Cu–spins are not ordered but the Nd–sublattice shows the same magnetic order (below $1.2~\mathrm{K}$) as in $\mathrm{Nd_2CuO_4}$ [62]. Furthermore, HF-like behaviour below 1 K was found in this compound for a doping range $0.15 \le x \le 0.2$ [63]. This feature probably arises from the combination of the coupling of the Nd and Cu moments and the Nd-Nd interaction. It is noted, that this behaviour is completely different to HF superconductors (see section 6.6). In the latter materials superconductivity occurs below $\approx 2 \text{ K}$ and the heavy quasi-particles carry the supercurrent. For the Nd_{1.85}Ce_{0.15}CuO₄ system however, the superconducting transition takes place at temperatures well above the formation of the state which bears strong resemblance to a HF system [63]. According to theoretical considerations [64], the low temperature state of $Nd_{1.85}Ce_{0.15}CuO_4$ is a new prototype of a HF system, where the Nd-moments interact with strongly correlated electrons at the Cu-site. In classical HF systems however, the rare–earth moments are coupling to conduction band electrons and their

correlation is negligible (see chapter 6). Presumably also $Y_{1-x}Pr_xBa_2Cu_3O_{7-\delta}$ ($\delta \approx 0.05$ and x = 0.2, 0.3) belongs to this new type of HF systems. Maple *et al.* [65] have observed a large value of the linear specific heat which yield a Sommerfeld coefficient well above 200 mJ/molK² and thus might point to low–lying magnetic excitations.

Pressure experiments on Pr_2CuO_4 showed that similar spin re-orientations as in Nd_2CuO_4 can be induced by volume compression but T_N hardly changes [66]. The latter finding is quite different from that found for La_2CuO_4 . Such a distinction can be caused by a different enhancement of inter-plane exchange coupling under pressure. If the pressure effects on T_N and T_c in both kind of superconductors (n- and p-doped) are related, than the AFM correlations might play an important role for superconductivity.

4.2 Structural phase transitions in $La_{2-x}Nd_xCuO_4$ (0.6 $\leq x \leq 2$) and Pr_2CuO_4

Depending on the size of the lanthanide ion, the Ln_2CuO_4 cuprates (Ln = rare earth) crystallize in three different structures. La₂CuO₄ is the only compound of this series able to adopt the tetragonal T-structure, but only either at temperatures above 573 K (at ambient pressure) or at pressures above 3.4 GPa (at room temperature) [67, 68]. At normal conditions (P=1 bar and room temperature) the T-structure is orthorhombically distorted due to a small tilt of the Cu-O octahedra, and hence forming the so called O-structure. Substituting La by the other lanthanides from praseodymium to thulium, results in compounds which crystallize in the related T'-structure [69]. In the T- and T'-structure the cations and one half of the oxygen ions (labelled O(1)) are occupying the same positions (see Fig. 4.1). However, the arrangement of the other half of the oxygen atoms (labelled O(2)) is quite different in both structures, resulting in different coordination polyhedra. In the T- and O-structure the Ln^{3+} and Cu^{2+} ions have respectively a ninefold (mono-capped quadratic antiprism) and sixfold (elongated octahedron) coordination, whereas they occupy an eightfold (pseudo-cubic) and fourfold (square-planar) coordinated site in the T'-structure. As a consequence of the lower coordination number in the T'- compared to the T- and O-structure, the latter should be favoured under high pressure according to the pressure–coordination rule [70].

This assumption is verified by synchrotron radiation experiments on LaNdCuO₄, Nd₂CuO₄, and Pr₂CuO₄ under high pressure [71, 72]. Figure 4.2 shows the evolution of the reduced volume with pressure for Nd₂CuO₄. The T'-structure is stable up to $P_T = 21.5$ GPa and then

Figure 4.2: Relative unit-cell volume V/V_0 of Nd₂CuO₄ versus pressure as derived from synchrotron x-ray data [71]. At $P_{\rm T}=21.5$ GPa the T'-phase (bold squares) starts to transform into the high pressure T-structure (\bullet). The T-phase fraction increases with pressure as is depicted in the inset. Upon releasing pressure (open symbols) the orthorhombic O-phase (\diamondsuit) appears and at low pressure the T'-phase (\square) is restored again.

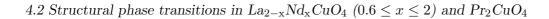
the K_2NiF_4 structure is adopted. In a wide pressure range both phases coexist (indicated by the vertical lines in Fig. 4.2). During pressure release the orthorhombic O-phase is attained before the initial T'-structure is recovered again at low pressure. The solid lines represent a fit of an EOS to the data (see section 4.3).

The stability of the different structures requires a bond–length matching between adjacent layers and is evaluated in terms of the Goldschmidt tolerance factor $t=(r_{\rm Ln^3+}+r_{\rm O^2-})/\sqrt{2}(r_{\rm Cu^2+}+r_{\rm O^2-})$, where $r_{\rm Ln^3+}$, $r_{\rm Cu^2+}$, and $r_{\rm O^2-}$ are the ionic radii of the lanthanide, the copper, and the six-fold coordinated oxygen ions, respectively [73, 74]. For the ${\rm La_{2-x}Nd_xCuO_4}$ solid–solution, t is a linear function in x, if an average lanthanide ionic radius $r_{\rm Ln^3+}=0.5[(2-x)r_{\rm La^3+}+xr_{\rm Nd^3+}]$, with $r_{\rm La^3+}=1.216$ Å and $r_{\rm Nd^3+}=1.163$ Å[75], is used. So far, the following phase diagram at normal conditions has been obtained [76, 77]: (i) the T–structure exists for $0.99 \ge t \ge 0.88$, (ii) the O–structure is present for $0.88 > t \ge 0.865$, (iii) the T'–structure is stable for $0.865 > t \ge 0.83$, and (iv) for 0.83 > t a mixture of ${\rm Ln_2O_3}$ and a new compound with the formula ${\rm Ln_2Cu_2O_5}$ is found [77, 78]. A special treatment of such a mixture at high pressure and high temperature has allowed to stabilize the T'–structure down to t=0.814 (for Ln=Tb, Dy, Ho, Er, Tm) [79].

In the T-structure compressive and tensile forces are present in the basal CuO₂ plane and along the c direction (Ln–O(2)), respectively. For La₂CuO₄, the Cu–O(1) distance (1.91 Å \approx a/2) is shorter than the sum of the ionic radii (2.13 Å, with $r_{\rm Cu^{2+}} = 0.73$ Å and $r_{\rm O^{2-}} = 1.40$ Å) leading to a compression. The two Cu–O(2) distances are significantly longer (2.46 Å, using c = 13.15 Å [67, 77]). The tension is due to the fact that eight out of nine Ln–O distances are longer (\approx 2.64 Å for Ln–O(1) and \approx 2.77 Å for Ln–O(2)) and only the distance between the lanthanide and the apical oxygen (\approx 2.30 Å) is shorter than the sum of the ionic radii (2.62 Å, using $r_{\rm La^{3+}} = 1.216$ Å). Both kinds of stresses are partially relieved by a cooperative tilting of the octahedra, resulting in the orthorhombic O–structure (i. e. the T \rightarrow O transition).

In La_{2-x}Nd_xCuO₄ the average size of the lanthanide as well as the tolerance factor t decrease with Nd substitution. According to the definition of t and the average radius $r_{\rm Ln^3+}$, a linear relation between t and x exists. When the critical value t=0.865 is reached, the O(2) ions move from the 4e sites of the O-structure $(0,0,z;\ 0,0,-z)$ to the 4d sites $(0,\frac{1}{2},\frac{1}{4};\ \frac{1}{2},0,\frac{1}{4})$ of the T'-structure (see Fig. 4.1). The O \rightarrow T' transition as a function of the average lanthanide ion size has been interpreted as optimization of the Ln–O distances [74, 76, 77]. The average Ln–O distance in the T'-structure is significantly shorter (2.51 Å instead of 2.64 Å) in the resulting fluorite-like arrangement (coordination number CN(Ln³⁺) = 8) compared to the O-structure (CN(Ln³⁺) = 9). Among the eight Ln–O distances in the T'-structure four are significantly shorter (2.32 Å, for Ln–O(2)) and four are longer (2.68 Å, for Ln–O(1)) than the sum of the ionic radii (2.51 Å). Therefore, a compression in the Ln–O(2) linkages is present. Furthermore, the oxygen ions at the 4d site are separated only by $a/\sqrt{2}$ (≤ 2.81 Å), which is very close to the sum of the ionic radii (2.80 Å). To diminish the O(2)–O(2) repulsion, the structure had to expand along the a- and b-axis. As a consequence the CuO₂-layers in the T'-structure are under tension.

The results of the high pressure studies on the $\text{La}_{2-x}\text{Nd}_x\text{CuO}_4$ solid-solution [71, 72, 80] and Pr_2CuO_4 [72] can be summarized by plotting the transition pressure P_{T} versus the tolerance factor t (see Fig. 4.3). We have chosen t as variable because it takes the Ln–O and Cu–O ionic bonding into account and gives an estimate of the structural stability. Nevertheless, the Nd–content x could also be used. The t-values of the T'– and O–structure have been calculated using rare earth ion radii in a ninefold and copper and oxygen ion radii in a sixfold coordination. Fitting a linear $P_{\text{T}}(t)$ -dependence (solid line in Fig. 4.3) to the data and extrapolating it down to $P_{\text{T}}=0$ GPa yields t=0.8669. This value is only slightly higher than t=0.865 which represents the border of stability of the T'–structure, indicated by the vertical line in Fig. 4.3.



27

Figure 4.3: Transition pressure $P_{\rm T}$ versus the tolerance factor t for ${\rm La_{2-x}Nd_xCuO_4}$ compounds and ${\rm Pr_2CuO_4}$. The straight line separates the T'- and T-phase. Above t=0.865 the orthorhombic O-phase is the stable low pressure phase. The point shown in this region represents ${\rm La_2CuO_4}$ which transforms into the T-phase at 3.4 GPa. The tolerance factor t versus $P_{\rm T}$ is plotted in the inset. Points at the t=0.865 (0.88) line represent the lowest pressures where the O-(T-)phase was observed.

An interesting insight in the phase sequence can be obtained if the tolerance factor is plotted versus pressure (see inset Fig. 4.3). The symbols at ambient pressure are the starting tolerance factor of the various compounds. The corresponding points at the borderline of the O- and T-phase (t = 0.88-line) represent the transition pressure $P_{\rm T}$ found in the La_{2-x}Nd_xCuO₄ compounds. In the plot are also included the transition pressures of La_{2-x}Nd_xCuO₄ (x = 0.6 and 0.7) [80] and La₂CuO₄ [68] obtained from measurements using conventional x-ray sources. Assuming a linear t(P)-relation the t(P = 0) and $t(P_{\rm T})$ -points can be connected by a straight line. This immediately gives an intersection with the t = 0.865-line, representing the lower limit of the O-phase. The points plotted at this line are the lowest pressure values where the O-phase was still observed in the diffraction pattern obtained during pressure release. They agree rather well with those deduced from the t versus P plot. This results implies further, that the O-phase should also occur in the solid-solution with lower Nd-content.

The fact that the intermediate O-phase is not observed during increasing pressure and the existence of a large T'- and T-phase domain (more than 25 GPa in the case of Pr_2CuO_4) is likely due to some hysteresis in the phase transitions, since the experiments were carried out at room temperature. This phenomenon is less pronounced during decreasing pressure, and the observed phase sequence $T \to O \to T'$ shows clearly how pressure is able to tune the value of the tolerance factor t. The reversibility of the transition proves that the T-structure is not induced by a change in composition, but results only from the pressure effect. This is also confirmed by the crystal structure refinement of the synchrotron x-ray data.

4.3 Compressibility of Ln_2CuO_4 compounds (Ln = La, Pr and Nd)

In our work we studied materials crystallizing in the T'-structure, having the cations M = Cu and Ln (Ln = La, Nd, and Pr) in a fourfold and an eightfold oxygen coordination, respectively. The unit-cell can be build up with $[MO_8]$ polyhedra. For each polyhedron the mean M-O distance defines an average bond length d_{M-O} . Hazen and Finger [81] reviewed many oxides, in particular those with the cubic rocksalt structure, and found the empirical expression $\kappa_V^{\text{poly}} = 3\kappa_{M-O}^{\text{poly}}$ for the volume compressibility κ_V^{poly} of the polyhedra. The linear compressibility $\kappa_{M-O}^{\text{poly}}$ for the distance d_{M-O} is given by

$$\kappa_{\rm M-O}^{\rm poly} = 0.44 \frac{d_{\rm M-O}^3}{Z_{\rm M}} \times 10^{-3} \quad ,$$
(4.1)

where $Z_{\rm M}$ is the valence of the cation M. In this relation $\kappa_{\rm M-O}^{\rm poly}$ is in GPa⁻¹ and d in Å. Using a

simple model, introduced by Cornelius et~al.~[82], the anisotropic compressibilities of the lattice parameters and the volume of the $\text{La}_{2-x}\text{Nd}_x\text{CuO}_4$ compounds can be calculated. Following their description, the unit–cell of the T'–structure can be build up with $[\text{LnO}_8]$ polyhedra and $[\text{CuO}_8]$ boxes. The latter are formed by the Cu–O(1) plane and the plane of the four O(2) ions. The polyhedra contain four Ln–O(1) and Ln–O(2) distances ($\approx 2.68~\text{Å}$ and $\approx 2.32~\text{Å}$, respectively). In the boxes four Cu–O(1) bonds and four Cu–O(2) distances ($\approx 1.97~\text{Å}$ and $\approx 3.62~\text{Å}$, respectively) are present. With the assumption that the $[\text{LnO}_8]$ polyhedra are compressed isotropically and the $[\text{CuO}_8]$ boxes are more rigid in the basal plane (Cu–O(1) bond) than perpendicular to it (long Cu–O(2) distance), the compressibilities of the crystal can be calculated. Since the two polyhedra each fill half the unit–cell volume, the compressibilities κ_a and κ_c along the a– and c-axis as well as the volume compressibility κ_V are given by

$$\kappa_a^{-1} = \frac{1}{2} \left(\kappa_{\text{Ln-O}}^{-1} + \kappa_{\text{Cu-O(1)}}^{-1} \right)$$
(4.2)

$$\kappa_c^{-1} = \frac{1}{2} \left(\kappa_{\text{Ln-O}}^{-1} + \kappa_{\text{Cu-O(2)}}^{-1} \right)$$
(4.3)

$$\kappa_V = 2\kappa_a + \kappa_c \quad . \tag{4.4}$$

Using the distances deduced from the synchrotron data [72] and the eqs. (4.1)–(4.4), the compressibilities and the bulk moduli of LaNdCuO₄, Nd₂CuO₄, and Pr₂CuO₄ can be calculated (see Tab. 4.1). The agreement to the measured values of κ_a and κ_V is in all cases better than 4% and 12%, respectively. The larger error in the latter is due to κ_c , which is about 20% higher than the measured values for the La_{2-x}Nd_xCuO₄ compounds with x = 1 and 2. A rather good agreement (better than 3%) is obtained for Pr₂CuO₄.

A similar approach can be made to calculate the compressibilities for the O-phase of La₂CuO₄. Again following the division of the unit-cell of La₂CuO₄ outlined in Ref. [82] the values listed in Tab. 4.1 are found. Also in this case the experimental values (apart from κ_b) are reasonably well reproduced. However, the calculated values reveal a rather isotropic compression whereas the experimental data show anisotropic compressibilities. It is noted that here κ_b corresponds to κ_c , since in the *Cmca* space group type the long axis is along the *b*-direction. From a crystal-chemistry point of view the model used here is only a crude approximation despite its good agreement with the measured values. The Cu-Ln distance (d < 2.79 Å) is much shorter than the Cu-O(2) distance (d = 3.62 Å) and this is not accounted for in eq. (4.1). Therefore, it is expected that this makes the structure more rigid along the *c*-axis than it is calculated. Furthermore, the compressibility κ_V is a combination of polyhedral compression and bond bending [81], especially in the orthorhombic structure of La₂CuO₄.

Table 4.1: Experimental compressibilities of the lattice parameters, unit–cell volume, some distances, and the c/a ratio of LaNdCuO₄, Nd₂CuO₄, and Pr₂CuO₄ in the T'–structure. The values of the bulk modulus B_0 and its pressure dependence B_0' are the average of fits according to the Murnaghan and Birch EOS. Numbers in parentheses represent standard deviations of the last digit. According to a model described in the text the axis and volume compressibilities can be calculated. In the last column data for La₂CuO₄ are given (P < 0.61 GPa) [59]. It adopts an orthorhombic crystal structure and the b–axis corresponds to the c–axis in the other compounds, crystallizing in a tetragonal crystal structure.

	$LaNdCuO_4$		Nd_2CuO_4		Pr_2CuO_4		La_2CuO_4 [59]	
	exp.	cal.	exp.	cal.	exp.	cal.	exp.	cal.
$\kappa_a = (10^{-3} \mathrm{GPa}^{-1})$	-1.9(2)	-2.0	-1.9(1)	-1.9	-2.0(1)	-2.0	-2.2	-2.5
$\kappa_b = (10^{-3} \mathrm{GPa}^{-1})$	-1.9(2)	-2.0	-1.9(1)	-1.9	-2.0(1)	-2.0	-4.2	-2.5
$\kappa_c = (10^{-3} \mathrm{GPa}^{-1})$	-3.0(1)	-3.9	-3.0(1)	-3.8	-3.7(2)	-3.8	-1.8	-2.5
$\kappa_V = (10^{-3} \mathrm{GPa^{-1}})$	-7.0(1)	-7.9	-6.9(1)	-7.7	-7.9(5)	-7.8	-8.2	-7.5
B_0 (GPa)	143(1)	127	145(2)	131	126(2)	129	122(2)	134
B_0'	4.0(4)	-	4.1(4)	-	5.0(6)	-	4	-
$\kappa_{\rm Ln-O(2)}(10^{-3}{\rm GPa^{-1}})$	-2.1(1)	-	-1.8(2)	-	-2.7(2)	-	-	-
$\kappa_{\rm Ln-O(1)}(10^{-3}{\rm GPa}^{-1})$	-3.2(1)	-	-2.9(1)	-	-2.4(2)	-	-	-
$\kappa_{\text{Cu-O(2)}}(10^{-3}\text{GPa}^{-1})$	-2.7(1)	-	-2.8(1)	-	-3.2(3)	-	-	-
$\kappa_{c/a}(10^{-3}\mathrm{GPa}^{-1})$	-1.0	-	-1.0	-	-1.4	-	+0.3	-

The compression of several M–O distances is also reported in Tab. 4.1. In the La_{2-x}Nd_xCuO₄ solid–solution the Ln–O(2) and Ln–O(1) distances vary like the a– and c–axis compressibilities, respectively. This is not surprising because the only way to diminish the internal stress is to decrease the largest Ln–O distance (i. e. Ln–O(1)). The compressibility of the remaining two Cu–O distances is the same as κ_a (for Cu–O(1)) and κ_c (for Cu–O(2)). These observations show that κ_a and κ_c are determined by the pressure dependence of the Ln–O(2) and Cu–O(1), and the Ln–O(1) and Cu–O(2) distances, respectively. The values given in Tab. 4.1 for Nd₂CuO₄ are in very good agreement with data obtained by neutron measurements [83].

In Pr_2CuO_4 , κ_a is the same as for the other two compounds but κ_c is significantly higher. This is nicely reproduced in the model calculations. However, it seems that the correlation between axis-compressibility and the pressure dependence of Ln–O distances found for the other two compounds is not valid in Pr_2CuO_4 : The Pr-O(2) distance is more compressible than the a-axis and the Pr-O(1) distance is significantly stiffer than the c-axis. The origin for this difference might be related to the Pr–ion, since the distances in Pr_2CuO_4 are comparable to those in $LaNdCuO_4$.

Upon decreasing pressure in all three compounds an orthorhombic structure was attained as pressure became lower than $P_{\rm T}$. The initial T'-structure was eventually obtained at pressures below 10 GPa, 5 GPa, and 2.5 GPa for Nd₂CuO₄, Pr₂CuO₄, and LaNdCuO₄, respectively. In the case of LaNdCuO₄ the O-phase occurred in a rather large pressure interval (2.5 < P < 10 GPa) and it was possible to record several diffraction pattern. Therefore, detailed structural information of this phase was obtained. Regarding the resemblance of the sequence of the structural transformations it is very likely that the following will be applicable to the other members of the La_{2-x}Nd_xCuO₄ solid-solution, too.

During pressure release the orthorhombic distortion defined as the difference between the c- and a-axis normalized in respect to the a-axis increases gradually in all the systems [72]. Simultaneously, the basal plane of the octahedra is rotated around the [100] direction. The rotation angle decreases continuously (7 degrees at 8.5 GPa to 3 degrees at 2.5 GPa). Furthermore, the [CuO₆] octahedra are distorted in the sense that the apex oxygen ion is shifted away from the fourfold rotation axis, present in the high pressure phase. All Ln–O distances increase as pressure is lowered which reflects in a certain way the decrease of the octahedra tilt and distortion.

The influence of high pressure on the T'-structure can be understood qualitatively in considering the coordination number of the rare earth ions and the density of the structure. As pressure is applied the density increases and a higher coordination number is favoured. Hence the T' \rightarrow T transition is very likely to occur. The observed increase of $P_{\rm T}$ as t decreases is determined by the Ln–O(2) and O(2)–O(2) interactions which are incorporated in the $P_{\rm T}(t)$ phase diagram of the La_{2-x}Nd_xCuO₄ solid–solution.

Chapter 5

$High-T_c$ superconductors under high pressure

In this chapter the important role of high pressure experiments in the field of high- T_c superconductors is discussed. Pressure–induced shifts in $T_{\rm c}$ helped to synthesized new compounds with higher $T_{\rm c}$ values at ambient pressure (section 5.1) and led C. W. Chu in 1994 to the statement that a maximum of $T_{\rm c}$ between 150 and 180 K may exist in hole–doped high– $T_{\rm c}$ cuprates at ambient pressure [84]. The increase or decrease of T_c under pressure supported the picture of a pressure-induced charge transfer between a charge reservoir and the superconducting CuO₂layers as one ingredient in a model to describe the $T_c(P)$ dependence (section 5.2). High pressure work on a well chosen compound with defined oxygen doping was performed to separate intrinsic and doping effects on T_c and is presented in section 5.3. Undoubtly, uniaxial pressure experiments on various YBa₂Cu₃O_{7- δ} compounds and T_c measurements on optimally doped systems discussed in section 5.4 support the idea, that the pressure dependence of the intrinsic $T_{c,max}$ is a second key parameter to be considered in explaining the $T_{\rm c}(P)$ variation. A pressure-induced charge transfer and a change of $T_{c,max}$ with pressure are incorporated in the model of inequivalent CuO_2 layers to explain the $T_c(P)$ dependencies observed in three and four layered Hgand Tl-based compounds (section 5.5). Other models to describe the pressure-induced changes in $T_{\rm c}$ will be discussed briefly at the end of this chapter. An extended description of the high pressure work in the field of high- T_c superconductors is given by Takahashi and Môri [85] and earlier reviews referred therein.

5.1 Role of pressure in the discovery of high- T_c compounds

Since the discovery of the high- T_c compounds the superconducting transition temperature T_c has risen from $T_c=35$ K in La_{1.85}Ba_{0.15}CuO₄ [1] to $T_c=133$ K in HgBa₂Ca₂Cu₃O_{8+ δ} [2]. In the research for higher T_c values, high pressure experiments played, and are still playing, an essential role. The fact that pressure could increase $T_{\rm c}$ in the La–Ba–Cu–O system from 32 K to $T_{\rm c}=40$ K (at P = 1.3 GPa) [53] triggered the synthesis of new compounds with transition temperatures well above the boiling point of liquid nitrogen. The working horse of solid-state physicists is $YBa_2Cu_3O_{7-\delta}$ [86], a member of the $MBa_2Cu_3O_{7-\delta}$ family (M = La \rightarrow Yb, without Ce, Pm, and Tb [87]). The key features of these orthorhombic compounds are the CuO₂-layers where superconductivity occurs and the CuO-chains along the crystallographic b-axis. The chains act as charge reservoir for the positive charged carriers of the superconducting current. Depending on the oxygen deficiency δ (0 \leq δ < 0.65), and hence, on the charge carrier density $n_{\rm h}$ defined as number of holes per CuO_2 -layer and Cu-atom — the T_c value can be adjusted in a wide temperature range. As was shown by neutron powder diffraction [88] the structural parameters and the Cu–O bond lengths vary smoothly with δ but do not correlate with the $T_{\rm c}(\delta)$ -dependence. Several experiments have established that pressure can enhance or decrease $T_{\rm c}~(-0.5 \le \partial T_{\rm c}/\partial P \le 2~{\rm K/GPa})$ depending on the initial $T_{\rm c}$ value, i. e. the oxygen deficiency [89, 90, 91]. This can be qualitatively understood under the assumption that pressure induces a charge transfer between the CuO-chains and CuO₂-layers.

Soon after the discovery of the MBa₂Cu₃O_{7- δ} compounds thallium—and later mercury—based systems were synthesized [92, 93]. These compounds are built up of alternating block–layers (either TlO– or HgO–layers) and CuO₂–layers as is schematically shown in Fig. 5.1. The former play the role of the charge reservoir as these compounds contain no CuO–chains. The general chemical formulae are Tl_mBa₂Ca_{n-1}Cu_nO_{2n+2+y} and HgBa₂Ca_{n-1}Cu_nO_{2n+2+ δ}, with m=1,2 and n=1-4 the number of block–layers and CuO₂–layers, respectively. In between these block–layers up to four CuO₂–layers are sandwiched. They have different surroundings in the n=3 and 4 layered systems and can thus be distinguished between inner and outer layers. The bilayered (m=2) Tl–compound with three CuO₂–layers held the previous record $T_c=128$ K [94] which has been increased up to $T_c=133$ K by applying 4 GPa [95]. Such a T_c value was then reported at ambient pressure for the Hg–based (n=3) compound HgBa₂Ca₂Cu₃O_{8+ δ} [2]. Its T_c value has been shifted up well beyond 150 K with pressure ($\partial T_c/\partial P \approx 1$ K/GPa), the highest transition temperature observed so far [17, 96, 97, 98, 99].

From the work on Bi– and Tl–based cuprates it was obvious that the number of CuO₂–

Figure 5.1: Schematic representation of the crystal structure of layered high– T_c superconductors. The unit–cell consists of CuO_2 –layers and block–layers which act as charge reservoir. The different surrounding of the CuO_2 –layers in the n=3 and 4 layered compounds leads to a distinction between inner (white) and outer (shaded) layers.

layers per unit-cell has a distinct effect on T_c . Within the same series, i. e. for a given cation-compound (either Tl, Bi or Hg) and a fixed m, T_c increases monotonically with n up to n=3. The $T_c(n)$ dependence reported for the Hg-based copper oxides ($1 \le n \le 7$) confirmed the previously found maximum for T_c at n=3 [100]. However, it might be possible that for still higher n-values, T_c declines asymptotically to a lower but still high value, comparable to the transition temperature of the infinite-layer cuprates [101].

As a demonstration that different high pressure techniques, using diverse pressure transmitting media/conditions do yield reliable results, the pressure–induced changes of $T_{\rm c}$ in YBa₂Cu₄O₈ are mentioned. The structure of this compound is related to that of YBa₂Cu₃O_{7- δ} but contains two CuO–chains. A deviation of the nominal oxygen concentration or oxygen–ordering phenomena do not occur. Many groups have enhanced $T_{\rm c}$ with pressure by more than 30 K and found a maximum of $T_{\rm c}=107$ K at around 8 GPa (for a summary see [102]). This shows that, as long as the examined sample is of the same quality, consistent results will be obtained.

This short overview illustrates the important contributions of high pressure experiments to increase $T_{\rm c}$ at ambient pressure: Each pressure driven increase of $T_{\rm c}$ could be interpreted as a sign that the system under examination is capable reaching higher $T_{\rm c}$ values at ambient pressure if only the system is suitably modified.

5.2 Pressure-induced charge transfer

It is now generally believed that the variation of T_c with the hole concentration follows an almost parabolic function of the hole concentration n_h [103]. As can be seen in Fig. 5.2, below a certain minimum hole concentration $n_h < 0.05$ the compounds are not superconducting and

a metallic ground state is found. Varying the oxygen content or applying pressure, holes can be transferred from a charge reservoir onto the ${\rm CuO_2}$ -layers and $T_{\rm c}$ increases. It reaches the maximum $T_{\rm c,max}$ at an optimal hole concentration $n_{\rm h,max}=0.16$. Further hole transfer will decrease $T_{\rm c}$ and superconductivity vanishes beyond ≈ 0.27 . Then the compounds behave as normal metals. All the compounds with $n_{\rm h} < n_{\rm h,max}$ are said to be underdoped while compounds with $n_{\rm h} > n_{\rm h,max}$ are said to be overdoped. Figure 5.2 is taken from Ref. [104] where p instead of $n_{\rm h}$ was used to denote the hole concentration. These data demonstrate that the onset of superconductivity occurs at the same hole concentration for the various compounds listed in the caption of Fig. 5.2. The solid line is a fit of

$$T_{\rm c} = T_{\rm c,max} \left\{ 1 - \beta [n_{\rm h} - n_{\rm h,max}]^2 \right\}$$
 (5.1)

to the data, with $\beta = 82.6$ and $n_{\rm h,max} = 0.16$ [105]. The idea that a certain charge transfer can be achieved by partial substitution or varying the oxygen deficiency had led to the picture of a pressure–induced charge transfer to explain the pressure effects on $T_{\rm c}$.

Almasan and coworkers [106] measured the $T_{\rm c}(P)$ dependence (P < 2 GPa) for many single crystals of YBa₂Cu₃O_{7- δ} (0 < δ < 0.65) and used eq. (5.1), but pressure was included as independent variable to explain their $\partial T_{\rm c}/\partial P$ data:

$$T_{\rm c}(n_{\rm h}, P) = T_{\rm c,max}(P) \left\{ 1 - \beta [n_{\rm h}(P) - n_{\rm h,max}(P)]^2 \right\}$$
 (5.2)

The analysis of the $T_{\rm c}(n_{\rm h},P)$ data within this phenomenological model led to the conclusion that the increase of $T_{\rm c}$ with pressure is produced not only by a pressure–induced charge transfer between CuO–chains and CuO₂–layers and other mechanisms, that yield a linear $T_{\rm c,max}(P)$ dependence, have to be considered.

Bucher et al. [107] also stated that in YBa₂Cu₃O_{7- δ} obviously another effect than the pressure–induced charge transfer plays an important role for the T_c increase. They applied pressure (P < 1.5 GPa) on polycrystalline samples of YBa₂Cu₃O_{7- δ} ($0 < \delta < 0.5$) and observed a variety of pressure effects systematically changing with δ in the interval 0.03 $< \delta < 0.19$. Within the charge transfer model an increase of the charge carrier density in this doping range ($T_c \approx 90$ K) is not expected to enhance T_c further. The authors correlated the variation of the c-axis parameter with δ and the $\partial T_c/\partial P$ dependence and argued that the strong pressure dependence of T_c (for $\delta = 0.19$) fades away as the c-axis approaches a critical value at $\delta = 0.09$. This observation is qualitatively supported by the pressure–enhanced T_c found in single crystals of YBa₂Cu₃O_{7- δ} [108].

Figure 5.2: Plot of $T_c/T_{c,max}$ against the hole concentration p for $Y_{1-x}Ca_xBa_2Cu_3O_6$ (\square), $La_{2-x}Sr_xCuO_4$ (+), and $La_{2-x}Sr_xCaCu_2O_6$ (\triangle). Also included is $T_c/T_{c,max}$ against the bond valence sum parameter, V_- , for $YBa_2Cu_3O_{7-\delta}$ (\circ), $Y_{1-x}Ca_xBa_2Cu_3O_{7-\delta}$ (\diamond), $YBa_2Cu_3O_{6.93}$ (\bullet), and $YBa_2(Cu_{0.93}Zn_{0.07})_3O_{6.925}$ (filled triangles). The plot is taken from Ref. [104]. The solid line is a fit to the data according to eq. (5.1).

The possibility that oxygen ordering effects could influence the $T_c(P)$ behaviour was mentioned by Kosuge and coworkers [109]. They reported high pressure transport measurements on Pb–based superconductors $Pb_{\frac{1+x}{2}}Cu_{\frac{1-x}{2}}Sr_2Y_{1-x}Ca_xCu_2O_{7+\delta}$ which are structurally similar to YBa₂Cu₃O_{7- δ}. In contrast to the latter compound the Pb-based system exhibits an unusually large charge transfer. The authors proposed a mechanism of pressure-induced delocalization of holes where pressure might enhance oxygen diffusion and thus leads to oxygen rearrangement and a decrease of disorder. Similar assumptions were expressed by other groups which have conducted time consuming experiments to study the oxygen ordering effect. Fietz and collaborators [110] reported a giant pressure effect on T_c in underdoped YBa₂Cu₃O_{7- δ} ($\delta \approx 0.6$) caused by pressure-induced oxygen ordering via oxygen motion between unit-cells. Evidence, that pressure can enhance the degree of oxygen defect ordering, was also obtained in an experiment on $\text{Tl}_2\text{Ba}_2\text{CuO}_{6+\delta}$ [111]. It was shown that in this compound $\partial T_c/\partial P$ changes both its sign and magnitude depending on whether the pressure is changed at high (300 K) or low (55 K) temperature [112]. This can be understood if in response to pressure changes, oxygen defects easily rearrange at higher temperature but are frozen in place at low temperature. Such oxygen ordering effects occur in the CuO-chains (for $\delta > 0$) and are manifested in a dramatic increase

in T_c with time in samples that have been quenched from high temperatures and annealed at room temperature [113].

Also in TlSr₂CaCu₂O_{7- δ} Schilling and coworkers [114] showed that T_c is not a unique function of pressure but rather depends in a complex fashion on the pressure—thermal—time history of the sample. The large annealing effects on TlSr₂CaCu₂O_{7- δ} ($T_c = 79$ K) gave strong evidence that the optimal T_c value is higher than 79 K. Optimizing the oxygen content and partially substituting Pb for Tl and Y for Ca, Liu and coworkers obtained $T_c = 108$ K in Tl_{0.5}Pb_{0.5}Sr₂Ca_{0.8}Y_{0.2}Cu₂O₇ [115].

5.3 Intrinsic pressure effects on T_c

The different effects for a pressure–induced T_c enhancement discussed so far show that systems for a high pressure research should be chosen carefully to separate intrinsic and doping effects on T_c . As already outlined at the end of the last section, T_c in the $Tl_{1-y}Pb_ySr_2Ca_{1-x}Y_xCu_2O_7$ solid–solution can be optimized if y=0.5 and x=0.2 are chosen [115]. Oxygen ordering effects are negligible since the sample is fully oxygenated. The compounds consist of (Tl,Pb)O–layers that act as charge reservoir and a double CuO_2 –layer. In this layers the charge carrier concentration n_h can be simply changed by varying x. Hence, samples which are at different points at the $T_c(n_h)$ curve could be separately studied under high pressure.

We have chosen the compounds $Tl_{0.5}Pb_{0.5}Sr_2Ca_{1-x}Y_xCu_2O_7$ with x = 0, 0.1, 0.2, and 0.35 to investigate $T_c(P)$ up to 20 GPa [116]. The electrical resistance R(T) was measured with the four-point method in a DAC and the pressure was obtained with the Ruby-fluorescence method at temperatures close to T_c . All pressure changes were done at room temperature to avoid as much as possible uniaxial stress. The transition temperatures were deduced from the R(T)-curves and/or their temperature derivatives. The results of the investigations on the four samples are summarized in Fig. 5.3. A single function $T_c(x, P)$ can be used to describe the full pressure and doping range:

$$T_{\rm c}(x,P) = T_{\rm c,max}(P) \left\{ 1 - \beta^{\star}(P) [x - x_{\rm max}(P)]^2 \right\}$$
 (5.3)

In this equation $T_{c,max}(P)$ is the intrinsic pressure dependence of T_c , while $\beta^*(P)$ is the pressure sensitive width of the $T_c(x)$ parabola, and $x_{max}(P)$ is the doping, corresponding to the highest T_c , at a pressure P. This equation is similar to eq. (5.2) but the pressure dependence of the width β^* is explicitly taken into account. The whole $T_c(x, P)$ landscape can be investigated and eq. (5.3) does fit the experimental $T_c(P)$ behaviour for each x [116]. A maximum $T_c = 112$ K

Figure 5.3: Contour plot of $T_c(x, P)$ for the solid-solution $Tl_{0.5}Pb_{0.5}Sr_2Ca_{1-x}Y_xCu_2O_7$ [116]. The maximum T_c which could be reached in this particular system is 112 K. This value can only be achieved under pressure and for an optimal yttrium content x = 0.21.

can be reached only under pressure at an optimal yttrium doping of x = 0.21. In this particular compound the pressure-induced T_c enhancement is intrinsic, i. e. achieved only by $T_{c,max}(P)$.

The pressure dependence of $T_{c,max}(P)$, $\beta^*(P)$, and $x_{max}(P)$ is depicted in Fig. 5.4. The $T_{c,max}(P)$ curve attains a maximum around 8 GPa. The initial slope of $T_{c,max}(P)$ is about 1 K/GPa. This value agrees rather well with that found by Neumeier and Zimmermann [91] who measured the $T_c(P)$ dependence of YBa₂Cu₃O_{6.97} as a function of carrier concentration that has been changed by substituting Ca for Y or La for Ba. Both Y– and Tl–based compounds are structurally related which might explain why the same intrinsic pressure enhancement of T_c is found. Also Kierspel et al. [117] found a value of $\partial T_{c,max}/\partial P = 0.9$ K/GPa in Bi₂Sr₂CaCu₂O_{8+ δ} for in–plane pressure. This points to the crucial role of the CuO₂–layers since they are the only common structural element in these systems. It is noted that Almasan et al. [106] estimated the $\partial T_{c,max}/\partial P$ value at the peak in the $T_c(n_h)$ relation and this had led to an underestimation in their $T_{c,max}(P)$ dependence.

The parameter β^* for the Tl_{0.5}Pb_{0.5}Sr₂Ca_{1-x}Y_xCu₂O₇ system is a monotonically increasing function in pressure. This implies a slight narrowing of the parabola, leading to the interpretation, that T_c is more sensitively dependent on doping as pressure increases. Thus, superconductivity occurs in a narrower doping range. An even more pronounced effect was found in HgBa₂CuO_{4+ δ} [118].

Figure 5.4: The pressure dependence of $T_{\text{c,max}}$, β^* , and x_{max} for the $\text{Tl}_{0.5}\text{Pb}_{0.5}\text{Sr}_2\text{Ca}_{1-x}\text{Y}_x\text{Cu}_2\text{O}_7$ system. The intrinsic pressure dependence of T_{c} is due to $T_{\text{c,max}}(P)$. For the definition of β^* and x_{max} see text.

In principle the parameter $x_{\rm max}$ comprises two contributions. Firstly, the effect of doping by Y and Pb and oxygen deficiency. There is practically no oxygen deficiency and its doping can be ignored. Secondly, the ambient pressure maximum in the $T_{\rm c}(n_{\rm h})$ curve is not at $n_{\rm h}=n_{\rm h,max}=0.16$. These two parts could not be separated in this experiment. But it is clear from Fig. 5.4 that, in ${\rm Tl}_{0.5}{\rm Pb}_{0.5}{\rm Sr}_2{\rm Ca}_{1-x}{\rm Y}_x{\rm Cu}_2{\rm O}_7$ a pressure–induced charge transfer does not play an important role and the $T_{\rm c}$ enhancement is largely determined by other effects. A tentative explanation should consider in detail the different nature of the charge reservoir layer, i. e. (Tl,Pb)O–layer versus CuO–chains.

The correlation between $T_c(n_h)$ and $T_c(P)$ is very striking in underdoped compounds where large $\partial T_c/\partial P$ values are correlated with large $\partial T_c/\partial n_h$ values. Gugenberger et al. [119] argued that in La_{2-x}Sr_xCuO₄ ($x=0.1,\ 0.15,\$ and 0.2) other mechanisms than a pressure–induced charge transfer should be considered to explain the $T_c(P)$ dependence since, in this structure, no charge reservoir exists. These authors performed uniaxial pressure experiments to determine the pressure dependence of T_c along the crystal directions. The uniaxial stress dependencies of

 $T_{\rm c}$ turned out to be largely anisotropic and almost no effect was found for hydrostatic conditions. Such experiments provide further evidence for other, intrinsic effects on $T_{\rm c}(P)$. The results of uniaxial pressure experiments will be discussed in the following section.

5.4 Uniaxial pressure dependence of T_c

In the preceding section, the influence of (quasi)hydrostatic pressure on the superconducting transition temperature was discussed and separated in intrinsic and doping related pressure effects on T_c . Now the dependence of T_c on uniaxial pressure, determined by thermal—expansion measurements is discussed. These results will show that the in–plane compression is important for $T_c(P)$.

Using an ultrahigh–resolution capacitance dilatometer, Meingast and coworkers [120] observed in untwinned YBa₂Cu₃O_{7- δ} at $T_c = 90.9$ K ($\delta \approx 0$) highly anisotropic jumps of the expansivities in the a-b plane (i. e. parallel to the CuO₂-layers). The magnitude of the expansivity jumps give via the Ehrenfest relation (see eq. (3.12)) the first–order uniaxial pressure dependence of T_c , $\partial T_c/\partial P_i$ (i=a,b,c). The values $\partial T_c/\partial P_a = -1.9$ K/GPa and $\partial T_c/\partial P_b = 2.2$ K/GPa indicate that uniaxial pressure along the respective axis has an opposite effect. Along the c-axis no change of T_c was observed ($\partial T_c/\partial P_c \approx 0$ K/GPa) like in Bi₂Sr₂CaCu₂O_{8+ δ} [117]. These values have been confirmed by direct measurements of $\partial T_c/\partial P_i$ as a function of uniaxial stress for an untwinned YBa₂Cu₃O_{7- δ} crystal ($T_c = 91.5$ K) by Welp et~al. [121]. In hydrostatic conditions the pressure effects perpendicular to the c-axis almost cancel each other and result in a small $\partial T_c/\partial P = 0.3$ K/GPa value, observed by many groups (see e. g. the review by Schilling and Klotz [102]).

A rather different behaviour is found in $\text{La}_{2-x}\text{Sr}_x\text{CuO}_4$ [119], where $\partial T_c/\partial P_c$ is always negative and between -7 and -14 K/GPa, depending on x. Along the a- and b-axis large positive but different values were obtained for the pressure derivative of T_c . This difference is probably due to the lack of a charge reservoir from which charge can be transferred to the $\text{CuO}_2-\text{layers}$ as pressure is applied. Therefore, other intrinsic effects are responsible for the $T_c(P)$ dependence and might be related with the $\text{CuO}_2-\text{layers}$. This argumentation is supported by experiments performed by Locquet et al. [122] who used epitaxial strain in a thin film (15 nm) of $\text{La}_{1.9}\text{Sr}_{0.1}\text{CuO}_4$ (bulk $T_c=25$ K), and shifted T_c up to 49 K. An identical film grown under tensile stress had only $T_c=10$ K. The authors ruled out that changes in the charge carrier concentration caused the high value of T_c which is significantly higher than the maximum in the solid–solution of $\text{La}_{2-x}\text{Sr}_x\text{CuO}_4$ (x=0.16, $T_c=37$ K) and raised the question whether T_c of other compounds

can be increased under compressive strain.

To elucidate the influence of the oxygen content on $\partial T_c/\partial P_i$ Kraut and coworkers [123] performed thermal–expansion measurements on untwinned YBa₂Cu₃O_{7- δ} crystals (0.06 $\leq \delta \leq$ 0.46). They found a positive value for $\partial T_c/\partial P_b$ (3 K/GPa) which is almost oxygen–content independent, except for $\delta = 0.27$ where the large value $\partial T_c/\partial P_b = 5$ K/GPa was observed. Along the a-axis a negative value $\partial T_c/\partial P_a = -2$ K/GPa was found except for $\delta = 0.27$ ($\partial T_c/\partial P_a = +2$ K/GPa). $\partial T_c/\partial P_c$ is slightly negative ($\delta < 0.1$) but increases strongly up to 4 K/GPa at $\delta = 0.37$. The $\partial T_c/\partial P$ versus δ dependence, obtained in summing up all uniaxial terms agrees well with hydrostatic pressure experiments [107, 108] but with the important difference that oxygen ordering effects can be ruled out since the data were obtained without applying pressure.

The $\partial T_{\rm c}/\partial P$ versus δ dependence supports quite nicely the model of a pressure-induced charge transfer. At the maximum of the $T_{\rm c}(\delta)$ dependence, i. e. at optimal doping, the pressure enhanced increase of $T_{\rm c}$ along the c-axis is zero. Towards underdoped (overdoped) the positive (negative) values of $\partial T_{\rm c}/\partial P_c$ are expected within this model, according to eq. (5.1). However, in this framework the large uniaxial-pressure effect along the a- and b-axis, even at optimal doping, cannot be explained. Furthermore, the almost doping independent $\partial T_{\rm c}/\partial P_a$ and $\partial T_{\rm c}/\partial P_b$ values (except for $\delta=0.27$) raise the question about the pressure effects besides the charge transfer, responsible for the $T_{\rm c}$ enhancement. Kraut et al. [123] suggest that the orthorhombic distortion plays a key role in the determination of $T_{\rm c}$ and the $\partial T_{\rm c}/\partial P_i$ should be regarded as the "intrinsic" pressure dependence of $T_{\rm c}$ where the pressure dependence of the electronic structure and pairing mechanism are incorporated.

An argument backing this idea is provided by the enhancement of T_c with the decrease of the orthorhombic distortion in MBa₂Cu₃O_{7- δ} either with pressure for a given M, or with increasing radius of the rare–earth ion [124]. For the former case Pickett [125] concluded from *ab initio* calculations on uniaxially strained YBa₂Cu₃O₇ that increasing T_c by internal strain is related to a decrease in orthorhombicity which then increases the charge carrier concentration in the CuO₂–layers. The latter case goes in line with the increase of the c-axis of the MBa₂Cu₃O_{7- δ} structure if the ionic radius of the rare–earth elements increases [87]. Thus, the highest T_c values should be found in Pr and La compounds. Zou and coworkers [126] reported bulk–superconductivity in oxygen annealed PrBa₂Cu₃O_x crystals with $T_c = 85$ K. This value is yet not higher than that reported in NdBa₂Cu₃O₇, but might be enhanced as soon as the preparation methods have been optimized. That PrBa₂Cu₃O_x has the potential for higher T_c values was shown by Ye *et al.* [127]

who achieved a pressure–induced $T_{\rm c}$ of 106 K at 8 GPa. Furthermore, Tallon and Flower [128] presented evidence that stoichiometric LaBa₂Cu₃O₇ should have a $T_{\rm c,max}\approx 100$ K. Motivated by this prediction Lindemer *et al.* [129] found $T_{\rm c}=96$ K in La_{1+z}Ba_{2-z}Cu₃O_y (0.1 $\leq z \leq$ 0.2) which is higher than that reported in stoichiometric LaBa₂Cu₃O₇ ($T_{\rm c}=80$ K) [130].

Until now the large anisotropy and the positive values for $\partial T_c/\partial P$ found in YBa₂Cu₄O₈ remain unexplained. Meingast and coworkers [131] reported the values $\partial T_c/\partial P_i = 3.7 - 5.0$, 0.3 – 0.4, and 0 ± 0.7 K/GPa along the a–, b–, and c–axis, respectively. Hence, the large $\partial T_c/\partial P = 5.5$ K/GPa value [132, 133] results mainly from the large uniaxial pressure dependence of T_c along the a–axis, i. e. perpendicular to the CuO–chains. Since YBa₂Cu₄O₈ is slightly underdoped the negligible pressure effect along the c–axis does not disprove a pressure-induced charge transfer. It is noted that the linear axis compressibilities of YBa₂Cu₃O_{7- δ} and YBa₂Cu₄O₈ are quite different [134] and could cause the difference in the absolute values $\partial T_c/\partial P_i$ in both systems, but this will not explain the different sign. The observed T_c enhancement is thus caused by other effects than charge transfer. On the other hand, Wijngaarden and coworkers [135, 136] deduced from the upper critical field $H_{c2}(P)$ and the $T_c(P)$ measurement a significant pressure–induced charge transfer in YBa₂Cu₄O₈ but stated an increase of $T_{c,max}$ as well to explain the initial pressure dependence of T_c [133].

Hints for a charge carrier redistribution between copper and oxygen ions in the conducting ${\rm CuO_2}$ -layers were deduced from the non-linear Raman-shift of the Cu-phonon mode in ${\rm YBa_2Cu_4O_8}$ under pressure [137]. Watanabe and coworkers [138] however, correlated the non-linear pressure dependence of ${\rm CuO_2}$ -layer oxygen mode frequency with the $T_{\rm c}(P)$ dependence. Earlier Raman experiments on poly- and single crystalline ${\rm YBa_2Cu_4O_8}$ under hydrostatic pressure conditions [34] revealed a non-linear increase of the chain-oxygen mode frequency which led to a rather large mode-Grüneisen parameter. The volume dependence of this phonon frequency correlates nicely with the $T_{\rm c}(V)$ data of Ref. [133]. These light scattering experiments show that the oxygen mode frequencies are strongly affected by pressure but at the present it is not clear if this is caused only by a pressure-induced charge transfer.

5.5 Inequivalent CuO₂-layers in Tl- and Hg-based compounds

So far, pressure effects on high– T_c compounds with two CuO₂–layers have been discussed. These two layers have equal surroundings (see Fig. 5.1). This is not longer the case in the HgBa₂Ca_{n-1}Cu_nO_{2n+2+ δ} and Tl₂Ba₂Ca_{n-1}Cu_nO_{2n+4+ δ} compounds with n=3 and 4 CuO₂–layers. Here a distinction between inner and outer CuO₂–layers has to be made. As was shown

Figure 5.5: (a) Possible charge distribution $n_{\rm h}$ as function of the total charge δ transferred between inner and outer ${\rm CuO_2}$ -layers in n=3 and 4 layered compounds. (b) $T_{\rm c}/T_{\rm c,max}$ versus $n_{\rm h}$ according to eq. (5.1). (c) the intrinsic $T_{\rm c}/T_{\rm c,max}(\delta)$ dependence of the inequivalent ${\rm CuO_2}$ -layers. The indicated paths show that a given δ results in different intrinsic $T_{\rm c}/T_{\rm c,max}$ values. Assuming, that δ increases linearly with pressure, a pressure axis can be used instead of the δ -axis. The figure is taken from Ref. [17].

in Fig. 5.1, the inner layers are sandwiched between the outer CuO_2 -layers whereas those are adjacent to one inner CuO_2 -layer and one block-layer (either HgO- or TlO-block-layer). As a consequence of these different surroundings the transferred charge from the block-layers may distribute non-homogeneously onto the inner and outer CuO_2 -layers. This effect is accounted for in a model developed by Haines and Tallon [139]. Their model is based on the assumption that each CuO_2 -layer can be considered as a superconducting unit with an inherent T_c that depends on the corresponding charge carrier density n_h given by eq. (5.1). Minimizing the total energy $U_{\text{tot}} = U_{\text{band}} + U_{\text{Mad}}$ of the charge carriers, with U_{band} the kinetic energy of the non-interacting holes and U_{Mad} the Madelung energy, the charge distribution among the CuO_2 -layers is found. In this pure ionic model U_{band} is given by

$$U_{\text{band}} = \frac{\pi\hbar^2}{2m^*a^2}n_{\text{h}}^2 \quad , \tag{5.4}$$

where a is the lattice parameter of the (almost quadratic) CuO_2 -layer and m^* the effective mass.

If the total doping induced by the block–layers is δ , a fraction $\frac{1}{2}(1-x)$ is distributed to each of the outer CuO_2 –layers. For n=3, a fraction x stays on the single inner CuO_2 –layer while for n=4 a fraction $\frac{1}{2}x$ is transferred to each of both inner CuO_2 –layers. Substituting these definitions into eq. (5.4) leads to

$$U_{\text{band}} = \frac{\pi\hbar^2}{2m^*a^2}\delta^2\left(\varphi x^2 - x + \frac{1}{2}\right) \quad , \tag{5.5}$$

with $\varphi = \frac{3}{2}$ for n = 3 and $\varphi = 1$ for n = 4.

The Madelung energy $U_{\rm Mad}$ takes all other charges not considered in eq. (5.4), the distribution of charges between copper and oxygen sites in the ${\rm CuO_2}$ -layers, and the crystal structure into account [140]. The charge distribution among the ${\rm CuO_2}$ -layers can now be found by minimizing $U_{\rm tot}$ with respect to x. This gives a rather complicated $x(\delta)$ dependence, but the pressure—induced charge distribution is in principle possible [141, 142].

In Fig. 5.5 we propose a possible charge distribution and its consequence on T_c in a schematic picture for a compound with three CuO_2 -layers [17]. The charge carrier density n_h of inner and outer CuO_2 -layer(s) is a linear function in δ but with different slopes (Fig. 5.5(a)). Assuming a parabolic $T_{\rm c}/T_{\rm c,max}(n_{\rm h})$ behaviour as in eq. (5.1) and plotted in Fig. 5.5(b), the intrinsic $T_{\rm c}/T_{\rm c,max}$ of each CuO₂-layer follows immediately (Fig. 5.5(c)). The δ -axis can be replaced by a pressure scale because experimental evidence exists that δ increases linearly with pressure [136]. Under pressure the total amount of transferred charge δ and hence $T_{\rm c}$ will increase. The resultant T_c will be the maximum of the two $T_c/T_{c,\text{max}}(\delta)$ curves of Fig. 5.5(c). Such a behaviour is quite different from that observed in the n=2 layered compounds as was discussed in the preceding sections. We used this model of a non-uniform charge distribution to give a qualitative explanation of the $T_c(P)$ dependence of $HgBa_2Ca_2Cu_3O_{8+\delta}$ and $HgBa_2Ca_3Cu_4O_{10+\delta}$ measured up to 30 GPa [17]. The n=3 compound holds the record ambient pressure T_c value of 133 K [2] which was shifted up enormously by several groups [17, 96, 97, 98, 143]. Despite the large spread in the maximum T_c reached under pressure all experiments yield almost the same initial pressure increase of T_c ($\partial T_c/\partial P \approx 2$ K/GPa). In this particular case, a pressure-induced enhancement of $T_{\rm c}$ cooperates with the charge transfer leading to the highest- $T_{\rm c,max}$ values reached for any superconductor so far.

A nice example for this model are the $T_c(P)$ data obtained in the n=3 and 4 layered $Tl_2Ba_2Ca_2Cu_3O_{10+\delta}$ and $Tl_2Ba_2Ca_3Cu_4O_{10+\delta}$ [142] reported in Fig. 5.6. For both compounds T_c as a function of pressure first follows one parabola and then a second parabola. At low pressure T_c is determined by the inherent T_c of the outer CuO_2 -layers while at higher pressure the T_c behaviour of the inner CuO_2 -layer(s) dominate(s). The different widths of the parabola

Figure 5.6: Pressure dependence of T_c in the n=3 and 4 layered Tl-based compounds $Tl_2Ba_2Ca_2Cu_3O_{10+\delta}$ and $Tl_2Ba_2Ca_3Cu_4O_{10+\delta}$ (from Ref. [141]). Each $T_c(P)$ dependence is described by two parabola according to a non-homogeneous charge distribution on inequivalent CuO_2 -layers (see text). For the n=3 (n=4) compound $T_c(P)$ follows the second parabola above 12 (10) GPa.

reflect the different slopes of the $n_h(\delta)$ (or $n_h(P)$) dependence shown in Fig. 5.5(a).

5.6 Other models to explain pressure–induced changes in T_c

Until now no microscopic model for the high– T_c superconductivity has been proposed. Thus, no microscopic arguments can be given for a pressure dependent intrinsic T_c , labelled $T_{c,\text{max}}$ in the preceding sections. In the following, other models proposed to explain $T_c(P)$ dependencies will be mentioned briefly.

Acha and coworker [144] showed that the change of the proximity effect induced by the decrease of the distance between CuO_2 -layers can account for the increase in T_c . This leads to a pressure–induced T_c enhancement, even if the samples are overdoped. These authors regarded the superconductor as a multilayer of superconducting and non–superconducting layers, i. e. CuO_2 - and block–layers as shown in Fig. 5.1 and calculated the T_c of such an arrangement in the Cooper–Werthammer–de Gennes model for proximity coupling. In this model, the large T_c increase in $HgBa_2Ca_2Cu_3O_{8+\delta}$ is then just the result of an inhomogeneous compression of the two kinds of layers. However, the enlarged proximity coupling due to pressure cannot be the only

reason for a pressure dependent $T_{c,\text{max}}$, as was pointed out recently by Wijngaarden *et al.* [145]. They argue that increasing the thickness ratio of superconducting and non–superconducting layers, resulting in higher T_c values in HgBa₂Ca_{n-1}Cu_nO_{2n+2+ δ} for various n at ambient pressure, does not agree with the pressure–enhanced T_c found in HgBa₂Ca₂Cu₃O_{8+ δ}.

Jansen and Block [146, 147] have undertaken a quantitative elucidation of the $T_c(P)$ dependence of Tl– and Hg–based superconductors. They propose an indirect–exchange mechanism of Cooper–pair formation via closed–shell oxygen (O^{2-}) in a s–wave BCS formalism. In their formalism a pressure enhancement of T_c is obtained even at optimal doping where the pressure–induced charge transfer cannot be responsible for an increase of T_c . Furthermore, these authors conclude from their expressions that a pressure–induced charge transfer is negligible at low pressure, and thus the intrinsic pressure effect must be held responsible for the large initial slope observed. The experimental $T_c(P)$ data of $Tl_2Ba_2Ca_{n-1}Cu_nO_{2n+4+\delta}$ and $HgBa_2Ca_{n-1}Cu_nO_{2n+2+\delta}$ for n=1-3 as well as $La_{2-x}Sr_xCuO_4$ are quantitatively reproduced and are due to two–dimensional characteristics of superconductivity in these systems.

Despite this excellent agreement between measured and calculated $T_c(P)$ dependence other charge carriers than 'bare' electrons may form Cooper-pairs. An increasing number of experiments have shown that polaronic charge carriers are present in the normal state of high- T_c superconductors. As was concluded by Zhao and coworkers [148] from their study of the isotopedependence of the diamagnetic signal in $\text{La}_{2-x}\text{Sr}_x\text{CuO}_4$, these bare charge carriers are accompanied by local lattice distortion (Jahn-Teller polaron) and condense by an unknown pairing mechanism into supercarriers.

With these considerations a qualitative description for the $T_c(P)$ behaviour can be given. Pressure approaches the block-layers and the CuO_2 -layers and the charge carrier density in the latter increases. In the case of an underdoped sample, T_c will increase whereas for an over-doped sample T_c will decrease. Simultaneously, intrinsic effects like the Cooper-pair formation mediated by indirect exchange between unpaired electrons on neighboring paramagnetic cations (Cu^{2+}) via closed-shell oxygen (O^{2-}) could enhance T_c , at least at low pressure. The observed T_c is finally determined by the sum of these effects.

Chapter 6

Strongly correlated f—electron systems

In the last two decades HF compounds were subject of intensive studies. These materials containing 4f- or 5f-elements show low temperature properties which can be most often well described within the FL theory, briefly presented in the first section of this chapter. The class of these materials consists mainly of Ce- and U-based compounds, but also some Yb-based materials exhibit these fascinating properties. The magnetic moments of the 4f- or 5f-ions can interact with the spin of the conduction band electrons and play an essential role in the magnetic and quadrupolar order observed at low temperature. On the other hand, this interaction can also build a singlet state of the localized magnetic moments and the spin of the conduction electrons. Section 6.2 is devoted to the competition between long-range magnetic order and a non-magnetic ground state.

A breakdown of the long-range magnetic order can be achieved by tuning a control parameter, such as the concentration x of a non-magnetic substitute or hydrostatic pressure to a critical value. At x_c or P_c the magnetic ordering temperature scales to zero (section 6.3) and some physical properties exhibit a weak power law or logarithmic divergence in temperature, which are striking deviations from the predictions of FL theory. These observations found in several non-stoichiometric compounds suggest the existence of a critical point at T=0 K, also called zero-temperature quantum phase transition. Section 6.4 describes briefly different possible mechanisms which are thought to produce such a departure from the FL picture close to the magnetic instability. Furthermore, examples for such a behaviour induced by pressure on stoichiometric and single crystalline compounds investigated in our laboratory are presented. Close to the critical point of these systems the anomalous behaviour persists down to very low

temperature (several 10 mK) and raises the question about the decomposition of the residual resistivity ρ_0 in a static disorder part and a part which is related to electronic correlations. This follows from the pressure variation of ρ_0 described in section 6.5. The increasing interest in these compounds is also associated with the unconventional superconductivity found in some of them in the vicinity of the magnetic instability. Section 6.6 is devoted to the HF superconductors and emphasize is put on the lately discovered compounds showing pressure—induced superconductivity.

6.1 Some characteristics of heavy–fermion compounds

In normal metals the motion of the electrons is well described within the Sommerfeld model [149]. The electrons are considered as free, non-interacting particles, i. e. the electron-electron interaction via Coulomb forces as well as the interaction with the lattice are neglected. Only external fields determine the electron motion in this free electron gas. In extension to this model, the Coulomb interaction between the electrons is included. Thus, the ensemble of the electrons can be regarded as a liquid rather than a gas. This leads to a one-to-one correspondence between the electron states and the new quasi-particle states of the (normal) FL. The free electron gas ideas however, require only small modifications if properties of the FL are calculated. In other words, certain parameters are renormalized. For example, the specific heat $C_V(T)$ and the spin susceptibility $\chi(T)$ are [150]

$$C_V = \gamma T = \frac{m^*}{m} \gamma^{(0)} T \tag{6.1}$$

$$\chi = \frac{m^*/m}{1 + F_0^a} \chi^{(0)} (6.2)$$

In these equations the bare and effective electron mass are denoted by m and m^* , respectively, and F_0^a characterizes the interaction of the quasi-particles. The quantities of zero order correspond to those of the electron gas. The Sommerfeld coefficient γ is given by

$$\gamma = \frac{\pi^2}{3} k_{\rm B}^2 N(E_{\rm F}) = \frac{1}{3} \left(\frac{k_{\rm B}}{\hbar}\right)^2 k_{\rm F} m^*$$
 (6.3)

with $k_{\rm F}$ the Fermi wave number and $N(E_{\rm F})$ the quasi-particle density of state at $E_{\rm F}$. The almost temperature independent Pauli-susceptibility $\chi =: \chi^{(0)}$ is

$$\chi = \mu_0 \mu_{\rm B}^2 N(E_{\rm F}) \tag{6.4}$$

with the permeability μ_0 and the Bohr magneton μ_B . The concept of FL was introduced by Landau to explain the low temperature properties of ³He but is successfully used to describe HF systems, i. e. systems of strongly correlated electrons.

A huge value of the Sommerfeld coefficient γ is found in CeCu₆, the prototype of a non-magnetic FL system. Below T=500 mK, $\gamma=1.53$ J/molK² [151] is very large in comparison to the value of a normal metal like Cu ($\gamma=0.7$ mJ/molK²) and is interpreted as an enhanced density of state at $E_{\rm F}$ (middle part of eq. (6.3)). In the picture of the FL the effective mass is enormously enhanced (right hand side of eq. (6.3)). A prove of a large effective mass was obtained by de Haas-van Alphen oscillation measurements. For example, in CeRu₂Si₂, another intensively investigated non-magnetic HF compound, $m^*=120m_0$ was found [152].

HF systems show a Curie–Weiss susceptibility of localized moments at high temperature and for some of them a signature in $\chi(T)$ at low temperature indicates the entrance into a magnetically ordered state. For other HF compounds, $\chi(T)$ does not show any sign of long–range magnetic order but at low temperature it is larger than for a simple metal. The enhancement of $\chi(T)$ points to a large value of $N(E_{\rm F})$ (see eq. (6.4)). Similar to simple metals, the magnetic susceptibility is proportional to the specific heat and the ratio of these two quantities defines the Wilson–Ratio

$$R = \frac{\chi}{\gamma} \frac{\pi^2 k_{\rm B}}{\mu_0 \mu_{\rm eff}^2} \tag{6.5}$$

with $\mu_{\text{eff}}^2 = g^2 \mu_{\text{B}}^2 J(J+1)$, where g is the Landé factor and J the angular quantum number. In the case of free electrons the Wilson–Ratio is equal to one but for the HF systems, values in the range 2 < R < 5 are found [153]. This deviation can be accounted for in the FL theory.

Another easily measurable property is the electrical resistivity $\rho(T)$ which shows for HF systems a characteristic temperature dependence at very low temperature (usually for T < 1 K). It is observed that $\Delta \rho(T) =: \rho(T) - \rho_0 = AT^2$, with ρ_0 the residual resistivity and a parameter A [154] that measures the scattering of quasi–particles among themselves in analogy to the electron–electron scattering $\rho_{\rm el-el} \propto (T/T_{\rm F})^2$ in normal metals. But in the latter case, the contribution $\rho_{\rm el-el}$ can be normally neglected since $T_{\rm F} \approx 10^4$ K. In HF systems however, $T_{\rm F}$ is much reduced and the T^2 dependence is observed well below a coherence temperature $T_{\rm coh}$ of the order of up to several 10 K, making quasi–particle scattering a considerable contribution in $\rho(T)$ at low temperature. Such a temperature dependence is found in many compounds and is expressed by the Kadowaki–Woods relation $A \propto \gamma^2$ [155]. This relation is supported by the observation $\sqrt{A} \propto 1/T_{\rm coh}$.

The first HF superconductor, $CeCu_2Si_2$ with $T_c = 650$ mK, was found in 1979 by Steglich and coworkers [3]. Upon cooling, heavy quasi-particles ($m^* = 300m_0$) are formed below 20 K and from the jump in specific heat at T_c it is concluded that the Cooper-pairs consist of these quasi-particles [156]. In contrast to normal BCS superconductors, where a small concentration

of magnetic impurities produces pair-breaking, magnetic correlations seem to be necessary for superconductivity in a HF compound. Several years later Jaccard and coworkers [10] found pressure-induced superconductivity in CeCu₂Ge₂, that orders antiferromagnetically at ambient pressure ($T_{\rm N}=4.1~{\rm K}$). Pressure decreases $T_{\rm N}$ and close to the magnetic instability (at $P\approx 9.4~{\rm GPa}$) superconductivity emerges. This observation revealed that short-range magnetic correlations might play an important role on the brink of superconductivity.

A long-range magnetic order can also be induced in the above mentioned compounds $CeCu_6$ and $CeRu_2Si_2$ if Cu is partially substituted by Au and Si is replaced by Ge. In the solid-solutions $CeCu_{6-x}Au_x$ and $CeRu_2(Si_{1-x}Ge_x)_2$ AFM order occurs at the critical concentration $x_c = 0.1$ [157] and 0.05–0.07 [158], respectively. This shows that an increase of the unit-cell volume (smaller atoms are replaced by larger ones) favours magnetic order. As was already mentioned in the context of the pressure experiments on $CeCu_2Ge_2$, a volume compression suppresses magnetism. In this sense, x and P are control parameters to tune the system between the magnetic and non-magnetic phases. A qualitative description for this gives the Doniach phase diagram, presented in the following section.

6.2 Exchange interaction and Doniach phase diagram

In his original work Kondo [159] described the properties of a single spin-1/2 magnetic impurity in a non-magnetic metallic host. He found an effective exchange interaction J between the conduction band electrons and the localized electrons. It is caused by the hybridization of the wavefunction of the localized electron and that of the conduction band electron and further due to the intra-atomic Coulomb interaction at the impurity. As a consequence, $N(E_{\rm F})$ is enhanced at low temperature, and the temperature scale is determined by the Kondo-temperature $T_{\rm K}$:

$$T_{\rm K} \propto \exp(-1/N(E_{\rm F})J)$$
 (6.6)

For $T \ll T_{\rm K}$, the magnetic moment of the impurity will be screened by the conduction electrons, i. e. they are quasi-bound antiferromagnetically to the local moment, forming a magnetic singlet ground state. Furthermore, a many-body Abrikosov-Suhl resonance of width $k_{\rm B}T_{\rm K} \ll \Delta$ and height $1/\Delta$ (Δ the Anderson width of the bare f-electron level well below $E_{\rm F}$) occurs in the density of state near $E_{\rm F}$ [156]. Resonance scattering close to $T_{\rm K}$ gives rise to the logarithmic increase in $\rho(T)$, observed as the temperature is lowered. It is noted that the density of state considered here $(N(E_{\rm F}) \propto 1/\Delta)$ is not the quasi-particle density of state that is used in FL theory to express thermodynamic quantities (see section 6.1). In the latter case heavy-mass

Figure 6.1: Temperature dependence of the electrical resistivity $\rho(T)$ of CeCu₆ [160] and LaCu₆ [161]. CeCu₆ shows the features of a HF compound and LaCu₆ behaves like a simple metal.

quasi-particles dominate the thermodynamic (low temperature) properties completely since the screening involves low-lying particle-hole excitations, hence $N(E_{\rm F}) \propto 1/k_{\rm B}T_{\rm K}$.

In this simple picture some observations are qualitatively explained, but it fails to explain the strong decrease of $\rho(T)$ found at low temperature. Such a behaviour of a lattice of 4f– or 5f–ions (Kondo lattice) is discussed in literature in terms of the entrance in a coherent scattering regime. At low temperature, coherence among the valence and spin fluctuations on different sites must occur in HF systems without any cooperative phase transition down to very low temperature.

The typical features of a HF compound in the electrical resistivity are depicted in Fig. 6.1 with the example of non-magnetic CeCu₆. Below room temperature $\rho(T)$ is large and almost temperature independent. In this temperature range, scattering on crystal field excitations contribute largely to $\rho(T)$. The logarithmic increase of $\rho(T)$ occurs towards low temperature and the maximum around ≈ 10 K is related to the Kondo effect ($T_{\rm K} = 6.2$ K). The onset of coherence is the origin for the strong decrease of $\rho(T)$ towards lower temperature. Below 200 mK the above mentioned $\Delta \rho(T) \propto T^2$ -dependence indicates the FL nature of CeCu₆. Its Lasubstituted counterpart, LaCu₆ however, exhibits a $\rho(T)$ similar to a simple metal, where $\rho(T)$ is determined by phonons and static disorder defects. This demonstrates that the local moments of the Ce-sublattice are responsible for the anomaly in $\rho(T)$ and other physical properties

(e. g. $C_V(T)$ and $\chi(T)$) [162].

In a Kondo lattice, i. e. a lattice with 10^{23} magnetic impurities, the magnetic moments at the f-sites can interact with each other via a spin polarization of the conduction electrons, induced by the local moments themselves. This means that in such a periodic lattice of Kondo impurities, the exchange interaction J is now responsible for coupling local moments through the Ruderman-Kittel-Kasuya-Yoshida (RKKY) interaction (measured by $T_{\rm RKKY}$) to produce AFM order at a Néel temperature [163]

$$T_{\rm N} \propto T_{\rm RKKY} \propto J^2 N(E_{\rm F})$$
 (6.7)

In eqs. (6.6) and (6.7) the same exchange interaction occurs and can lead either to non–magnetic singlets or to long–range magnetic order in compounds containing 4f– or 5f–elements with local moments. This raises the possibility of a competition of these two phenomena for the ground state.

Considering the absolute value of J in eqs. (6.6) and (6.7) makes a crude classification of the HF systems possible (see Fig. 6.2). For small values of J the RKKY interaction dominates and the system orders magnetically. As J exceeds a critical value J_c , a Kondo compensation of the local moments should dominate the RKKY interaction. The long–range magnetic order should be suppressed. This argumentation is supported theoretically by the work of Doniach [164] who considered the competition between RKKY and Kondo interaction in a one–dimensional Kondo lattice. The Doniach phase diagram in Fig. 6.2 is experimentally verified by many measurements. Starting with a Ce–based magnetic material and tuning J towards larger values, for example by pressure, the non–magnetic phase can be reached. As soon as the non–magnetic region is reached the FL behaviour is manifested below a temperature $T_{\rm FL}$, for example by values than J_c , pressure decreases J and the magnetic phase will be reached at high pressure and the FL properties are lost.

Since several years, transport, thermal, and magnetic measurements on several HF compounds have revealed anomalous low temperature properties, that present pronounced deviations from the predictions of FL theory. These new phenomena are therefore summarized under the label NFL behaviour [165]. A certain consensus seems to be established that these features occur in a region around J_c , indicated by the vertical lines in Fig. 6.2. Consequently the proximity of the magnetic instability seems to play a key role for the unusual low temperature behaviour, predominately observed in chemically substituted, i. e. disordered rare earth and actinide alloys. Evidence for a departure of FL behaviour close to the magnetic instability

Figure 6.2: Kondo temperature $T_{\rm K}$ and the RKKY interaction, measured by $T_{\rm RKKY}$, as a function of the exchange interaction J. The magnetic ordering temperature $T_{\rm ord}$ scales to zero as J approaches a critical value $J_{\rm c}$. In a region around $J_{\rm c}$ (indicated by the vertical lines) anomalous low temperature properties are observed in some HF compounds. However, many other HF systems reveal a FL behaviour, for example in electrical resistivity, in the non–magnetic phase below a temperature $T_{\rm FL}$.

in stoichiometric compounds, with as low as possible disorder, was found by resistivity measurements under pressure by several groups (see Ref. [35] and references therein). This kind of experiments will be the subject of section 6.4. In the following we would like to demonstrate that volume compression of initially magnetic Ce-compounds or non-magnetic Yb-systems changes the electronic properties in such a way that the respective other phase in the Doniach phase diagram is reached at high pressure. Many other systems confirmed qualitatively the Doniach diagram and for more details the reader is referred to the reviews by Brandt and Moschchalkov [166], Grewe and Steglich [156], Bauer [167], and Thompson and Lawrence [168].

6.3 From magnetism to heavy-fermion behaviour and vice versa

The Doniach phase diagram discussed in the preceding section can also be used to describe the solid-solutions $\text{CeRu}_2(\text{Si}_{1-x}\text{Ge}_x)_2$ and $\text{CeCu}_{6-x}\text{Au}_x$, where alloying experiments tuned the HF compounds (x=0) into magnetically ordered compounds (x=1). The interpretation of the results of such experiments has always to account for disorder effects, introduced via the nonstoichiometry. Applying pressure on a stoichiometric and single crystalline compound, that shows long—range magnetic order, offers the possibility to drive the system towards the magnetic instability. At first sight these results can then be discussed on a basis, where disorder plays a minor role.

As a first example, pressure experiments on CeRu₂Ge₂ will be discussed. This compound is now subject of several investigations [158, 169, 170] and almost at the same time as we have presented the (T, P) diagram [171], Kobayashi et al. [172] published a similar phase diagram. CeRu₂Ge₂ has a FM groundstate [173] and the Kondo effect is negligible [174]. A more specific feature of CeRu₂Ge₂ is the strong competition between AFM and FM couplings $(T_N = 8.5 \text{ K} \text{ and } T_C = 7.4 \text{ K [35]})$ [175]. They persist in the solid–solution CeRu₂(Si_{1-x}Ge_x)₂ down to the magnetic instability at $x_c = 0.05 - 0.07$ [158]. Moreover, experiments and band structure calculations confirmed that the Fermi surface of the pure Ge (x = 1) and Si (x = 0) compounds enclose a volume which differs by one electron, i. e. the 4f electron of Ce [176]. A structural phase transition can be ruled out up to 20 GPa, as was shown with conventional and synchrotron x–ray experiments [177, 178].

The (T, P) diagram of single crystalline $CeRu_2Ge_2$ obtained by $\rho(T)$ measurements under pressure in our laboratory [35], resembles qualitatively the (T, x) diagram of $CeRu_2(Si_{1-x}Ge_x)_2$ [158, 179] as can be seen in Fig. 6.3. The analogy of pressure and x-variation (equivalent to a chemical pressure) in this ternary Ce-system is additionally supported by the appearance of the three critical magnetic fields B_a , B_c , and B_M in CeRu₂Ge₂ at high pressure [35], reminiscent to the characteristic fields in $CeRu_2(Si_{0.9}Ge_{0.1})_2$ at ambient pressure [180]. Thus, a quantitative comparison between CeRu₂Ge₂ and its Si substituted alloys can be made if the unit-cell volume V is taken as a common variable. Both, pressure and a decrease in x correspond to a reduction in the unit-cell volume. From x-ray diffraction studies of the alloys reported in Ref. [181] the relation $V(x) = 172.38 \text{ Å}^3 + 10.67x$ is deduced. The volume for a given pressure applied on $CeRu_2Ge_2$ can be calculated with an EOS if the bulk modulus B_0 is known. This is not the case for $CeRu_2Ge_2$ and therefore its T(V(P)) data were matched to the T(V(x))-data of the alloys by adjusting B_0 . In this procedure, the unit-cell volume of $CeRu_2Ge_2$ at the critical pressure $P_{\rm c} = 8.7$ GPa was assumed to be the same as that of $\text{CeRu}_2(\text{Si}_{1-x}\text{Ge}_x)_2$ for x = 0.05, which seems to be very close to the critical concentration x_c . Then the Murnaghan EOS (eq. (3.14)), with $B'_0 = 4$, gives $B_0 = 135$ GPa, which is a good estimate for the bulk modulus in comparison with similar compounds [177, 178, 182, 183].

The transition temperatures for $CeRu_2(Si_{1-x}Ge_x)_2$ and $CeRu_2Ge_2$ are plotted versus the

Figure 6.3: Magnetic ordering temperatures T_N , T_C , and T_L plotted versus the relative unit–cell volume V/V_0 for $CeRu_2Ge_2$ (bold symbols) and the solid–solution $CeRu_2(Si_{1-x}Ge_x)_2$ (open symbols, taken from Ref. [158, 179]). The volume is normalized to the value $V_0 = 183.03 \text{ Å}^3$ of $CeRu_2Ge_2$ at ambient pressure.

reduced volume in the (T,V) diagram shown in Fig. 6.3. In the case of $CeRu_2(Si_{1-x}Ge_x)_2$ the transition temperatures obtained by Haen and coworkers [158, 179] from specific heat measurements are plotted and the upper abscissa has to be used to obtain the Ge-content. At low pressure, i. e. large V/V_0 -values, the agreement is very good and for intermediate volume compression the T_L -values agree also well except for the two values x=0.4 and x=0.2. Close to the magnetic instability the T_N -values of the solid-solution are slightly higher than those obtained in the pressure experiment. One point may be emphasized here. As can be seen from Fig. 6.3 the AFM transition temperature first increases and after passing a maximum it decreases rather rapidly. The extrapolation $T_N \propto (P_c - P)^m \to 0$, made for $P \geq 6.0$ GPa, led to a critical pressure $P_c = 8.70(5)$ GPa and an exponent m = 0.71(8). Values for m are predicted in the framework of the spin fluctuation theory (see section 6.4.1) and should be equal 2/3 (AFM) or 3/4 (FM).

In this phase diagram four regions with different ground states can be distinguished:

(i) A double transition region (AFM plus FM) exists for $0.7 \le x \le 1.0$ [158] or P < 3.5 GPa. The

long-range magnetic order in the AFM phase is modulated with a wave vector $\vec{k}_1 = (0.309, 0, 0)$ [175], identical to that of the short-range magnetic correlations in CeRu₂Si₂ [184]. In the FM phase the magnetic moment ($\mu = 1.9 \mu_{\rm B}$) is aligned along the c-axis [175, 185].

- (ii) Two AFM phases seem to exist for $0.1 \le x < 0.7$ (3.5 GPa $\le P < 7.8$ GPa) characterized by $T_{\rm L}$ and $T_{\rm N}$, with $T_{\rm L} < T_{\rm N}$. Detailed neutron studies on CeRu₂(Si_{0.9}Ge_{0.1})₂ [180] revealed a complex (B,T) phase diagram. At low temperature and up to a field $B_{\rm a}$ the neutron reflection patterns associated with \vec{k}_1 are unchanged (phase I), even on crossing $T_{\rm L}$. However, at the latter temperature some modifications in the intensity of the third harmonic of the moment modulation occurred [186]. Above $B_{\rm a}$, two distinct AFM phases were found, depending on temperature. In the high temperature phase (phase III) not only \vec{k}_1 was seen but also $\vec{k}_2 = (0.309, 0.309, 0)$ (which is the other wavevector characterizing the AFM correlations in CeRu₂Si₂) plus a FM component. The low temperature phase (phase II) is commensurate with $\vec{k}_3 = (\frac{1}{3}, \frac{1}{3}, 0)$. The transition from phase III to phase II is described as a lock—in of \vec{k}_2 to a commensurate value [186]. Thus, it is very likely that a transition in low field $(B < B_{\rm a})$ at $T_{\rm L} < T_{\rm N}$ occurs also in CeRu₂Ge₂ at intermediate pressure like in CeRu₂(Si_{1-x}Ge_x)₂ alloys.
- (iii) Only one transition was detected in the range 7.8 GPa $< P < P_{\rm c}$ (0.05 < x < 0.1) with the electrical resistivity measurements. This might point to the possibility that $T_{\rm L}$ is very close to zero. To clarify this, detailed neutron scattering experiments below 2 K have to be performed for 0.05 < x < 0.1.
- (iv) No long-range magnetic order is observed above $P_c = 8.7$ GPa, but the electrical resistivity reveals a deviation from a FL behaviour in the pressure range up to 9.5 GPa (discussed in section 6.4). Above this pressure, the FL region is eventually entered and the characteristic $\Delta \rho(T) \propto AT^2$ -dependence below $T_{\rm FL} \approx 500$ mK was seen analogously to CeRu₂Si₂ [35]. This upper temperature limit for the $\rho(T) \propto AT^2$ fits starts to increase just above P_c up to 2 K at 10.8 GPa, the highest pressure reached [35]. Unfortunately no comparison to the temperature dependence of the electrical resistivity of CeRu₂(Si_{1-x}Ge_x)₂ with x close to x_c is possible because they are not measured yet.

These considerations about the (T,V) phase diagram show that the unit–cell volume (and therefore the change of interatomic distances) is a crucial parameter. The changes in the interatomic distances enter in the exchange coupling J [187]

$$J \propto V_{\rm cf}^2 / (E_{\rm F} - E_f) \tag{6.8}$$

via $V_{\rm cf}$, the hybridization of conduction and 4f-electrons. E_f denotes the energy of the 4f-band. The hybridization can be written as $V_{\rm cf} \propto 1/d^{l+l'+1}$ [188], with l and l' the angular momentum $(l, l'=0, 1, 2, \dots$ for s, p, d, \dots orbitals, respectively) and the interatomic distance d between Ce and a ligand. Our calculations showed that the main effect arises from the f-d hybridization. Therefore, the V_{df} hybridization is solely considered in the following. With the assumption that $E_{\rm F}-E_f$ hardly changes at low pressure the volume dependence of the exchange interaction J normalized to its value $J_{\rm c}=:1$ (at $P_{\rm c}$) was deduced (inset of Fig. 6.3). The $J/J_{\rm c}$ variation with the reduced volume V/V_0 should, in principle, allow to calculate the pressure variation of $T_{\rm K}$ using $T_{\rm K} \propto \exp\left(-1/Jn(E_{\rm F})\right) \propto 1/\sqrt{A}$. This gives a $T_{\rm K}$ -value in CeRu₂Ge₂ at ambient pressure of 4 K, which is slightly higher than that reported in Ref. [189] if at $P_{\rm c}$ the value $T_{\rm K}=24$ K of CeRu₂Si₂ [190] is used. It is mentioned that at high pressure the system approaches the intermediate valence regime and therefore $E_{\rm F}-E_f$ should decrease and the $J/J_{\rm c}$ ratio should be further enhanced.

The difference between CeRu₂Si₂ and CeRu₂Ge₂ at ambient pressure becomes also evident in the thermoelectric power S(T). In the former compound a broad maximum is centered around 220 K whereas S(T) of the latter is always negative for T < 290 K (see Fig. 6.4 P = 0 curve). The most striking features in S(T) of $CeRu_2Ge_2$ at ambient pressure are the minima present at $T_{\rm min,S}^{(1)}=80$ K and $T_{\rm min,S}^{(2)}=6$ K, with $S=-9.7~\mu{\rm V/K}$ and $-3.5~\mu{\rm V/K}$, respectively. Comparing this temperature dependence to that reported for other magnetic Ce-compounds, e. g. CePd₂Si₂ [191] and CeCu₂Ge₂ [10] reveals a clear difference. The latter compound shows a positive bump at high temperature like CeRu₂Si₂ followed by a negative minimum around 20 K. A second positive peak in S(T) develops at lower temperature and a sign change occurs around $T_0 = 50 \text{ K}$. The high temperature maximum was attributed to the interplay of the Kondo effect and the crystal field (CF) effect while the negative values of S(T) were assigned to spin interactions. The absence of a positive contribution at high temperature in S(T) of $CeRu_2Ge_2$ can be attributed to the fact that CF effects play a minor role because both $\Delta_{\rm CF}^{(1)}=500$ K and $\Delta_{\rm CF}^{(2)}=750$ K [185, 192] are well above room temperature and $T_{\rm K}$ is assumed to be very small [189]. The appearance of a minimum in S(T) at $T_{\min,S}^{(1)}$ seems to be too high in temperature to be explained by spin interactions. This minimum also occurs in S(T) of the non-magnetic LaRu₂Ge₂ and is thus unambiguously not related to the magnetic sublattice [193]. The anomaly around $T_{\min,S}^{(2)}$ is interpreted as a sign for the opening of a magnetic gap, in good agreement with the findings of the specific heat and electrical resistivity, reported in [35].

As soon as pressure is applied to $CeRu_2Ge_2$, S(T) at room temperature becomes positive and a pronounced high–temperature maximum develops. It is related to the CF splitting [193]. At low temperature, signs of T_N and T_L are clearly visible. This is nicely demonstrated by the

Figure 6.4: The absolute thermoelectric power of $CeRu_2Ge_2$ versus temperature at various pressures. The magnetic ordering temperatures T_N , T_C , and T_L as well as the opening of a FM gap are clearly visible at low pressure. The signature of the Kondo effect (T_K) and the CF splitting (T_{max}) start to develop at intermediate pressures.

S(T) curves obtained at 0.9 and 5.7 GPa (Fig. 6.4). The maximum in S(T) around 10 K in the latter curve is interpreted as a signature of the Kondo effect. The Kondo temperature $(T_{\rm K})$ has become of the order the CF splitting at 10.4 GPa and the intermediate valence regime is entered. No pronounced features are found in the low temperature part of S(T) anymore. The magnetic ordering temperatures extracted from these thermopower measurements confirm the (T, V) diagram presented above and further details are discussed in Ref. [193].

The T(V) phase diagram of the $\text{CeRu}_2(\text{Si}_{1-x}\text{Ge}_x)_2$ solid-solution in Fig. 6.3 shows very nicely that resistivity measurements on a stoichiometric and single crystalline compound under high pressure are able to deliver detailed information about changes in the magnetic order. High pressure transport data can be used as a guide for e. g. neutron experiments. In such experiments the critical pressure of CeRu_2Ge_2 ($P_c = 8.7 \text{ GPa}$) seems beyond the technical limits. Hence, by choosing an appropriate alloy of $\text{CeRu}_2(\text{Si}_{1-x}\text{Ge}_x)_2$, neutron experiments performed within their pressure limit could shed more light on the magnetic order in CeRu_2Ge_2 close to magnetic instability.

As a second example for a pressure-induced non-magnetic state the experiments on stoichio-

metric and single crystalline CeCu₅Au will be discussed. The partially substitution of Cu by Au induces in the $CeCu_{6-x}Au_x$ solid-solution a long-range magnetic order [157]. The RKKY interaction dominates the Kondo effect ($T_{\rm K}=1.8~{\rm K}$) and an AFM order occurs below $T_{\rm N}=2.35~{\rm K}$ at ambient pressure [194]. This can be explained qualitatively with the decrease of the hybridization between localized and conduction band electrons, and therefore, of the exchange interaction J, due to the enlarged unit-cell volume. The high pressure resistivity study of CeCu₅Au has allowed us to determine the pressure dependence of $T_{\rm N}$ and to establish the evolution of other characteristic temperatures (see Fig. 6.5). At pressures below 3.2 GPa the intersection of two tangents drawn to the $\rho(T)$ -curve was used to extract T_N . The values agree with the temperatures where the slope of the temperature derivative of $\rho(T)$ changes considerably. At higher pressures no anomaly was visible in $\rho(T)$. Furthermore, at low pressure two maxima in the $\rho(T)$ curves are present. After a phononic contribution has been subtracted the positions of these maxima were determined to be at $T_{\rm max}^{\rm low}$ and $T_{\rm max}^{\rm high}$. Above ≈ 3 GPa only one maximum is visible in $\rho(T)$ as in the case of CeCu₆ (Fig 6.1). This demonstrates the analogy between CeCu₅Au and CeCu₆ if a certain pressure shift is taken into account. The rapid (almost exponential) rise of $T_{\rm max}^{\rm low}$ in CeCu₅Au of almost two orders of magnitude corresponds to an enhancement of the Kondo coupling which dominates the RKKY interaction at high pressure. This is supported by the decrease of $T_{\rm N}$ and agrees well with the Doniach picture described in section 6.2.

In Fig. 6.5 results obtained on two different pieces cut from the same single crystal are shown. The open squares (\square) show that in one experiment the magnetic order was still visible at P=3.84 GPa. At this particular pressure a pronounced drop in $\rho(T)$ occurred at a temperature $T_{\rm c}=100$ mK (\diamondsuit). At a slightly higher pressure (P=4.19 GPa) this drop was less pronounced but still visible at the same temperature. Details of this pressure—induced new phase will be given in section 6.6. In a second experiment no signs of magnetism above 3.2 GPa (bold squares) have been found. Also no indications for a drop in $\rho(T)$ at low temperature have been seen. The $T_{\rm N}(P)$ dependence (bold squares in Fig. 6.5) scales to zero like $T_{\rm N} \propto (P_{\rm c} - P)^m$ at a critical pressure $P_{\rm c}=4.1\pm0.3$ GPa with an exponent $m=0.68\pm0.11$. Within the spin fluctuation theory the exponent should be n=2/3 for AFM ordering which is consistent with the observed value.

The Kondo temperature in CeCu₅Au at low pressure is small in comparison to the crystal field (CF) splitting $\Delta_{\rm CF}^{(1)} \approx 100$ K and $\Delta_{\rm CF}^{(2)} \approx 160$ K [195]. Therefore, as often observed in this situation for other compounds, the magnetic resistivity has two maxima at $T_{\rm max}^{\rm low}$ and $T_{\rm max}^{\rm high}$, reflecting the Kondo scattering on the ground state and excited CF levels, respectively. As soon

Figure 6.5: Pressure dependence of some characteristic temperatures in $\rho(T)$ of CeCu₅Au in a semilogarithmic plot. The Néel temperature $(T_{\rm N})$ scales to zero at $P_{\rm c}=4.1(3)$ GPa. Two maxima in $\rho(T)$ at $T_{\rm max}^{\rm low}$ (bold diamonds) and $T_{\rm max}^{\rm high}$ (circles), related to the Kondo effect, seem to merge above 4 GPa. In one experiment (open symbols) a new phase (probably superconducting) below $T_{\rm c}=100$ mK was found.

as pressure is higher than ≈ 2 GPa, a low temperature resistivity maximum emerges at $T_{\rm max}^{\rm low}$ and starts to increase with pressure. This might point to the possibility of an enhanced screening of the magnetic moments by the conduction electrons and thus to an increasing role of the Kondo effect. Consequently, the anomaly at $T_{\rm max}^{\rm low}$ has to be related to $T_{\rm K}$. Both anomalies in $\rho(T)$ seem to merge above 4 GPa, indicating the entrance in an intermediate valence regime when the Kondo temperature becomes of the order of the CF splitting.

In the case of two excited CF levels Hanazawa et al. [196] have introduced a second Kondo temperature at high temperature (T_K^h) . It is related with T_K by $T_K^h = \sqrt[3]{T_K \Delta_1 \Delta_2}$. With the assumption that Δ_1 and Δ_2 are hardly changed at low pressure (P < 4 GPa), the T_K^h values can be calculated if T_K is known. This is the case for several compounds of $\text{CeCu}_{6-x}\text{Au}_x$ [197]. Their relative unit–cell volumes $V(x)/V_0$, with V_0 the unit–cell volume of CeCu_5Au at ambient pressure, have to be transformed into the corresponding pressure values. With the Murnaghan EOS (see eq. (3.14)) a $T_K(P)$ relation, applicable for CeCu_5Au , can be deduced (with $B_0 = 110 \text{ GPa}$ and $B'_0 = 4$). This (linear) function then yields the $T_K^h(P)$ dependence. The $T_K^h(P)$ values are practically identical to $T_{\text{max}}^{\text{high}}(P)$ in the pressure range 2 < P < 3 GPa. At lower

pressure the agreement is not so good which might be related to the presence of magnetic order.

As a last example, the pressure-induced magnetic order in non-magnetic HF compounds will be discussed briefly. HF behaviour is not only observed in Ce- and U-based intermetallics but has also been found in Yb-compounds. In a review by Bauer [167], the anomalies of Yb-Cubased HF systems are discussed in detail. The physical properties of the Yb-compounds can be compared to those of the Ce-based HF systems using the electron-hole analogy. In this picture the missing 4f-electron in the $4f^{13}$ -configuration of the Yb³⁺-ion can be interpreted as a 4fhole, analogously to the 4f-electron in the Ce^{3+} -ion. The ternary YbCu₂Si₂ is of particular interest after the discovery of its pressure-induced magnetism (around 8 GPa) [198] and its close relation to the superconducting HF compound CeCu₂Si₂. At ambient pressure the Sommerfeld coefficient is $\gamma = 135 \text{ mJ/molK}^2$ and the valence of Yb is close to 2.8 at T = 4.2 K, both indicating the moderate HF and intermediate valence character of YbCu₂Si₂ ($T_{\rm K}=200$ K). The electrical resistivity and the magnetic susceptibility do not show any evidence of magnetic order down to 400 mK at ambient pressure. The electrical resistivity measurements on YbCu₂Si₂ under pressure revealed that the transition temperature $T_{\rm M}=1.3~{\rm K}$ (at $P=8.5~{\rm GPa}$) increases up to 3 K at 25 GPa, the highest pressure reached in this experiment [199]. Using the electronhole analogy the pressure effect on YbCu₂Si₂ can be explained qualitatively. Starting from an intermediate valence state, pressure drives YbCu₂Si₂ into the HF region and at the critical pressure a magnetically ordered phase with a weak Kondo effect is entered.

The effect of pressure on the electrical resistivity of two other Yb-based intermediate valence compounds was also studied in our laboratory [200]. In YbCuAl and YbInAu₂ the Kondo temperature decreases with pressure. In the former compound a FL behaviour is found at low pressures, but the maximum in $\rho_0(P)$ around 7 GPa and the $\rho(T)$ anomaly at 1 K (at 8 GPa) are interpreted as signs of magnetic order. In YbInAu₂ a minimum in $\rho(T)$ develops at low temperature and the pressure dependence of the low temperature resistivity was explained in the context of the Kondo hole effect which leads to an increase of ρ_0 upon approaching the magnetic instability.

6.4 Non-Fermi-liquid behaviour

In the preceding section the appearance (disappearance) of HF behaviour in Ce– (Yb–)based compounds was discussed. Close to the magnetic instability a deviation from the quadratic temperature variation of $\rho(T)$ points to unconventional low–temperature properties. This NFL

behaviour attracted much interest in recent years and several, conceptually different origins have been proposed, briefly described at the beginning of this section. Then, in the second part, evidence for NFL behaviour in a pressure range around the critical pressure will be described with the example of CeCu₅Au and CeRu₂Ge₂.

6.4.1 Different models to account for unusual low temperature properties

The multi-channel Kondo model introduced by Nozières and Blandin [201] treats the interaction of a magnetic impurity with spin \mathbf{S} and the conduction electrons. A local FL due to the Kondo effect arises if the impurity spin is completely screened by the conduction electrons. This occurs when the condition $\mathbf{S} = N/2$ is fulfilled, where N is the number of conduction electron channels. For N=1 and $\mathbf{S}=1/2$ this requirement is satisfied. If the spin \mathbf{S} however, interacts with several channels (N>2), the Kondo screening is enhanced and the spin \mathbf{S} is over-screened. In the case of strong coupling, a magnetic moment results which in turn then interacts with the conduction electron channels. Thus, the extension of the Kondo screening diverges. Nozières and Blandin calculated the situation for $\mathbf{S}=1/2$ and N=2 and predicted a logarithmic divergence of C/T and $\chi(T)$. Such a local NFL has not been found yet unequivocally.

The two–channel quadrupolar Kondo effect has been considered by Cox [202]. In this scenario the electrical quadrupolar moment of the f–ion interacts with the conduction electrons and their spins provide the two channels. The C/T data of $U_xY_{1-x}Pd_3$ alloys [203, 204] showed the logarithmic divergence, predicted in this model. However, many open questions remain. For example, the NFL behaviour found in $U_xY_{1-x}Pd_3$ for x=0.2 cannot be explained on the basis of a diluted system of isolated quadrupolar impurities. The observed $\Delta\rho \propto -T$ dependence is in contradiction to the expected \sqrt{T} -behaviour. Furthermore, $\chi(T)$ does not diverge upon approaching zero temperature. Apart from the possible microscopic origin of the NFL behaviour in this U–based system, it remains unclear, whether the NFL properties are intrinsic or related to a small distribution of local U concentration, as was shown with a detailed metallurgical analysis [205].

Almost all systems that show NFL properties are non-stoichiometric compounds and are therefore partly disordered materials. A model known as "Kondo-disorder" emphasizes a disorder-driven mechanism as possible origin of NFL behaviour [206]. A system of dilute magnetic impurities in a disordered metallic host leads to a probability distribution of Kondo temperatures which is sufficiently singular to induce a divergence in the magnetic susceptibility as $T \to 0$ [207]. This model was successfully applied to thermodynamic data $(C_V(T))$ and $\chi(T)$

of $UCu_{5-x}Pd_x$ [208]. A nominally ordered alloy that presents NFL behaviour is UCu_4Pd [209]. Muon spin rotation experiments reported by MacLaughlin *et al.* indicate that the U–ion susceptibility is inhomogeneous at low temperature. This is due to the inherent and unavoidable lattice disorder which also favours a disorder–driven mechanism to explain the NFL behaviour in UCu_4Pd .

Such a route to NFL behaviour that incorporates furthermore the competition between the Kondo– and RKKY–interaction was suggested by Castro Neto and coauthors [13]. In this model the presence of disorder leads to the coexistence of a paramagnetic metallic phase (dominated by the Kondo–effect) with magnetic clusters (mainly RKKY–interaction) in the proximity of the magnetic instability. As a consequence, various physical properties diverge with decreasing temperature. This theory is in good agreement with C_V and $\chi(T)$ data for various alloys over appreciable ranges of substitute concentration [210]. Important constraints on this scenario were however, provided by the experiments on UCu₄Pd mentioned above. First, the magnetic clusters seem to be limited to a few f-ions and second, the fluctuation rate of the spins in the clusters is rather large.

Very recently, Coleman [12] has put forward the idea of a quantum critical point (QCP). If AFM and FL behaviour are considered as two competing attractive fixed points of a renormalization group trajectory, which are linked by a new fixed point, then a QCP exists. Upon lowering temperature, the system evolves towards one of the two attractive fixed points. Using pressure or other means to reach a critical $T_{\rm K}/T_{\rm RKKY}$ value, the system is forced towards the QCP. The properties of the system will be dominated over a wide temperature range by the physics of this QCP, and NFL behaviour can be interpreted as a generic feature in the vicinity of a QCP [211].

All these proposals have had a certain success in describing the anomalies at low temperature in stoichiometric as well as non–stoichiometric (highly disordered) compounds. But none of them can claim general applicability to a wide range of f–electron systems.

The occurrence of NFL behaviour in $CeRu_2Ge_2$ and $CeCu_5Au$ at high pressure (see below) can be unambiguously attributed to the fact, that both systems are tuned to the magnetic instability. In the framework of the spin fluctuation theory [212], predictions for the temperature dependence of $\rho(T)$ as well as the variation of the ordering temperature with pressure can be made. Moriya and Takimoto [212] showed that the spin fluctuation theory developed for itinerant d-electrons can be modified and applied to nearly localized f-electron systems. The key ingredient of this theory is the dynamical susceptibility $\chi(q,\omega)$ arising from overdamped spin

fluctuation modes. Their population can be calculated quantitatively, once $\chi(q,\omega)$ is known. The rate at which these modes become occupied with increasing temperature enters in the transport properties and the exponent n in the power law of the resistivity can be calculated. If the magnetic order occurs in three dimensions, n=3/2 (n=5/3) for AFM (FM) order is predicted. Furthermore, the ordering temperature should depend on pressure as $T_{\rm N} \propto (P_{\rm c}-P)^{2/3}$ or as $T_{\rm c} \propto (P_{\rm c}-P)^{3/4}$ if the magnetic instability at $P_{\rm c}$ is approached [212, 213].

It is worthwhile mentioning that NFL behaviour is also observed in one–dimensional systems and described theoretically in the Luttinger–liquid model. In these systems the electron–electron interaction is much larger than in a FL and leads to a spin–charge separation [214]. Some organic superconductors [215] and quantum wires [216] can be described as a Luttinger–liquid. Furthermore, the normal state properties of the high– T_c cuprates brought up the question whether the $\rho(T) \propto T$ dependence observed in these systems suggests a NFL (marginal FL) behaviour [217]. These systems are close to AFM order although this might be not the important argument for the marginal FL behaviour.

In the following, strongly correlated electron systems, that are driven by pressure toward the magnetic instability, will be discussed. It is of great interest to understand, whether the NFL behaviour represents an asymptotic behaviour upon approaching zero temperature or a crossover to a FL fixed point. For NFL behaviour in $CeCu_{6-x}Au_x$ induced by concentration tuning, the reader is referred to a review article by v. Löhneysen [218]. The unusual low temperature properties of $CeCu_2Si_2$ and $CeNi_2Ge_2$ are reviewed by Steglich and coworkers [219] and in the articles by Gegenwart and collaborators [220, 221] the latest results on these two systems can be found. Experimental evidence for NFL behaviour in the recently discovered HF superconductors $CePd_2Si_2$ [222] are given in Ref. [223].

6.4.2 Temperature dependence of the electrical resistivity

Applying pressure on stoichiometric and single crystalline CeCu_5Au offers the unique possibility to study the low temperature properties close to the magnetic instability and to make a comparison to the $\text{CeCu}_{6-x}\text{Au}_x$ solid–solution (with $x \to x_c$). That pressure can induce the same magnetic properties as alloying does was shown by the (T, V) phase diagram of CeRu_2Ge_2 .

The electrical resistivity of CeCu₅Au below 300 mK was described with

$$\rho = \rho_0 + \tilde{A}T^n \tag{6.9}$$

at all pressures [224]. The exponent n and the coefficient \tilde{A} are fitting parameters. The only "constraint" to the fit was the fixation of the upper temperature limit $T_{\rm FL}=300$ mK. It is

Figure 6.6: The exponent n used in the power law of eq. (6.9) to describe the $\rho(T)$ data of CeCu₅Au below T = 300 mK. Around P = 3.5 GPa a clear deviation from a FL (n = 2) behaviour is observed. The dashed line is a guide to the eye.

a compromise between an as narrow as possible temperature interval (30 mK< T < 300 mK) and the reliability of the deduced parameters, i. e. n and \tilde{A} . Figure 6.6 illustrates how the deviation of a FL description (n=2) evolves with pressure. Below 1.2 GPa n=2 is consistent with residual electron-magnon scattering in a magnetic system. Then at 1.8 GPa, n suddenly attains a value of 1.75 and decreases as pressure increases. At 3.5 GPa n=1.51 is reached, close to the critical value n=3/2, predicted by theory (see section 6.4.1). Increasing pressure further, leads to a higher n value which finally reaches n=2 well inside the non-magnetic region (P=5.37 GPa). The minimum in n vs P is not an artefact of the limited temperature interval in the fitting procedure. The fits for various $T_{\rm FL}$ values (up to 600 mK) showed always a minimum in n(P) around 3.5 GPa, where n is the smaller (n=1.2) the higher the $T_{\rm FL}$ limit (600 mK) is chosen. In the non-magnetic region however, the FL value n=2 was found in temperature intervals which became enlarged with pressure, i. e. $T_{\rm FL}$ increased with pressure.

This behaviour immediately raises the question whether these results could be compared to the observations in $\text{CeCu}_{6-x}\text{Au}_x$ with different Au–concentrations. It is clear that the unit–cell volume variation is a crucial parameter. Thus a correspondence of the x-values in $\text{CeCu}_{6-x}\text{Au}_x$ to the pressure values in CeCu_5Au should be deduced. Using the relation

Figure 6.7: Left panel: $\rho(T)$ of CeCu₅Au at selected pressures. Well inside the magnetic region a NFL behaviour is already found at P=1.8 GPa, which corresponds to the alloy with x=0.5. A variation as $\Delta\rho(T)\propto T^{1.51}$ is observed at 3.5 GPa, close to the magnetic instability. The comparison to the x=0.1 alloy is qualitative, since the exponent is still larger than one. In the non–magnetic region (P=5.37 GPa) a FL behaviour is observed below 300 mK, as for CeCu₆. Right panel: $\rho(T)$ for various alloys of CeCu_{6-x}Au_x taken from Ref. [226]. For x=0 (bottom) the quadratic temperature dependence (FL–like) is nicely demonstrated by the straight line in the $\rho(T^2)$ –plot. The linear temperature dependence for the x=0.1 compound (middle) suggests a NFL behaviour below 600 mK. A FL description is suggested for x=0.5 below 300 mK.

 $V(x) = 420.225 \text{ Å}^3 + 13.988x$, deduced from x-ray data given in Ref. [225] and e. g. the Murnaghan EOS (eq. (3.14)), a correspondence between x and P can be obtained. For CeCu₅Au, a bulk modulus $B_0 = 110$ GPa (with $B_0' = 4$) was deduced in section 6.3. This gives the correspondence $x = 0.5 \Leftrightarrow P = 1.8$ GPa, $x = 0.1 \Leftrightarrow P = 3.4$ GPa, and $x = 0 \Leftrightarrow P = 3.85$ GPa. These values should be taken as a guide rather than as a strict prediction.

The correspondence between x and P is nicely demonstrated in Fig. 6.7 where the $\rho(T)$ –data of $CeCu_{6-x}Au_x$ for x=0, 0.1, and 0.5 [226] (right panel) and of $CeCu_5Au$ at different pressures (left panel) are shown. In all cases the current flow was parallel to the b–axis of the orthorhombic crystal structure. The right panel of this figure shows a FL behaviour for the non–magnetic $CeCu_6$ below ≈ 200 mK as is indicated by the straight line in the $\rho(T^2)$ –plot. At the critical Au–concentration $x_c=0.1$ the linear $\rho(T)$ variation up to 600 mK nicely demonstrate the NFL behaviour. It should be noted that in $CeCu_{5.9}Au_{0.1}$ a linear $\rho(T)$ variation

was also found for the other current directions [227]. CeCu_{5.5}Au_{0.5} is well inside the ordered magnetic phase $(T_{\rm N}\approx 1~{\rm K})$ and the straight line in the $\rho(T^2)$ -plot suggests the validity of a FL description up to 300 mK. But a closer look might allow the conclusion, that this is not the case. This is supported by the $\rho(T)$ dependence measured in CeCu₅Au at 1.8 GPa, which corresponds to the Au-content x=0.5, shown at the top of the left panel in Fig. 6.7. The electrical resistivity follows a $T^{1.75}$ temperature law, suggesting that already at this pressure the NFL region is entered. The $\rho(T)$ curve obtained at 3.5 GPa, which corresponds roughly to the critical Au-concentration, shows a $\Delta\rho(T) \propto T^{1.51}$ variation below 300 mK rather than a linear temperature dependence. May be a linearity in $\rho(T)$ of CeCu₅Au can be found only at a pressure exactly corresponding x_c . Well inside the non-magnetic region $(P=5.37~{\rm GPa}) \rho(T)$ of CeCu₅Au is in agreement with the FL picture up to 300 mK.

The same description (eq. (6.9)) of the $\rho(T)$ data has been made for the temperature dependence of the electrical resistivity of CeRu₂Ge₂ throughout the entire pressure range below $T_{\rm FL}=1.5~{\rm K}$ [35]. The result of this procedure is shown in Fig. 6.8. The exponent decreases from $n\approx 4$ at low pressure to $n\approx 3$ at $P=2.7~{\rm GPa}$. The variation of n starting at 3.5 GPa is attributed to a change of the magnetic ordering [35]. The exponent approaches n=2 around 7 GPa. Then a rather large pressure interval around $P_{\rm c}$ exists (7.8 $\leq P \leq$ 9.5 GPa) where n attains values between $3/2 \leq n \leq 5/3$. At pressures higher than 9.5 GPa the $\rho(T)$ -curves show a T^2 -dependence and the FL region is entered. This can be seen for the curves measured at P=9.9 and 10.8 GPa, plotted in the inset of Fig. 6.8. The other $\rho(T)$ -curves clearly demonstrate a deviation from a T^2 -dependence around $P_{\rm c}=8.7~{\rm GPa}$.

The deviation from FL behaviour in the temperature range 30 mK < $T_{\rm FL}$ < 1.5 K around $P_{\rm c}$ raises the question of whether a FL description is applicable below a certain temperature which is, in this case, enormously suppressed. As can be seen in the inset of Fig. 6.8, such a temperature limit might exist well below 300 mK but more accurate measurements are necessary to clarify this point. However, these findings might stimulate further experiments on ${\rm CeRu_2}({\rm Si_{1-x}Ge_x})_2$ compounds (with x close to x_c) at ambient pressure, to investigate the NFL properties also by other means, like susceptibility and specific heat, in more detail.

A non- T^2 dependence of $\rho(T)$ was already observed in the structurally identical CePd₂Si₂ [222] and CeNi₂Ge₂ compounds [219, 228]. The NFL behaviour found in these compounds seems to depend strongly on the value of the residual resistivity ρ_0 . A relatively large $\rho_0 = 20 \ \mu\Omega$ cm in CePd₂Si₂ yields $\rho(T) \propto T^2$ near P_c [229], whereas $\rho(T) \propto T^{1.2}$ in a sample with $\rho_0 = 5 \ \mu\Omega$ cm was found [222]. In a high quality CeNi₂Ge₂ polycrystal ($\rho_0 = 0.3 \ \mu\Omega$ cm) $\rho(T)$ obeyed a $T^{1.37}$

Figure 6.8: The exponent n used in the power law of eq. (6.9) to describe the $\rho(T)$ data of CeRu₂Ge₂ below T=1.5 K. The two different symbols denote the values obtained from two parts of one sample in the high pressure cell. In the inset $\rho(T) \propto T^2$ below 1 K is plotted. The FL behaviour is unequivocally found at pressures $P \geq 9.9$ GPa.

power law at low temperature [230]. The residual resistivity in $CeRu_2Ge_2$ is also relatively small $(\rho_0 \approx 2 \ \mu\Omega cm)$ and a NFL behaviour around P_c is detected. In single crystalline $CeCu_5Au \ \rho_0$ is between 20 and $\approx 60 \ \mu\Omega cm$ and yet, a clear deviation from a FL description is found. This suggests that disorder plays a key role for the appearance of the unusual low temperature properties in these materials.

6.5 Anomalies in the residual resistivity

The analysis of the $\rho(T)$ data is often done under the assumption that various scattering mechanisms give additive contributions to the residual resistivity ρ_0 . It is ascribed to disorder (all types of defects, such as vacancies, impurities, etc.) and is considered as temperature independent. Here we would like to emphasize, that the expression "residual resistivity" in this context refers to the resistivity measured at the lowest temperature (between 30 mK and 40 mK) accessible in our experiments.

Figure 6.9 shows that in various HF compounds ρ_0 varies considerably between the magnetic and non–magnetic regions. It appears that ρ_0 depends strongly on electronic correlations

(charge and spin fluctuations) present in these systems. The structures in $\rho_0(P)$, with different magnitudes, are not necessarily centered at P_c . The magnitude of the ρ_0 -peak in the superconducting $CeCu_2Si_2$ and $CeCu_2Ge_2$ at pressures close to the $T_c(P)$ maximum, is very sample dependent [18]. The occurrence of this peak can be associated to charge fluctuations [231] or even to a valence transition. For YbCu₂Si₂ only one part of the Yb ions orders magnetically [232] at $P_c \approx 8$ GPa and then the $\rho_0(P)$ maximum may correspond to full ordering at higher pressure. Even in the case of CeRu₂Ge₂ [35] or CeAl₃ [233], large residual magnetoresistance effects showed that the magnetic contribution to ρ_0 is not negligible at all in comparison to the static disorder contribution. This becomes evident for CeCu₅Au where the pronounced peak in ρ_0 well inside the magnetic region seems to be correlated to the magnetic modulation wave vector. Furthermore, observations in other systems indicate that a part of ρ_0 is caused by various scattering centers such as Kondo hole [234], uncompensated spin [235] or magnetic cluster [236]. Their contribution should decrease with increasing temperature and could be involved in the formation of a low temperature $\rho(T)$ minimum. Such a dependence was observed in YbInAu₂ [200] and attributed to the Kondo-hole scattering. Thus, there is little evidence that the disorder can be reduced to a temperature independent term ρ_0 . It is more likely that only one part of ρ_0 due to static disorder can be subtracted from the total resistivity according to the Matthiessen rule. As an example for the pronounced pressure effects on the residual resistivity, the $\rho_0(P)$ -dependence observed for CeCu₅Au will be discussed in detail [237].

In CeCu₅Au a large value of ρ_0 ($\approx 30~\mu\Omega$ cm) compared to other ternary Ce–systems, is already found at ambient pressure. Applying a moderate pressure (P < 2 GPa) enhances ρ_0 by almost a factor of two (Fig. 6.10). A pronounced maximum at P = 1.8 GPa is observed and increasing pressure by only 2 GPa further, ρ_0 has fallen below the ambient pressure value. Above 4 GPa an almost linear decrease of ρ_0 with pressure is found. The ρ_0 values of CeCu_{6-x}Au_x (see inset of Fig. 6.10) are almost consistent with the Nordheim relation $\rho_0 \propto x(1-x)$. The Au impurities can be regarded as strong scatters. They probably change the Kondo effect of the nearby Ce ion in a subtle way without changing strongly $T_{\rm K}$. This has led to the assumption, that the increase of ρ_0 with x is related to the Kondo effect [238].

The different slopes of the linear $\rho(T)$ variation in CeCu_{5.9}Au_{0.1} along the a- and b-direction (discussed in section 6.4.2) point to the influence of the magnetic order on the scattering of electrons [227]. Thus, the strong pressure dependence of ρ_0 in CeCu₅Au seems also to be related to the magnetic order at low temperature. It is very likely that pressure on CeCu₅Au changes the magnetic ordering vector \vec{k} as alloying does in CeCu_{6-x}Au_x. That pressure can provide

Figure 6.9: Residual resistivity of different heavy Fermion compounds versus pressure. In case of Cecompounds $\Delta P = P - P_c$ whereas for YbCu₂Si₂ $\Delta P = P_c - P$ has to be used. The critical pressures $P_c(\text{GPa})$ are 4.1,8, 8.7, 9.4, and -1 for CeCu₅Au, YbCu₂Si₂, CeRu₂Ge₂, CeCu₂Ge₂, and CeCu₂Si₂, respectively.

such a possibility is supported by the magnetic phase diagram of $\text{CeRu}_2(\text{Si}_{1-x}\text{Ge}_x)_2$ presented in section 6.3. Neutron data revealed a magnetic ordering wave vector $\vec{k}=(0.59,0,0)$ and $\vec{k}=(0.62,0,0.27)$ for $\text{CeCu}_{6-x}\text{Au}_x$ with $x\geq 0.5$, and $0.1\leq x\leq 0.3$, respectively [239]. We assume that the magnetic ordering vector in CeCu_5Au (for $P\leq 1.8$ GPa) is the same as in the alloys with $x\geq 0.5$. In the pressure range 1.8 < P < 4 GPa it is very probable that the magnetic order in CeCu_5Au , can be compared with $\text{CeCu}_{6-x}\text{Au}_x$ for $0.1\leq x\leq 0.3$. This correspondence between pressure and Au-content was introduced in section 6.4.2 to match qualitatively the NFL behaviour in CeCu_5Au to that in $\text{CeCu}_{6-x}\text{Au}_x$ alloys. The analogy allows now to sketch an explanation for the observed $\rho_0(P)$ dependence shown in Fig. 6.10.

At first, a non-magnetic Kondo system is considered. Below $T_{\rm K}$ coherence sets in and $\rho(T)$ decreases towards T=0. If now $T_{\rm K}$ is increased (without introducing impurities, for example by applying pressure), the temperature interval where coherent scattering develops is enlarged. Thus, at very low temperature, $\rho(T)$ approaches the residual resistivity inherent to the system. This shows in a qualitative way that ρ_0 of a non-magnetic Kondo compound should decrease with pressure as is found for ${\rm CeCu}_5{\rm Au}$ in the paramagnetic phase above 4 GPa (Fig. 6.10) where a rather linear decrease of ρ_0 is observed up to 8 GPa. Extrapolating this dependence down to

Figure 6.10: Residual resistivity of CeCu₅Au as a function of pressure. The initial increase of ρ_0 is attributed to the weakening of the AFM order. Above P=1.8 GPa the scattering of electrons is related to the magnetic ordering wave vector. As soon as the magnetic instability is reached ρ_0 decreases linearly with pressure. Different symbols denote different experiments. In the inset the ρ_0 variation with the Au–concentration x is shown. The solid line is a fit according to the Nordheim relation ($\rho_0 \propto x(1-x)$).

P=0 shows clearly a contribution in $\rho_0(P)$ that very likely has its origin in the magnetic order. In CeCu₅Au $T_{\rm N}=2.35~{\rm K}$ and $T_{\rm K}=1.8~{\rm K}$ are of the same order of magnitude. The 50% decrease of $\rho(T)$ between $T_{\rm N}$ and 30 mK at ambient pressure [224] is thus partly due to the occurrence of magnetic order and coherence. Pressure drives $T_{\rm N}$ towards zero temperature, decreasing the temperature interval where a complete magnetic order can develop. It is noted, that in CeCu₅Au $T_{\rm N}$ varies rather strongly with pressure in contrast to $T_{\rm K}$, which is enlarged only by a factor of two in the pressure range up to 4 GPa, deduced from the x-P correspondence. Thus, the smaller the $T_{\rm N}$, the higher the residual resistivity. This can be qualitatively understood if the $T_{\rm N}$ value is related to the exchange interaction J (see eq. (6.7)). A low ordering temperature suggests also a weak coupling between the magnetic moments. This favours an appreciable contribution of scattering by spin fluctuations to the residual resistivity. However, this explanation does not account for the maximum in $\rho_0(P)$ at 1.8 GPa, well inside the magnetically ordered phase.

A probable explanation for this pronounced maximum is provided by a model presented by v. Löhneysen and coworkers [238] to explain the $\rho_0(x)$ -variation in CeCu₅Au. In their theoretical

considerations they related the initial decrease of $\rho(T)$ below $T_{\rm N}$ to the magnetic moment present in the alloys of ${\rm CeCu_{6-x}Au_x}$. For $x\geq 0.5$ the static magnetisation associated with the magnetic order is thought to act like an additional periodic structure, which changes the electronic band structure. These effects led in the calculations for the alloy with x=0.5 (which can be compared to ${\rm CeCu_5Au}$ at P=1.8 GPa) to a decrease of $\rho(T)$ below $T_{\rm N}$ partly caused by the magnetic order and the entrance of coherence. For the compounds with x=0.2 and 0.3 the calculations ascribed the resistivity decrease below $T_{\rm N}$ mainly to the formation of coherence. Hence, above $x\approx 0.5$ (i. e. below 1.8 GPa) the effects of the increasing magnetic moment changes the electronic band structure is such a way that the main contribution in the decrease of $\rho(T)$ below $T_{\rm N}$ is of magnetic origin. Below $x\approx 0.5$ (i. e. above 1.8 GPa) the coherent scattering becomes more and more dominant. This model furthermore suggests, that the coherence temperature $T_{\rm coh}$ in ${\rm CeCu_5Au}$ is lower than $T_{\rm N}$ for $P\leq 1.8$ GPa and larger as $T_{\rm N}$ at higher pressures.

In this scenario the interplay of magnetism and electrical resistivity in $CeCu_5Au$ under pressure is described in a rather crude way. The detailed $\rho(P)$ dependence presented in Fig. 6.10 might stimulate theoretical work to achieve a better understanding of the contributions to the residual resistivity.

6.6 Superconductivity on the verge of magnetic order

So far, five U-based and one ternary Ce-based HF superconductors at ambient pressure are known and a second ternary Ce-compound, CeNi_2Ge_2 , is still discussed controversially. Pressure—induced superconductivity was detected only in Ce-based systems. More convincing data for a superconducting state has to be furnished for CeCu_2 and CeCu_5Au since none of them showed zero resistivity. The pronounced drops in $\rho(T)$ and their field dependence at a temperature T_c can only be treated as hints for superconductivity.

Table 6.1 shows the transition and magnetic ordering temperature together with the magnetic moment. All the transition temperatures are lower than 2 K and all the magnetic moments are rather small, except for $CeCu_5Au$. Many experimental evidence for an unconventional type of superconductivity was deduced from the temperature dependence of the specific heat, ultrasound attenuation, and NMR spin–lattice relaxation rate below T_c (see e. g. the review by Grewe and Steglich [156]). Their non–exponential temperature dependence points to the existence of nodes in the superconducting gap function. In contrast to the effect of non–magnetic impurities to BCS–like superconductors, HF superconductors are strongly affected by small amounts of such impurities (like Y, La or Th). They are as effective at pair breaking as magnetic impurities, like

Table 6.1: Superconducting (T_c) and magnetic ordering temperature (T_N) , the critical pressure (P_c) where superconductivity emerges, the magnetic moment (μ) as well as the space group type of stoichiometric HF superconductors. The references given are mainly review articles where further information can be found.

compound	$T_{ m c}$	$T_{ m N}$	$P_{ m c}$	μ	space group	reference
	(K)	(K)	(GPa)	$(\mu_{ m B})$	type	
$CeCu_2Si_2$	0.65	≈ 1	-1	0.1-0.3	I4/mmm	[3, 156]
URu_2Si_2	1.2	17	0	0.03	I4/mmm	[156]
UPd_2Al_3	2.0	14.5	0	0.85	P6/mmm	[156, 240]
UNi_2Al_3	1.0	4.3	0	0.24	P6/mmm	[241]
UPt_3	0.48, 0.52	5	0	0.02	$P6_3/mmc$	[242, 243]
UBe_{13}	0.9	-	0	-	Fm3c	[244, 245]
$\mathrm{CeNi}_{2}\mathrm{Ge}_{2}$	0.1-0.4	-	≈ 0	-	I4/mmm	[221, 246]
$CeCu_2Ge_2$	0.7	4.1	9.4	0.74	I4/mmm	[10]
$CeRh_2Si_2$	0.35	39	0.9	1.28	I4/mmm	[247, 248]
$\mathrm{CePd}_2\mathrm{Si}_2$	0.5	10	2.8	0.62	I4/mmm	[156, 222, 248]
CeIn_3	0.1	10.2	2.6	0.65	$Pm\bar{3}m$	[228]
CeCu_2	0.2	3.5	6	0.33	Imma	[249]
$\mathrm{CeCu}_{5}\mathrm{Au}$	0.1	2.35	3.8	2.66	Pnma	[194, 224]

Gd which is well described by the theory of Abrikosov and Gor'kov [250]. Thus, a non-s-wave pairing is very likely in HF superconductors. This is supported by the existence of more than one superconducting phase in UPt₃ [251] and probably also in Th-doped UBe₁₃ [245].

In CeCu₂Si₂ μ SR measurements revealed a new picture of the interplay between superconductivity and magnetism, as was pointed out by Amato [252]. The two states do not coexist on a microscopic level and both types of ground states arise from instabilities of the electrons involved in the HF state. This is different to URu₂Si₂, UPd₂Al₃, and UNi₂Al₃, all exhibiting a coexistence of superconductivity with magnetic order at a microscopic scale. Despite this coexistence, the μ SR data show that both ground states do not strongly interact, although in each state f-electrons are involved [252]. This is the important difference to magnetic superconductors such as the Chevrel phases [253]. In these compounds the Cooper-pairs are formed by the conduction electrons which only weakly interact with the local moment. Without going into details, UPt₃ and UBe₁₃ are showing evidence that the superconducting pairing mecha-

nism is mediated by spin fluctuations (see Ref. [252] and references therein). Such a magnetic pairing mechanism is now claimed by Mathur and coworkers [11] to operate in CePd₂Si₂ and CeIn₃. Applying moderate pressure (≈ 2.5 GPa), the magnetically ordered state is weakened in both compounds and just before the magnetic instability is reached, superconductivity emerges ($T_{\rm c} < 500$ mK).

In $CeCu_2Ge_2$ superconductivity can be induced by a pressure of about 9.4 GPa ($T_c = 600 \text{ mK}$) [10]. Experimentally the coexistence of magnetism and superconductivity at a microscopic scale cannot be proven due to the pressure gradient in the pressure cell and sample inhomogeneity [254]. Only signs of a coexistence are observed, like in $CeCu_2$ [249] and it can be stated that this situation agrees with a pairing mechanism mediated by AFM spin fluctuations.

No agreement about the low temperature properties of CeNi_2Ge_2 is yet found. Grosche and coworkers [246] claimed the occurrence of superconductivity in high purity single crystals of CeNi_2Ge_2 at ambient pressure. This phase was suppressed by a pressure as low as 0.4 GPa. The same authors furthermore reported a pressure—induced superconducting phase in another sample of CeNi_2Ge_2 (P > 1.2 GPa, $T_c = 400$ mK), similar to the observation published by the same group earlier [228]. On the other hand, Gegenwart et al. [221] recently found in polycrystalline CeNi_2Ge_2 only a 30% drop of $\rho(T)$ below 100 mK at ambient pressure and assigned this observation to the onset of superconductivity. This inconsistency shows that the sample quality seems to be an important parameter for the low temperature phase of CeNi_2Ge_2 .

The same statement is applicable to CeRh₂Si₂, another pressure–induced HF superconductor reported by Movshovich and coworkers [247]. In the pressure range 0.9 < P < 1.7 GPa the onset of superconductivity occurs at 350 mK. But also in this system complete and incomplete transitions have been observed, and Movshovich *et al.* pointed to the question whether precise stoichiometry, low residual resistivity or perhaps some other properties are the important criteria for superconductivity. Low residual resistivity (ρ_0 in the low $\mu\Omega$ cm range) was also said to play a key role for the occurrence of superconductivity in CePd₂Si₂ [11]. This seems not to be the case in CeCu₅Au ($\rho_0 = 28 \ \mu\Omega$ cm), where we believe to have found traces of superconductivity ($T_c = 100 \ \text{mK}$ and $P = 3.84 \ \text{GPa}$) close to the magnetic instability.

The pressure dependence of $\rho(T)$ of single crystalline CeCu₅Au was investigated in our group [224] and details were already given in the preceding sections. Here, the peculiar low temperature behaviour of the $\rho(T)$ curves recorded close to the magnetic instability are of particular interest (see Fig. 6.11). At P=3.84 GPa the entrance into a magnetically ordered phase at $T_{\rm N}\approx 1$ K is still visible (see inset Fig. 6.11) but at T=100 mK, $\rho(T)$ drops suddenly more than 10%. This

Figure 6.11: Electrical resistivity $\rho(T)$ of CeCu₅Au at pressures close to the magnetic instability. The strong drop in $\rho(T)$ at 100 mK is interpreted as the entrance to a (probably) superconducting phase. Inset: The anomaly in $\rho(T)$ at ≈ 1 K is interpreted as a sign of magnetic order.

effect can be suppressed if the measuring current density $(\vec{j} \parallel \vec{b})$ is increased or a small magnetic field $(\vec{B} \parallel \vec{c})$ is applied. Traces of this transition are also present at P=4.19 GPa. The resistivity starts to decrease but not as strong as at the preceding pressure. No signs of a magnetically ordered phase were found at higher temperature. Hence, if magnetism and superconductivity coexist, it occurs in a very narrow pressure range. Well above this pressure, no anomalies in the low temperature part of $\rho(T)$ are found (see curve at P=5.37 GPa in Fig. 6.11). Thus, these effects can be interpreted as hints for the occurrence of superconductivity in CeCu₅Au. But it is clear that additional experiments are necessary to clarify this point.

If the new phase should be found unequivocally to be a superconducting phase, the statement of low residual resistivity as an important ingredient for superconductivity will be obsolete. Just before $\rho(T)$ of CeCu₅Au starts to decrease, the resistivity is close to 40 $\mu\Omega$ cm (at 100 mK and P=3.84 GPa). As in the other pressure–induced HF superconductors, the superconductivity then would emerge in the vicinity of the magnetic instability. Therefore, it would be very likely, that AFM spin fluctuations could provide the "glue" for the Cooper–pairs.

Chapter 7

Conclusion

In this work we have attempted to shed more light on the structural evolution of the rare–earth based cuprates, to summarize the results of pressure–induced $T_{\rm c}$ changes in the high– $T_{\rm c}$ cuprates, and to supply more evidence for the unusual low temperature properties of heavy–fermion systems close to the magnetic instability. Synchrotron radiation was used to obtain the structural parameters of ${\rm La_{2-x}Nd_xCuO_4}$ (x=1,2) and ${\rm Pr_2CuO_4}$. The electrical resistance was measured on Hg– and Tl–based high– $T_{\rm c}$ compounds. Electrical resistivity and thermoelectric power measurements have been used to study the heavy–fermion systems.

The tetragonal T'-structure (Nd₂CuO₄-type) of La_{2-x}Nd_xCuO₄ (0.6 $\leq x \leq 2.0$) and Pr₂CuO₄ transforms into the T-structure (K₂NiF₄-type) at pressures $P_{\rm T}$. This transition pressure increases linearly with x and decreases linearly with the tolerance factor t, that is a measure for the stability of the structure. The stability is related to compressive stress in parts of the structure that weakens with decreasing average lanthanide ion size (i. e. $x \to 2$). As a consequence higher pressure is necessary to induce the structural transition. The occurrence of the orthorhombic O-phase, upon pressure release, can be understood if the (t, P) phase diagram is taken into account. The axis and volume compressibilities have been well described by a simple model that considers the linear compressibilities of different polyhedra building up the unit-cell.

The $T_c(P)$ dependence found for the high- T_c superconductors can be qualitatively explained in the scenario of a pressure-induced charge transfer. In originally underdoped cuprates, pressure induces a charge transfer, i. e. holes are transferred from a charge reservoir into the CuO₂-layers. The critical temperature increases as long as the charge carrier concentration n_h is below an optimum value. If the sample is overdoped, T_c decreases with pressure since n_h has passed the maximum of the parabolic $T_c/T_{c,max}$ versus n_h relation. The clear deviation of a parabolic $T_c(P)$ dependence in three and four layered Hg- (and Tl-) based superconductors was ascribed 7 Conclusion 77

to the presence of inequivalent CuO_2 –layers. Due to the weak proximity coupling between these layers, T_c is determined by the CuO_2 –layers with the highest pressure–induced T_c . At the same time, intrinsic effects contribute to a T_c enhancement. This has been demonstrated by pressure experiments on an optimally doped Tl–Pb–based superconductor. Pressure hardly induces any charge transfer and the main contribution to the T_c increase is thus due to intrinsic effects.

The experiments in the field of heavy–fermion compounds have contributed results to clarify several aspects of these strongly correlated electron systems. Magnetically ordered Ce–systems and non–magnetic Yb–compounds are tuned by pressure to the magnetic instability. In the former, long–range magnetic order is destroyed whereas in the latter magnetism starts to develop as pressure approaches a critical value P_c . The magnetic ordering temperature follows qualitatively the dependence given in the Doniach phase diagram, i. e. the exchange interaction J between the localized 4f– and conduction band electrons changes with pressure. In the case of CeRu₂Ge₂ and CeCu₅Au the $T_N(P)$ dependence scales to zero with a critical exponent predicted in the spin–fluctuation theory. Furthermore, a good agreement with the magnetic phase diagrams known from the solid–solutions CeRu₂(Si_{1-x}Ge_x)₂ and CeCu_{6-x}Au_x is observed if a certain correspondence between pressure and substitution content x is assumed.

A deviation of the electrical resistivity from a quadratic temperature dependence supports the idea of non–Fermi–liquid behaviour in $CeRu_2Ge_2$ and $CeCu_5Au$ close to $P_c=8.7\pm0.1$ GPa and 4.1 ± 0.3 GPa, respectively. The evolution of this behaviour with pressure might help to understand whether this behaviour is determined by the generic features of a quantum critical point or by the combination of a distribution of Kondo–temperatures, caused by disorder, and the competition of Kondo effect and RKKY–interaction.

The strong pressure dependence of the residual resistivity ρ_0 (measured at temperatures as low as 30 mK) in the HF compounds raises the question whether low–lying excitations contribute to a static part of ρ_0 , caused by all kinds of lattice imperfections. In CeCu₅Au the $\rho_0(P)$ dependence is clearly correlated with the magnetic ordering vector. This is supported by the similarity of $\rho_0(P)$ to the $\rho_0(x)$ variation observed in CeCu_{6-x}Au_x.

An new phase in $\text{CeCu}_{6-x}\text{Au}_x$ has been found below 100 mK in the pressure range 3.8 < P < 4.2 GPa. The sensitivity of $\rho(T)$ to the electrical current density and the magnetic field does not exclude a superconducting phase even if the resistivity drop was not complete. This feature and the anomalies in the residual resistivity mentioned above, suggest that charge and spin fluctuations might be present in this particular strongly correlated electron system.

78 7 Conclusion

Acknowledgement

This work comprises my scientific work carried out at different laboratories during the last six years. The structural investigations on ternary rare—earth based cuprates started at the Institut de Chimie de la Matière Condensée de Bordeaux (former Laboratoire de Chimie du Solide du CNRS). Many discussions with Dr. C. Cros helped me to set—up the x—ray measurements. This work was financially supported under the scope of the *Human Capital and Mobility Program* of the European Community (contract no. ERBCHBGCT920144). The investigation of the pressure induced changes in these compounds was completed with two runs at the European Synchrotron Radiation Facility in Grenoble at the beamline ID09. The success of the measurements is also due to the excellent technical support by Dr. M. Hanfland.

The high pressure work on the high– T_c compounds has been performed at the Vrije Universiteit Amsterdam. For this work I am again grateful for the financial support from the European Community under the same scope as mentioned above (contract no. ERBCHBICT940952). Fruitful discussions with Dr. D. Tristan Jover and the hospitality of Prof. R. Griessen's group are acknowledged.

In Geneva I studied the influence of pressure on the transport properties of heavy–fermion systems. At first I would like to thank Prof. J. Sierro for giving me the opportunity to become deeply involved in the high pressure physics of heavy–fermion compounds and supporting the composition of the present work. Many fruitful discussions with Dr. D. Jaccard, Dr. K. Alami–Yadri, and Dr. S. Raymond contributed much to the success of the high pressure work we did together. I am grateful to R. Cartoni for preparing the technical and schematic drawings and Dr. H. Kohlmann for carefully reading the whole manuscript. During the time in Geneva I received financial support from the Swiss National Science Foundation. I also express my thanks to all the other members of the Département de Physique de la Matière Condensée who supported me during my stay in Geneva.

- [1] J. G. Bednorz and K. A. Müller, Z. Phys. B 64, 189 (1986).
- [2] A. Schilling, M. Cantoni, J. D. Guo, and H. R. Ott, Nature 363, 56 (1993).
- [3] F. Steglich, J. Aarts, C. D. Bredl, W. Lieke, D. Meschede, W. Franz, and H. Schäfer, Phys. Rev. Lett. 43, 1892 (1979).
- [4] K. Miyake, S. Schmitt-Rink, and C. M. Varma, Phys. Rev. B 34, 6554 (1986).
- [5] C. C. Tsuei, J. R. Kirtley, C. C. Chi, L.-S. Yu-Jahnes, A. Gupta, T. Shaw, J. Z. Sun, and M. B. Ketchen, Phys. Rev. Lett. 73, 593 (1994).
- [6] H. Yasuoka, T. Imai, and T. Shimizu, in Strong Correlation and Superconductivity, edited by H. Fukuyama, S. Maekawa, and A. P. Malozemoff, Springer Verlag, 1989, p. 254.
- [7] J. Rossat-Mignod, L- P. Regnault, C. Vettier, P. Burges, P. Burlet, J. Bossy, J. Y. Henry, and G. Laperlot, Physica C 169, 58 (1991).
- [8] T. R. Chien, Z. Z. Wang, and N. P. Ong, Phys. Rev. Lett. 67, 2088 (1991).
- [9] M. Takigawa, A. P. Rayers, P. C. Hammel, J. D. Thompson, R. H. Heffner, Z. Fisk, and H. R. Ott, Phys. Rev. B 43, 247 (1991).
- [10] D. Jaccard, K. Behnia, and J. Sierro, Phys. Lett. A 163, 475 (1992).
- [11] N. D. Mathur, F. M. Grosche, S. R. Julian, I. R. Walker, R. K. W. Haselwimmer, and G. G. Lonzarich, Nature 394, 39 (1998).
- [12] P. Coleman, Physica B **259-261**, 353 (1999).
- [13] A. H. Castro Neto, G. Castilla, and B. A. Jones, Phys. Rev. Lett. 81, 3531 (1998).
- [14] M. Eremets, High Pressure Experimental Methods, Oxford University Press, Oxford, 1996.
- [15] A. Jayaraman, Rev. Mod. Phys. **55**, 65 (1983).
- [16] A. Jayaraman, Rev. Sci. Instrum. 57, 1013 (1986).
- [17] D. Tristan Jover, R. J. Wijngaarden, H. Wilhelm, S. M. Loureiro, J.-J. Capponi, A. Schilling, and H. R. Ott, Phys. Rev. B 54, 4265 (1996).
- [18] D. Jaccard, E. Vargoz, K. Alami-Yadri, and H. Wilhelm, Rev. High Pressure Sci. Technol. 7, 412 (1998).
- [19] E. S. Itskevich and V. F. Kraidenov, Instrum. Exp. Techn. 21, 1640 (1979).
- [20] V. Diatschenko and C. W. Chu, Rev. Sci. Instrum. 46, 1291 (1975).
- [21] D. L. Decker, J. Appl. Phys. 42, 3239 (1971).
- [22] J. D. Barnett, S. Block, and G. J. Piermarini, Rev. Sci. Instrum. 44, 1 (1973).
- [23] G. J. Piermarini, J. D. Barnett, and S. Block, J. Appl. Phys. 44, 5377 (1973).
- [24] H. K. Mao, P. M. Bell, J. W. Shaner, D. J. Steinberg, J. Appl. Phys. 49, 3276 (1978).
- [25] R. A. Noack and W. B. Holzapfel, High Pressure Sci. Technol. 1, 748 (1979).
- [26] D. D. Ragan, R. Gustavsen, and D. Schiferl, J. Appl. Phys. 72, 5539 (1992).
- [27] D. E. McCumber and M. D. Sturge, J. Appl. Phys. **34**, 1682 (1963).
- [28] A. Goñi and K. Syassen, in Semiconductors and Semimetals, Vol. 54, edited by R. K. Willardson and A. C. Beer, Academic Press, New York, 1998, p. 247.

- [29] L. D. Jennings and C. A. Swenson, Phys. Rev. 112, 31 (1958).
- [30] B. Bireckhoven and J. Wittig, J. Phys. E **21**, 841 (1988).
- [31] D. Erskine and P. Y. Yu, Rev. Sci. Instrum. 58, 406 (1987).
- [32] J. Thomasson, C. Ayache, I. L. Spain, M. Villedieu, J. Appl. Phys. 68, 5933 (1990).
- [33] J. H. Burnett, H. M. Cheong, and W. Paul, Rev. Sci. Instrum. 61, 3904 (1990).
- [34] H. Wilhelm, Ph.D. thesis, University Stuttgart, 1993.
- [35] H. Wilhelm, K. Alami-Yadri, B. Revaz, and D. Jaccard, Phys. Rev. B 59, 3651 (1999).
- [36] P. Bolsaitis and I. L. Spain, in *High Pressure Technology*, edited by I. L. Spain and J. Paauwe, Dekker, New York, Vol. 1, 1977, p.485.
- [37] W. B. Holzapfel, in *Molecular Systems Under High Pressure*, edited by R. Pucci and G. Piccitto, Elsevier Publisher, North-Holland, 1991, p. 61.
- [38] F. D. Murnaghan, Proc. Natl. Acad. Sci. USA 30, 244 (1944).
- [39] R. Jeanloz, Phys. Rev. B 38, 805 (1988).
- [40] F. Birch, Phys. Rev. **71**, 809 (1947).
- [41] P. Vinet, J. Ferrante, J. R. Smith, and J. H. Rose, J. Phys. C: Solid State Phys. 19, L467 (1986).
- [42] B. Coqblin, The Electronic Structure of Rare-Earth Metals and Alloys: the Magnetic Heavy Rare-Earths, edited by B. Coqblin, Academic Press, 1977.
- [43] F. J. Blatt, P. A. Schroeder, C. L. Foiles, and D. Greig, in *Thermoelectric Power of Metals*, Plenum Press, New York, 1976.
- [44] R. D. Barnard, Thermoelectricity in Metals and Alloys, Taylor and Francis Ltd., London, 1972.
- [45] S. M. M. Evans, A. K. Bhattacharjee, and B. Coqblin, Phys. Rev. B 45, 7244 (1992).
- [46] J. M. Ziman, Electron and Phonons, Claredon Press, Oxford, 1960.
- [47] D. L. Cox and N. Grewe, Z. Phys. B 57, 281 (1988).
- [48] K. H. Fischer, Z. Phys. B **76**, 315 (1989).
- [49] R. P. Huebner, in Solid State Physics, Vol. 27, edited by H. Ehrenreich, F. Seitz, and D. Turnbull, Academic Press, New York, 1972, p.63.
- [50] N. F. Mott, Ann. Phys. (France) 10, 55 (1985).
- [51] Y. Tokura, H. Takagi, and S. Uchida, Nature **337**, 345 (1989).
- [52] Y. Maeno, H. Hashimoto, K. Yoshida, S. Nishizaki, T. Fujita, J. G. Bednorz, and F. Lichtenberg, Nature 372, 532 (1994).
- [53] C. W. Chu, P. H. Hor, R. L. Meng, L. Gao, Z. J. Huang, and Y. Q. Wang, Phys. Rev. Lett. 58, 405 (1987).
- [54] N. Shirakawa, K. Murata, S. Nishizaki, Y. Maeno, and T. Fujita, Phys. Rev. B 56, 7890 (1997).
- [55] S. Katano, N. Môri, H. Takahashi, and H. Takei, J. Phys. Soc. Jpn. 58, 3890 (1989).
- [56] N. Yamada and M. Ido, Physica C 203, 240 (1992).
- [57] J.-S. Zhou, H. Chen, and J. B. Goodenough Phys. Rev. B 49, 9084 (1994).
- [58] J.-S. Zhou, J. B. Goodenough, H. Sato, and M. Naito, Phys. Rev. B 59, 3827 (1999).
- [59] H. Takahashi, H. Shaked, B. A. Hunter, P. G. Radaelli, R. L. Hitterman, D. G. Hinks, and J. D. Jorgensen, Phys. Rev. B 50, 3221 (1994).
- [60] C. Murayama, N. Môri, S. Yomo, H. Takagi, S. Uchida, and Y. Tokura, Nature 339, 293 (1989).
- [61] N. M. Pyka, A. Metz, M. Loewenhaupt, R. van de Kamp, Physica B 241-243, 865 (1998).
- [62] J. W. Lynn, I. W. Sumarlin, S. Skanthakumar, W.-H. Li, R. N. Shelton, J. L. Peng, Z. Fisk, and S.-W. Cheong, Phys. Rev. B 41, 2569 (1990).
- [63] T. Brugger, T. Schreiner, G. Roth, P. Adelmann, and G. Czjek, Phys. Rev. Lett. 71, 2481 (1993).
- [64] P. Fulde, V. Zevin, and G. Zwicknagl, Z. Phys. B **92**, 133 (1993).
- [65] M. B. Maple, B. W. Lee, J. J. Neumeier, G. Nieva, L. M. Paulius, and C. L. Seaman, J. Alloys Comp. 181, 135 (1992).

[66] S. Katano, N. Môri, H. Takahashi, T. Kobayashi, and J. Akimitsu, J. Phys. Soc. Jpn. 59, 1928 (1990).

- [67] B. Grande, H. Müller-Buschbaum, and M. Schweitzer, Z. Anorg. Allg. Chem. 428, 120 (1977).
- [68] J. Shu, J. Akella, J. Z. Liu, H. K. Mao, and L. Finger, Physica C 176, 503 (1991).
- [69] H. Müller-Buschbaum and W. Wollschläger, Z. Anorg, Allg. Chem. 414, 76 (1975).
- [70] A. Neuhaus, Chimia 18, 93 (1964).
- [71] H. Wilhelm, C. Cros, E. Reny, G. Demazeau, and M. Hanfland, J. Mater. Chem. 8, 2729 (1998).
- [72] H. Wilhelm, C. Cros, E. Reny, G. Demazeau, and M. Hanfland, to be published in J. Solid State Chem.
- [73] V. M. Goldschmidt, Akad. Oslo I. Mater. Natur. No.2, 7 (1926).
- [74] P. Ganguly and C. N. Rao, J. Solid State Chem. 53, 193 (1984).
- [75] R. D. Shannon, Acta Crystallogr. Sect. A 32, 751 (1976).
- [76] A. Manthiram and J. B. Goodenough, J. Solid State Chem. 87, 402 (1990).
- [77] J. F. Bringley, S. S. Trail, and B. A. Scott, J. Solid State Chem. 86, 310 (1990).
- [78] N. Kimizuka, E. Takayama, and S. Horiuchi, J. Solid State Chem. 42, 322 (1962).
- [79] H. Okada, M. Takano, and Y. Takeda, Physica C 166, 111 (1990).
- [80] H. Wilhelm, C. Cros, F. Arrouy, and G. Demazeau, J. Solid State Chem. 126, 88 (1996).
- [81] R. M. Hazen and L. W. Finger, Comparative Crystal Chemistry, Wiley Chichester, 1982.
- [82] A. L. Cornelius, S. Klotz, and J. S. Schilling, Physica C 197, 209 (1992).
- [83] T. Kamiyama, F. Izumi, H. Takahashi, J. D. Jorgensen, D. Dabrowski, R. L. Hitterman, D. G. Hinks, H. Shaked, T. O. Mason, and M. Seabaugh, Physica C 229, 377 (1994).
- [84] C. W. Chu, J. Supercond. 7, 1 (1994).
- [85] H. Takahashi and N. Môri, in *Studies of High Temperature Superconductors*, Vol. 16, edited by A. V. Narlikar, Nova Science Publisher Inc., New York, 1997, p. 1.
- [86] M. K. Wu, J. R. Ashburn, C. T. Torng, P. H. Hor, R. L. Meng, L. Gao, Z. J. Huang, Y. Q. Wang, and C. W. Chu, Phys. Rev. Lett. 58, 908 (1987).
- [87] T. A. Vanderah and C. K. Lowe-Ma, J. Supercond. 7, 107 (1994).
- [88] J. D. Jorgensen, B. W. Veal, A. P. Paulikas, L. J. Nowicki, G. W. Crabtree, H. Claus, and W. K. Kwok, Phys. Rev. B 41, 1863 (1990).
- [89] A. Driessen, R. Griessen, N. Koeman, E. Salomons, R. Brouwer, D. G. de Groot, K. Heeck, H. Hemmes, and J. Rector, Phys. Rev. B 36, 5602 (1987).
- [90] S. Klotz, W. Reith, and J. S. Schilling, Physica C 172, 423 (1991).
- [91] J. J. Neumeier and H. A. Zimmermann, Phys. Rev. B 47, 8385 (1993).
- [92] Z. Z. Sheng and A. M. Herrmann, Nature 332, 55 (1988).
- [93] S. N. Putilin, E. V. Antipov, O. Chmaissem, and M. Marezio, Nature 362, 226 (1993).
- [94] R. S. Liu, J. L. Tallon, and P. P. Edwards, Physica C 182, 119 (1991).
- [95] D. Tristan Jover, R. J. Wijngaarden, R. S. Liu, J. L. Tallon, and R. Griessen, Physica C 218, 24 (1993).
- [96] C. W. Chu, L. Gao, F. Chen, Z. J. Huang, R. L. Meng, and Y. Y. Xue, Nature 365, 323 (1993).
- [97] M. Nuñez-Regueiro, J. L. Tholence, E. V. Antipov, J.-J. Capponi, and M. Marezio, Science 262, 97 (1993).
- [98] H. Takahashi, A. Tokiwa-Yamamoto, N. Môri, S. Adachi, H. Yamauchi, and S. Tanaka, Physica C 218, 1 (1993).
- [99] L. Gao, Y. Y. Xue, F. Chen, Q. Xiong, R. L. Meng, D. Ramirez, C. W. Chu, J. H. Eggert, and H. K. Mao, Phys. Rev. B 50, 4260 (1994).
- [100] B. A. Scott, E. Y. Suard, C. C. Tsuei, D. B. Mitzi, T. R. McGuire, B.-H. Chen, and D. Walker, Physica C 230, 239 (1994).
- [101] M. Takano, M. Azuma, Z. Hiroi, Y. Bando, and Y. Takeda, Physica C 176, 441 (1991).

[102] J. S. Schilling and S. Klotz, in *Physical Properties of High Temperature Superconductors*, edited by D. M. Ginsburg, World Scientific, Singapore, 1992, Vol. 3, p. 59.

- [103] M. R. Presland, J. L. Tallon, R. G. Buckley, R. S. Liu, N. E. Flower, Physica C 176, 95 (1991).
- [104] G. V. M. Williams and J. L. Tallon, Phys. Rev. B 59, 3911 (1999).
- [105] J. L. Tallon, C. Bernhard, H. Shaked, R. L. Hitterman, and J. D. Jorgensen, Phys. Rev. B 51, 12911 (1991).
- [106] C. C. Almasan, S. H. Han, B. W. Lee, L. M. Paulius, M. B. Maple, B. W. Veal, J. W. Downey, A. P. Paulikas, Z. Fisk, and J. E. Schirber, Phys. Rev. Lett. 69, 680 (1992).
- [107] B. Bucher, E. Kaldis, Ch. Krüger, and P. Wachter, Europhys. Lett. 34, 391 (1996).
- [108] R. Benischke, T. Weber, W. H. Fietz, J. Metzger, K. Grube, T. Wolf, and H. Wühl, Physica C 203, 293 (1992).
- [109] M. Kosuge, T. Maeda, K. Sakuyama, T. Miyatake, N. Koshizuka, H. Yamauchi, H. Takahashi, C. Murayama, and N. Môri, Phys. Rev. B **45**, 10713 (1992).
- [110] W. H. Fietz, R. Quenzel, H. A. Ludwig, K. Grube, S. I. Schlachter, F. W. Hornung, T. Wolf, A. Erb, M. Kläser, and G. Müller-Vogt, Physica C **270**, 258 (1996).
- [111] R. Sieburger and J. S. Schilling, Physica C 173, 403 (1991).
- [112] A. K. Klehe, C. Looney, J. S. Schilling, H. Takahashi, N. Môri, Y. Shimakawa, Y. Kubo, T. Manako, S. Doyle, A. M. Herrman, Physica C 257, 105 (1996).
- [113] B. W. Veal, H. You, A. P. Paulikas, H. Shi, Y. Fang, and J. W. Downey, Phys. Rev. B 42, 4770 (1990).
- [114] J. S. Schilling, C. Looney, S. Sadewasser, and Y. Wang, Rev. High Pressure Sci. Technol. 7, 425 (1998).
- [115] R. S. Liu, P. P. Edwards, Y. T. Huang, S. F. Wu, and P. T. Wu, J. Solid State Chem. 86, 334 (1990).
- [116] D. Tristan Jover, H. Wilhelm, R. J. Wijngaarden, and R. S. Liu, Phys. Rev. B 55, 11832 (1997).
- [117] H. Kierspel, H. Winkelmann, T. Auweiler, W. Schablitz, B. Büchner, V. H. M. Duijn, N. T. Hien, A. A. Menovsky, and J. J. M. Franse, Physica C 262, 177 (1996).
- [118] X. D. Qiu, Q. Xiong, L. Gao, Y. Cao, Y. Y. Xue, and C. W. Chu, Physica C 282-287, 885 (1997).
- $[119]\,$ F. Gugenberger, C. Meingast, G. Roth, K. Grube, V. Breit, T. Weber, and H. Wühl, Phys. Rev. B ${\bf 49},\,13137$ (1994).
- [120] C. Meingast, O. Kraut, T. Wolf, H. Wühl, A. Erb, and G. Müller-Vogt, Phys. Rev. Lett. 67, 1634 (1991).
- [121] U. Welp, M. Grimsditch, S. Fleshler, W. Nessler, J. Downey, G. W. Crabtree, and J. Guimpel, Phys. Rev. Lett. 69, 2130 (1992).
- [122] J.-P. Locquet, J. Perret, J. Fompeyrine, E. Mächler, J. W. Seo, and G. Van Tendeloo, Nature **394**, 453 (1998).
- [123] O. Kraut, C. Meingast, G. Bräuchle, H. Claus, A. Erb, G. Müller-Vogt, and H. Wühl, Physica C 205, 139 (1993).
- [124] G. V. M. Williams and J. L. Tallon, Physica C 258, 41 (1996).
- [125] W. Pickett, Phys. Rev. Lett. **78**, 1960 (1997).
- [126] Z. Zou, J. Ye, K. Oka, and Y. Nishihara, Phys. Rev. Lett. 80, 1074 (1998).
- [127] J. Ye, Z. Zou, A. Matsushita, J. K. Oka, Y. Nishihara, and T. Matsumoto, Rev. High Pressure Sci. Technol. 7, 577 (1998).
- [128] J. L. Tallon and N. E. Flower, Physica C **204**, 237 (1993).
- [129] T. B. Lindemer, B. C. Chakoumakos, E. D. Specht, R. K. Williams, and Y. J. Chen, Physica C 231, 80 (1994).
- [130] S. A. Sunshine, L. F. Schneemeyer, J. V. Waszczak, D. W. Murphy, S. Miraglia, A. Santoro, and F. Beech, J. Cryst. Growth 85, 632 (1987).
- [131] C. Meingast, J. Karpinski, E. Jilek, and E. Kaldis, Physica C **209**, 591 (1993).
- [132] B. Bucher, J. Karpinski, E. Kaldis, and P. Wachter, Physica C 157, 478 (1989).

[133] E. N. van Eenige, R. Griessen, R. J. Wijngaarden, J. Karpinski, E. Kaldis, S. Rusiecki, and E. Jilek, Physica C **168**, 482 (1990).

- [134] W. H. Fietz, H. A. Ludwig, B. P. Wagner, K. Grube, R. Benischke, and H. Wühl, in *Frontiers of High Pressure Research*, edited by H. D. Hochheimer and R. D. Etters, NATO ASI, Vol. B 286, Plenum Press, New York, 1992, p. 433.
- [135] R. J. Wijngaarden, E. N. van Eenige, J. J. Scholtz, and R. Griessen, Physica C 185-189, 787 (1991).
- [136] R. J. Wijngaarden, J. J. Scholtz, E. N. van Eenige, and R. Griessen, in Frontiers of High Pressure Research, edited by H. D. Hochheimer and R. D. Etters, NATO ASI, Vol. B 286, Plenum Press, New York, 1992, p. 399.
- [137] M. Kakihana, H. Arashi, M. Yashima, M. Yoshimura, L. Börjesson, and M. Käll, Physica C 230, 199 (1994).
- [138] N. Watanabe, M. Kosuge, N. Koshizuka, S. Adachi, and H. Yamauchi, Phys. Rev. B 49, 9226 (1994).
- [139] E. M. Haines and J. L. Tallon Phys. Rev. B 45, 3172 (1992).
- [140] see AID Document No. E-PAPS: E-PRBMD-54-10175-0.254MB. The E-PAPS document file may be retrieved free of charge from the FTP server http://www.aip.org/epaps/epaps.html.
- [141] D. Tristan Jover, Ph.D. thesis, Free University Amsterdam, 1996.
- [142] D. Tristan Jover, R. J. Wijngaarden, R. Griessen, E. M. Haines, J. L. Tallon, and R. S. Liu, Phys. Rev. B 54, 10175 (1996).
- [143] L. Gao, Y. Y. Xue, F. Chen, Q. Xiong, R. L. Meng, D. Ramirez, C. W. Chu, J. H. Eggert, and H. K. Mao, Physica C 235-240, 1493 (1994).
- [144] C. Acha, M. Nuñez-Regueiro, S. Le Floch, P. Bordet, J.-J. Capponi, C. Chaillant, and J. L. Tholence, Phys. Rev. B 57, R5630 (1999).
- [145] R. J. Wijngaarden, D. Tristan Jover, and R. Griessen, Physcia B 265, 128 (1999).
- [146] L. Jansen and R. Block, Physica A **212**, 143 (1994).
- [147] L. Jansen and R. Block, Physica A 247, 265 (1997).
- [148] G. M. Zhao, M. B. Hunt, H. Keller, and K. A. Müller, Nature 385, 236 (1997).
- [149] N. W. Ashcroft and N. D. Mermin, Solid State Physics, W. B. Saunders Company, 1976.
- [150] D. Pines and P. Nozières, The Theory of Quantum Liquids, W. A. Benjamin, 1966.
- [151] H. R. Ott, H. Rudigier, Z. Fisk, J. O. Willis, and G. R. Steward, Solid State Commun. 53, 235 (1985).
- [152] H. Aoki, S. Uji, A. K. Albessard, Y. Ōnuki, J. Phys. Soc. Jpn. 61, 3457 (1992).
- [153] Z. Fisk, H. R. Ott, and G. Aeppli, Jpn. J. Appl. Phys. 26, Suppl. 3, 1882 (1987).
- [154] P. Nozières, J. Low Temp. Phys. 17, 31 (1974).
- [155] K. Kadowaki and S. B. Woods, Solid State Commun. 58, 507 (1986).
- [156] N. Grewe and F. Steglich, in Handbook of Physics and Chemistry of Rare Earths, Vol. 14, edited by K. A. Gschneidner Jr. and L. Eyring, Elsevier, Amsterdam, 1991, p. 343.
- [157] H. v. Löhneysen, A. Schröder, T. Trappmann, and M. Welsch, J. Magn. Magn. Matter. 108, 45 (1992).
- [158] P. Haen, H. Bioud, and T. Fukuhara, Physica B **259-261**, 85 (1999).
- [159] J. Kondo, Prog. Theor. Phys. **32**, 37 (1964).
- [160] S. Raymond, private communication.
- [161] Y. Ōnuki, Y. Shimizu, and T. Komatsubara, J. Phys. Soc. Jpn. 54, 304 (1985).
- [162] H. R. Ott, in *Progress in Low Temperature Physics*, Vol. XI, edited by D. F. Brewer, Elsevier Science Publishers B. V., Amsterdam, 1987, p. 215.
- [163] T. Kasuya, in *Magnetism*, Vol. IIb, edited by G. T. Rado and H. Suhl, Academic Press, Amsterdam, 1966.
- [164] S. Doniach, Physica B **91**, 231 (1977).

[165] See for example the *Proceedings of the Conference on Non-Fermi-Liquid Behaviour in Metals*, Santa Barbara, edited by P. Coleman, M. B. Maple, and A. Millis, J. Phys.: Condens. Matter **8** (1996).

- [166] N. B. Brandt and V. V. Moschchalkov, Adv. Phys. 33, 374 (1984).
- [167] E. Bauer, Adv. Phys. 40, 417 (1991).
- [168] J. D. Thompson and J. M. Lawrence, in *Handbook of Physics and Chemistry of Rare Earths*, Vol. 19, edited by K. A. Gschneidner Jr., L. Eyring, G. H. Lander, and G. R. Choppin, Elsevier Science B. V., 1994, p. 383.
- [169] S. Raymond, P. Haen, R. Calemczuk, S. Kambe, B. Fåk, P. Lejay, T. Fukuhara, and J. Flouquet, to be published in J. Phys.: Condens. Matter.
- [170] S. Süllow, M. C. Aronson, B. D. Rainford, and P. Haen, Phys. Rev. Lett. 82, 2963 (1999).
- [171] H. Wilhelm and D. Jaccard, Solid State Commun. 106, 239 (1998).
- [172] T. C. Kobayashi, T. Miyazu, K. Shimizu, K. Amaya, Y. Kitaoka, Y. Ōnuki, M. Shirase, and T. Takabatake, Phys. Rev. B 57, 5025 (1998).
- [173] A. Böhm, R. Caspary, U. Habel, L. Pawlak, A. Zuber, F. Steglich, and A. Loidl, J. Magn. Magn. Matter. 76&77, 150 (1988).
- [174] J. Dakin, G. Rapson, and B. D. Rainford, J. Magn. Magn. Matter. 108, 117 (1992).
- [175] S. Raymond, D. Raoelison, S. Kambe, L. P. Regnault, B. Fåk, R. Calemczuk, J. Flouquet, P. Haen, and P. Lejay, Physica B 259-261, 48 (1999).
- [176] P. Fulde, Physica B 230-232, 1 (1997).
- [177] I. L. Spain, F. Steglich, U. Rauchschwalbe, and H. D. Hochheimer, Physica B 139&140, 449 (1986).
- [178] C. Wassilew–Reul, private communication, and C. Wassilew-Reul, M. Kunz, M. Hanfland, D. Häusermann, C. Geibel, and F. Steglich, Physica B **230-232**, 310 (1997).
- [179] P. Haen, F. Mallmann, M. J. Besnus, J. P. Kappler, F. Bourdarot, P. Burlet, and T. Fukuhara, J. Phys. Soc. Jpn. 65, Suppl. B, 16 (1996).
- [180] J.-M. Mignot, L. P. Regnault, J.-L. Jacoud, J. Rossat-Mignod, P. Haen, and P. Lejay, Physica B 171, 357 (1991).
- [181] P. Lehmann, Ph. D. Thesis, University of Strasbourg, 1987.
- [182] P. Haen, J.-M. Laurant, K. Payer, and J.-M.Mignot, in *Transport and Thermal Properties of felectron systems*, by G. Oomi et al., Plenum Press 1993, p. 145.
- [183] R. Mock, B. Hillebrands, H. Schmidt, G. Güntherodt, Z. Fisk, and A. Meyer, J. Magn. Magn. Matter. 47&48, 312 (1985).
- [184] L. P. Regnault, W. A. C. Erkelens, J. Rossat-Mignod, P. Lejay, and J. Flouquet, Phys. Rev. B 38, 4481 (1988).
- [185] A. Loidl, K. Knorr, G. Knopp, A. Krimmel, R. Caspary, A. Böhm, G. Sparn, C. Geibel, F. Steglich, and A. P. Murani, Phys. Rev. B 46, 9341 (1992).
- [186] J.-M. Mignot, J.-L. Jacoud, L. P. Regnault, J. Rossat-Mignod, P. Haen, P. Lejay, Ph. Boutrouille, B. Hennion, and D. Petitgrand, Physica B **163**, 611 (1990).
- [187] J. R. Schrieffer and P. A. Wolff, Phys. Rev. B 149, 491 (1966).
- [188] W. A. Harrison and G. K. Straub, Phys. Rev. B **36**, 2695 (1987).
- [189] B. D. Rainford, J. Dakin, and A. Severing, J. Magn. Magn. Matter. 108, 119 (1992).
- [190] M. J. Besnus, J. P. Kappler, P. Lehmann, and A. Meyer, Solid State Commun. 55, 779 (1985).
- [191] P. Link, D. Jaccard, and P. Lejay, Physica B 225, 207 (1996).
- [192] R. Felten, G. Weber, and H. Rietschel, J. Magn. Magn. Matter. **63&64**, 383 (1987).
- [193] H. Wilhelm, D. Jaccard, and T. Kobayashi, to be published.
- [194] C. Paschke, C. Speck, G. Portisch, and H. v. Löhneysen, J. Low Temp. Phys. 97, 229 (1994).
- [195] B. Stroka, A. Schröder, T. Trappmann, H. v. Löhneysen, M. Loewenhaupt, and A. Severing, Z. Phys. B 90, 155 (1993).
- [196] K. Hanazawa, K. Yamada, and K. Yoshida, J. Magn. Magn. Mater. 47&48, 357 (1985).

[197] H. v. Löhneysen, M. Sieck, O. Stockert, and M. Waffenschmidt, Physica B 223&224, 471 (1996).

- [198] K. Alami-Yadri and D. Jaccard, Solid State Commun. 100, 385 (1996).
- [199] K. Alami-Yadri, H. Wilhelm, and D. Jaccard, Eur. Phys. J. B 6, 5 (1998).
- [200] K. Alami-Yadri, H. Wilhelm, and D. Jaccard, Solid State Commun. 108, 279 (1998).
- [201] P. Nozières and A. Blandin, J. Phys. 41, 193 (1980).
- [202] D. L. Cox, Phys. Rev. Lett. **59**, 1240 (1987).
- [203] B. Andraka and A. M. Tsvelik, Phys. Rev. Lett. 67, 2886 (1991).
- [204] C. L. Seaman, M. B. Maple, B. W. Lee, S. Ghamaty, M. S. Torikachvili, J.-S. Kang, L. Z. Liu, J. W. Allen, D. L. Cox, Phys. Rev. Lett. 67, 2882 (1991).
- [205] S. Süllow, unpublished, 1994.
- [206] E. Miranda, V. Dobrosavljević, and G. Kotilar, Phys. Rev. Lett. 78, 290 (1997).
- [207] V. Dobrosavljević, T. R. Kirkpatrick, G. Kotilar, Phys. Rev. Lett. 69, 1113 (1992).
- [208] O. O. Bernal, D. E. MacLaughlin, H. G. Lukefahr, and B. Andraka, Phys. Rev. Lett. 75, 2023 (1995).
- [209] D. E. MacLaughlin, R. H. Heffner, G. J. Nieuwenhuys, G. M. Luke, Y. Fudamoto, Y. J. Ummura, R. Chau, M. B. Maple, and B. Andraka, Phys. Rev. B 58, R11849 (1998).
- [210] M. C. de Andrade, R. Chau, N. R. Dilly, E. J. Freeman, D. A. Gajewski, M. B. Maple, R. Movshovich, A. H. Castro Neto, G. Castilla, and B. A. Jones, Phys. Rev. B 81, 5620 (1998).
- [211] S. Sachdev, N. Read, and R. Oppermann, Phys. Rev. B 52, 10286 (1995).
- [212] T. Moriya and T. Takimoto, J. Phys. Soc. Jpn. **64**, 960 (1995).
- [213] A. J. Millis, Phys. Rev. B 48, 7183 (1993).
- [214] F. D. M. Haldane, Phys. Rev. Lett. 45, 1358 (1980).
- [215] B. Dardel, D. Malterre, M. Grioni, P. Weibel, Y. Baer, J. Voit, and D. Jérôme, Europhys. Lett. 24, 687 (1993).
- [216] X. G. Wen, Phys. Rev. B 41, 12838 (1990).
- [217] C. M. Varma, P. B. Littlewood, S. Schmitt-Rink, E. Abrahams, and A. E. Ruckenstein, Phys. Rev. Lett. 63, 1996 (1989).
- [218] H. v. Löhneysen, J. Phys.: Condens. Matter 8, 9689 (1996).
- [219] F. Steglich, B. Buschinger, P. Gegenwart, M. Lohmann, R. Helfrich, C. Langhammer, P. Hellmann, L. Donnevert, S. Thomas, A. Link, C. Geibel, M. Lang, G. Sparn, and W. Assmus, J. Phys.: Condens. Matter 8, 9909 (1996).
- [220] P. Gegenwart, C. Langhammer, C. Geibel, R. Helfrich, M. Lang, G. Sparn, F. Steglich, R. Horn, L. Donnevert, A. Link, and W. Assmus, Phys. Rev. Lett. 81, 1501 (1998).
- [221] P. Gegenwart, F. Kromer, M. Lang, G. Sparn, C. Geibel, and F. Steglich, Phys. Rev. Lett. 82, 1293 (1999).
- [222] F. M. Grosche, S. R. Julian, N. D. Mathur, and G. G. Lonzarich, Physica B 223&224, 50 (1996).
- [223] S. R. Julian, F. V. Carter, F. M. Grosche, R. K. W. Haselwimmer, S. J. Lister, N. D. Mathur, G. J. McMullan, C. Pfleiderer, S. S. Saxena, I. R. Walker, N. J. Wilson, and G. G. Lonzarich, J. Magn. Magn. Mater. 177-181, 265 (1998).
- [224] H. Wilhelm, S. Raymond, D. Jaccard, O. Stockert, and H. v. Löhneysen, to be published in the Proceedings of the 17th AIRAPT conference, Hawaii, 1999.
- [225] H. G. Schlager, A. Schröder, M. Welsch, and H. v. Löhneysen, J. Low Temp. Phys. 90, 181 (1993).
- [226] H. v. Löhneysen, J. Magn. Magn. Mater. 157/158, 601 (1996).
- [227] A. Neubert, T. Pietrus, O. Stockert, H. v. Löhneysen, A. Rosch, and P. Wölfle, Physica B 230-232, 587 (1997).
- [228] S. J. S. Lister, F. M. Grosche, F. V. Carter, R. K. W. Haselwimmer, S. S. Saxena, N. D. Mathur, S. R. Julian, and G. G. Lonzarich, Z. Phys. B 103, 263 (1997).
- [229] P. Link, D. Jaccard, and P. Lejay, Physica B **223&224**, 303 (1996).

[230] F. Steglich, P. Gegenwart, R. Helfrich, C. Langhammer, P. Hellmann, L. Donnevert, C. Geibel, M. Lang, G. Sparn, W. Assmus, G. R. Stewart, and A. Ochiai, Z. Phys. B 103, 235 (1997).

- [231] K. Miyake, O. Narikiyo, and Y. Onishi, Physica B 259-261, 676 (1999).
- [232] H. Winkelmann, M. M. Abd-Elmeguid, H. Micklitz, J. P. Sanchez, P. Vulliet, K. Alami-Yadri, and D. Jaccard, Phys. Rev. B. 60, 3324 (1999).
- [233] J. Flouquet, P. Haen, F. Lapierre, C. Fierz, A. Amato, and D. Jaccard, J. Magn. Magn. Matter. 76-77, 285 (1988).
- [234] J. M. Lawrence, J. D. Thompson, and Y. Y. Chen, Phys. Rev. Lett. 54, 2537 (1985).
- [235] F. G. Aliev, N. B. Brandt, V. V. Moschchalkov, V. I. Sidorov, and R. V. Lutsiv, Sov. Phys. Solid State 24, 1786 (1982).
- [236] T. Graf, R. Movshovich, J. D. Thompson, Z. Fisk, P. C. Canfield, Phys. Rev. B 52, 3099 (1995).
- [237] H. Wilhelm, S. Raymond, D. Jaccard, O. Stockert, and H. v. Löhneysen, to be published.
- [238] H. v. Löhneysen, A. Neubert, A. Schröder, O. Stockert, U. Tutsch, M. Loewenhaupt, A. Rosch, and P. Wölfle, Eur. Phys. J. B 5, 447 (1998).
- [239] O. Stockert, H. v. Löhneysen, A. Rosch, N. Pyka, and M. Loewenhaupt, Phys. Rev. Lett. 80, 5627 (1998).
- [240] C. Geibel, C. Schank, S. Thies, H. Kitazawa, C. D. Bredl, A. Böhm, M. Rau, A. Granel, R. Caspary, R. Helfrich, U. Ahlheim, G. Weber, and F. Steglich, Z. Phys. B 84, 1 (1991).
- [241] C. Geibel, S. Thies, D. Kaczorowski, A. Mehner, A. Granel, B. Seidel, U. Ahlheim, R. Helfrich, K. Petersen, C. D. Bredl, and F. Steglich, Z. Phys. B 83, 305 (1991).
- [242] G. Bruls, D. Weber, B. Wolf, P. Thalmeier, B. Lüthi, A. de Visser, and A. Menovsky, Phys. Rev. Lett. 65, 2294 (1990).
- [243] S. M. Hayden, L. Taillefer, C. Vettier, and J. Flouquet, Phys. Rev. B 46, 8675 (1992).
- [244] H. R. Ott, H. Rudigier, Z. Fisk, and J. L. Smith, Phys. Rev. Lett. 50, 1595 (1983).
- [245] H. R. Ott, H. Rudigier, Z. Fisk, and J. L. Smith, Phys. Rev. B 31, 1651 (1985).
- [246] M. Grosche, P. Agarwal, S. R. Julian, N. J. Wilson, R. K. W. Haselwimmer, S. J. S. Lister, N. D. Mathur, F. V. Carter, S. S. Saxena, and G. G. Lonzarich, cond-mat/9812133.
- [247] R. Movshovich, T. Graf, D. Mandrus, J. D. Thompson, J. L. Smith, and Z. Fisk, Phys. Rev. B 53, 8241 (1996).
- [248] B. H. Grier, J. M. Lawrence, V. Murgai, and R. D. Parks, Phys. Rev. B 29, 2664 (1984).
- [249] E. Vargoz, P. Link, D. Jaccard, T. Le Bihan, and S. Heathman, Physica B 229, 225 (1997).
- [250] A. A. Abrikosov and L. P. Gor'kov, Sov. Phys. JETP 12, 1243 (1961).
- [251] R. A. Fisher, S. Kim, B. F. Woodfield, N. E. Phillips, L. Taillefer, K. Hasselbach, J. Flouquet, A. L. Giorgi, and J. L. Smith, Phys. Rev. Lett. 62, 1411 (1989).
- [252] A. Amato, Rev. Mod. Phys. **69**, 1119 (1997).
- [253] Ø. Fischer, Appl. Phys. **16**, 1 (1978).
- [254] D. Jaccard, H. Wilhelm, K. Alami-Yadri, and E. Vargoz, Physica B **259-261**, 1 (1999).

- [255] H. v. Löhneysen, Physica B **206&207**, 101 (1995).
- [256] S. Kambe, S. Raymond, L.-P. Regnault, J. Flouquet, P. Lejay, and P. Haen, J. Phys. Soc. Jpn. 65, 3294 (1996).
- [257] P. W. Anderson, in Valence Fluctuations in Solids, edited by L. M. Falicov, W. Hanke, and M. B. Maple, North-Holland Publishing Company, Amsterdam, 1981, p. 451.
- [258] H. Wilhelm and D. Jaccard, Physica B **259-261**, 79 (1999).
- [259] H. Okumura, K. Kakurai, Y. Yoshida, Y. Onuki, and Y. Endoh, J. Magn. Magn. Mater. 177-181, 405 (1998).
- [260] U. Walter, D. Wohlleben, and Z. Fisk, Z. Phys. B 62, 325 (1986).
- [261] A. Amato. Ph.D. Thesis, University of Geneva (1988).
- [262] A. Germann and H. v. Löhneysen, Europhys. Lett. 9, 367 (1989).
- [263] M. Ruck, G. Portisch, H. G. Schlager, M. Sieck, and H. v. Löhneysen, Acta Cryst. B 49, 936 (1993).
- [264] H. v. Löhneysen, T. Pietrus, G. Portisch, H. G. Schlager, A. Schröder, M. Sieck, and T. Trappmann, Phys. Rev. Lett. **72**, 3262 (1994).
- [265] A. Schröder, J. W. Lynn, R. W. Erwin, M. Loewenhaupt, and H. v. Löhneysen, Physica B 199&200, 47 (1994).
- [266] S. Mock, C. Paschke, A. Schröder, J. Sereni, M. Sieck, and H. v. Löhneysen, Physica B 199&200, 39 (1994).
- [267] M. Sieck, F. Huster, and H. v. Löhneysen, Physica B **230-232**, 583 (1997).
- [268] H. v. Löhneysen, Physica B **230-232**, 550 (1997).
- [269] A. Rosch, A. Schröder, O. Stockert, and H. v. Löhneysen, Phys. Rev. Lett. 79, 159 (1997).
- [270] H. v. Löhneysen, S. Mock, A. Neubert, T. Pietrus, A. Rosch, A. Schröder, O. Stockert, and U. Tutsch, J. Magn. Magn. Mater. 177-181, 12 (1998).
- [271] A. Rosch, Phys. Rev. Lett. 82, 4280 (1999).
- [272] D. M. Adams, R. Appleby, and S. K. Sharma, J. Phys. 9, 1140 (1976).
- [273] W. H. Fietz, C. A. Wassilew, D. Ewert, M. R. Dietrich, H. Wühl, D. Hochheimer, and Z. Fisk, Phys. Lett. A 142, 300 (1989).
- [274] R. P. Gupta and M. Gupta, Physica C 171, 465 (1990).
- [275] R. P. Gupta and M. Gupta, Physica C 178, 414 (1991).
- [276] A. Erb, E. Walker, J.-Y. Genoud, and R. Flükiger, Physica C 282-287, 89 (1997).
- [277] J.-M. Mignot, A. Ponchet, P. Haen, F. Lapierre, and J. Flouquet, Phys. Rev. B 40, 10917 (1989).
- [278] S. Imada, M. Tsunekawa, T. Iwasaki, S. Suga, Y. Ōnuki, F. Iga, M. Kasaya, Y. Kawasaki, K. Ishida, Y. Kitaoka, and K. Asayama, J. Magn. Magn. Matter. 177-181, 387 (1998).
- [279] E.-W. Scheidt, T. Schreiner, K. Heuser, S. Koerner, and G. R. Stewart, Phys. Rev. B 58, R10104 (1998).
- [280] Continetino, Phys. Rev. B 48, 7183 (1993).